Systematic Design of Microscope Objectives

Dissertation

for the acquisition of the academic title

Doktor Rerum Naturalium (Dr. rer. nat.)

submitted to

the Council of the Faculty of Physics and Astronomy

of the Friedrich-Schiller-Universität Jena

by **M.Sc. Yueqian Zhang**

born on 15.08.1991 in Tianjin

Reviewers:

1. Prof. Dr. Herbert Gross

2. Prof. Dr. Alois Herkommer

3. Prof. Dr. Julie Bentley

Date of the Disputation: 13.12.2019

Abstract

The modern microscope objective is the most sophisticated optical component in light microscopes, providing high contrast images with diffraction-limited resolution. The design of microscope objectives has been developed for over a hundred of years. However, after 1970s, the review of advanced application-oriented systems is limited, and the design principles are not clear to most optical designers who are not the specialist from a few microscope manufacturers. To subtract off the hidden assumptions during the historical development and turn back to the intrinsic building blocks of the high numerical aperture (NA) systems, in this work, a systematic analysis and synthesis approach for microscope objectives is worked out, which is not found in available literature.

The microscope objective patents are collected worldwide. Concentrating on the standardized objectives with color correction at least in the visible spectrum, a large system database is built up within Zemax/OpticStudio$^{\mathrm{TM}}$. According to a systematic review of the historical development, new classifications of the modern microscope objectives are proposed to understand the system complexity. Thereby, systematic analysis of the systems can be conducted to decouple the impact of aberration correction, application and manufacturing requests. Based on the decoupled results, the building blocks and design principles of the modern microscope objectives are systematically analyzed and summarized. Lens modules are sorted with respect to the general optical power distribution and individual structural lens groups. The reasons for many commonly used complicated structures are explained. Utilizing the lens modules, the microscope objective design can be more systematic. Both the modification of existing systems and the synthesis of new structures are realized, which give optical designers new ideas or possible opportunities to keep away from the restriction of other patents.

This work provides a new point of view on the conventional microscope objectives, which can be applied to other classical optical systems as well. This point of view may help optical designers respond to the increasing demand for systems with extended etendue and follow the recent trend of AI-aided optical design.

This page is left blank intentionally.

Zusammenfassung

Das Objektiv ist die wichtigste optische Komponente eines Lichtmikroskops, da dessen Qualität den Bildkontrast und die Auflösung vordergründig bestimmt. Am Design des Mikroskop-Objektives wird über einem Jahrhundert gearbeitet. Seit den 1970er Jahren findet sich jedoch nur noch wenig Literatur, die sich der Entwicklung von „Advanced application-oriented Systems“ widmet. Die Prinzipien des Designs sind daher selbst für die meisten Designer nicht übersichtlich. Diese Arbeit handelt der systematischen Analyse- und dem Syntheseansatz für Mikroskop-Objektive. Dies wurde bis jetzt nicht in der Literatur erwähnt.

Für diese Arbeit wurden die Patente im Sektor vom Mikroskop-Objektiven weltweit gesammelt. Eine systematische Datenbank ist basierend auf Zemax/OpticStudio^{TM} aufgebaut, welche sich auf standardisierte Objektive mit einer Farbkorrektur zumindest für den sichtbaren Bereich konzentriert. Eine neue Klassifikation der modernen Mikroskop-Objektive wird vorgeschlagen, basierend auf einem systematischen Rückblick der historischen Entwicklung. Dies ziehet darauf ab, deren Komplexität zu verstehen. Eine systematische Analyse der Systeme kann verwendet werden, um den Einfluss der Abbildungsfehlerskorrektur, der Anwendung und der Herstellungsanforderungen zu entkoppeln. Diese Ergebnisse sind der Grundstein, um die Designprinzipien der modernen Mikroskop-Objektive in dieser Arbeit systematisch zu analysieren und zusammenzufassen. Die Linsenmodule werden nach der allgemeinen optischen Brechkraftverteilung und den einzelnen konstruktionsbedingten Linsengruppen sortiert. Etliche komplizierte Strukturen werden begründet. Angesichts der Anwendung der Linsenmodule wird das Design des Mikroskop-Objektives strukturierter. Sowohl die Veränderung bekannter Systeme als auch die Synthese neuer Strukturen wurden realisiert. Hierdurch bieten sich dem Optikdesigner neuen Ideen und Chancen, um die Einschränkung bestehender Patente zu vermeiden.

Diese Arbeit vermittelt eine neue Betrachtungsweise im Hinblick auf konventionelle Mikroskop-Objektive, welche aber auch bei anderen klassischen optischen Systemen angewendet werden kann. Sie hilft möglicherweise auch den Optikdesignern der

steigenden Nachfrage nach Systemen mit erhöhtem Leitwert geredet zu werden und folgt dem Trend „AI“-gestütztem Design.

Contents

1. Introduction

Modern microscope objective lenses, which correct various aberrations, are the most sophisticated optical components in light microscopes. They are typically high numerical aperture (NA) optical systems, which provide high contrast images with diffraction-limited resolution. Since Lister created the two-group Lister-type objective in 1830s and Abbe built up the modern microscopy theory in 1880s, the microscope objectives have been developed over centuries and thousands of systems have been patented in hundreds of patents for various applications.

The early age of microscope objective development (1830s to mid-20th century) has been well described in literature [1-5]. However, from 1970s, the modern microscope systems became highly standardized and objective design appeared strongly application-oriented. Each vendor developed their own technology roadmap, which is based on their own design ideas and manufacturing technologies. There are only two articles reviewing these modern objectives, which were reported by Riesenberg in 1988 [6] and Broome in 1992 [7]. From the mid-1990s, the growing demand from fluorescence microscopy and the semiconductor industry significantly influenced the development of microscope objectives. Due to the lack of review of the latest arts, the impact of applications and manufacturing considerations on the increased system complexity is not clear. Furthermore, unlike the well-known photographic objective databases with thousands of entries, the available database of microscope objectives usually only has 20-30 examples [8-10]. Lacking enough data, a systematic analysis of modern systems is also missing.

The design principles of the simple systems were well known [4-6, 11, 12], such as the achromatic glass selection for color correction and the use of thick meniscus lens for field flattening. However, when it comes to the modern objectives, only the structural parameters are carefully defined in the patents, whereas the design principles and functionality of the structures are seldom discussed. In the industrial community, each vendor keeps its own design technique as a secret and only some pieces of ideas were published [13]. In the academic community, several systematic synthesis approaches have been reported in the recent two decades, but most of them only work for low NA cases [14, 15]. Frolov published a series of papers about the modern objective construction [16-19], but the approach only shows the technology roadmap of the LOMO and Labor projects, which cannot demonstrate the design principle of most standardized modern systems.

Since modern microscope objectives have not been systematically reviewed and analyzed, optical designers, who are not the specialists of microscopes, are often confused with two questions:

- What to design? — How does the various application and manufacturing requests impact the specification? How to specify the system parameters, and which correction level is required?
- How to design? — How to classify the microscope objectives according to their correction level to understand the relation between their performance and system complexity? What are the design principles applied in microscope objectives and how to understand them from the existing systems? How to utilize the experience to aid the new system design?

"Zu den Sachen selbst" (back to the things themselves) is a key concept of phenomenological Epoché in Husserl's phenomenology, where "Sachen" or "things" in English refer to any phenomenon that may confront the ego in consciousness, such as a law of nature [20]. In optical design, it is also necessary to subtract off the hidden assumptions to reach the reality [21]. To answer the questions above, it is important to operate the Epoché to efficiently utilize the experience in conventional microscope objective designs.

In this work, as the first step, most of the published modern microscope objective patents (448) are collected and 484 systems with different structures are built up within Zemax/OpticStudio^{TM} as a database. Second, new classification methods are proposed to analyze the relationship between the system parameters and system complexity. Third, a systematic analysis of the systems is conducted with respect to three concepts: aberration correction, impact of applications and the consideration of manufacturing and technology. For each phenomenological model in the objective design, each concept is discussed with certain Epoché. Fourth, based on these three concepts, the structural lens modules are extracted, and their functionalities are systematically summarized. As a last step, the summarized lens modules are utilized to generate new objective structures.

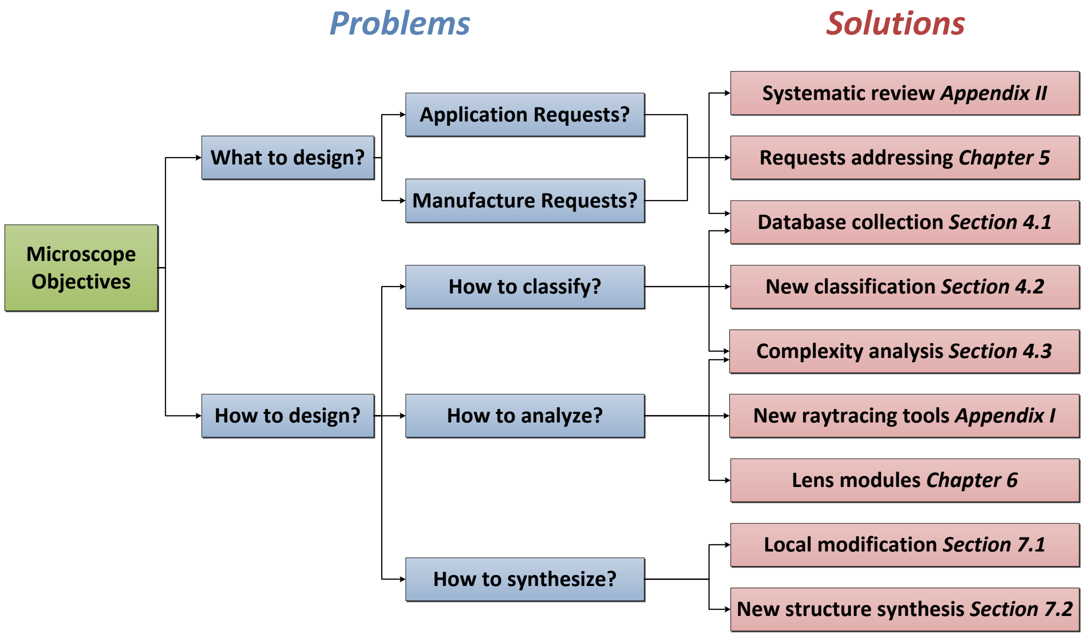

Figure 1.1: Problems in microscope objective design and the solutions, which are marked with the corresponding chapter or section numbers in the thesis.

Figure 1.1 gives a summary of the problems in microscope objective design and the solutions proposed in this work, in which the structure of the thesis is also outlined. In Chapter 2, a brief introduction of the optical system in light microscopes is given. Imaging and aberration theory of the high NA systems is described, and the necessary analysis tools are demonstrated as well. In Chapter 3, the trend of the microscope objective development is reviewed. During the historical development of microscope objectives, some lens modules and correction schemes are widely used by most of the systems, which can be regarded as the state-of-the-art design approaches. These well-described correction schemes are also summarized in Chapter 3. A purpose of this work is to analyze these lens modules more systematically and to further summarize other lens modules. The objective database implementation and complexity analysis are demonstrated in Chapter 4, which combines the first two steps of this work. According to the systematic analysis in the third step, the impacts of application and manufacturing requests are well sorted in Chapter 5. Design principles of microscope objectives are introduced in Chapter 6, including the general aberration correction strategies, material selection strategies and power distribution methods. The detailed lens modules are also summarized in Chapter 6 and then they are utilized in Chapter 7 for system synthesis. The new system synthesis can be considered as both an interpolation and an extrapolation of the microscope objective solution space. By inserting the lens modules locally into the lens groups of existing systems or synthesizing new structures from basic lens modules, new combinations of system parameters and correction levels can be obtained (extrapolation), and new system structures can be achieved to realize the conventional combinations (interpolation). The thesis will be summarized in Chapter 8, after a brief discussion of future perspectives.

As a conclusion, the design methods and correction schemes for conventional microscope objectives are summarized in the first three chapters. From Chapter 4 to Chapter 7, as the main contribution of this work, the new systematic classification, systematic analysis of application and manufacturing requests, systematic analysis of lens modules and systematic synthesis of new structures are proposed for the modern objectives.

There are two general remarks on the plots of the system performance criterion and system layouts. In this thesis, in all the system layouts, the crown glasses are colored with light yellow, the flint glasses are colored with orange and the fluorites or fluorite glasses (d-line Abbe number $\nu_d > 90$) are colored with light green. With special consideration of color correction and for extended spectrum, it is possible to cement two crown glasses or two flint glasses together. In the corresponding system layouts, the cemented element is plotted with two components with the same color. When it comes to the performance plots, when the aberrations, spot sizes, RMS wavefront errors are evaluated in the image space of an infinite-conjugate microscope objective, a tube lens is always combined with the objective for calculation, but it is not shown on the system layouts.

2. Fundamentals

In this chapter, the fundamentals of light microscope and microscopic imaging, which are relevant to this work, are summarized. In Section 2.1, the optical system in light microscopes is briefly introduced. Subsequently, the basic aberration theory of high NA systems is illustrated in Section 2.2, which also introduces the analysis tools for the lens module extraction. As an optical system with diffraction-limited performance, the resolution of microscope objectives should be considered with diffraction theory, which is demonstrated in Section 2.3. This knowledge will be necessary for the system analysis and synthesis in this work.

2.1 Optical System in Light Microscopes

The optical system of a complete microscope consists of two parts: the detection/imaging path and the illumination path. Regarding the imaging path, the conventional light microscope is mostly a two-stage imaging system. The objective lens collects information from an object with high NA and forms an intermediate image with low NA, which is then transferred by an eyepiece and observed by human eye. In the digital microscopes, the intermediate image can be transferred by a relay system and captured by image sensors. But in some recent developed microscopes, such as the virtual slide microscope, the image sensor can be place at the intermediate image position as well, resulting in a one-stage imaging system.

Figure 2.1(a) gives the classical setup of the compound microscope, which has a finite location for the intermediate image, namely finite conjugate. The tube length is defined as the distance between the rear focal plane of the objective lens and the intermediate image. It was standardized as 160 mm by Royal Microscopical Society (RMS) in late 19th century. From 1980s, all the major manufacturers developed their own standardized microscope systems, which utilize an infinite-corrected objective instead of the objective with finite tube length: UIS (Universal Infinity System) for Olympus, CFI (Chrome-Free Infinity-corrected system) for Nikon, ICS (Infinity Color Corrected System) for Carl Zeiss and HCS

(Harmonic Component/Compound System) for Leica (also with DELTA system in the early 1990s) [22]. According to Figure 2.1(b), to get a real intermediate image, a tube lens is inserted behind the objective lens. Concerning both the incidence angle on the tube lens and the mechanical track of the whole system, the optimal focal length of the tube lens should be selected between 150 and 250 mm. The four major vendors are using 180, 200, 164.5 and 200 mm in their standardized systems, respectively. Since the light path leaving the objective is collimated, various additional equipment can be inserted into the infinity space without changing the image scale or the intermediate image position, including: a beam splitter for epi-illumination, a Bertrand lens to observe the pupil, color filters, DIC prisms for contrast imaging, polarization components [3], etc.

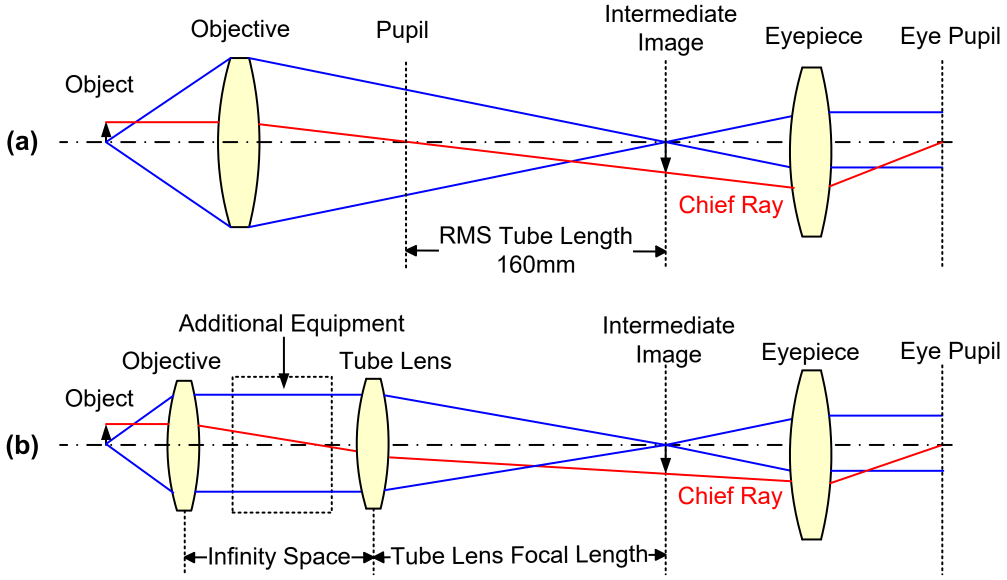

Figure 2.1.: (a) Finite-conjugate microscope system with standardized tube length. (b) Infinite-conjugate microscope system with standardized tube lens.

All manufacturers define the size of the intermediate image as a fixed diameter D_{img}. The major vendors usually use the values of 18, 20, 22, 23, 25, 26.5, 28 and 30 mm in their standardized setups, which are denoted as SF18, SF20, SF22, SF23, SF25, SF26.5, SF28 and SF30 in this thesis, respectively. From this value, the object height can be calculated with the help of objective magnification m_{obj} as:

$$y_{\text{obj}} = \frac{D_{\text{img}}}{2m_{\text{obj}}}. \tag{2.1}$$

It is notable that for the infinite-conjugate objective with a tube lens with focal length f_{tube}, the magnification between the object space and the intermediate image is given by:

$$m_{\mathrm{obj}} = \frac{f_{\mathrm{tube}}}{f_{\mathrm{obj}}}, \tag{2.2}$$

where f_{obj} is the focal length of the objective lens. The throughput of an optical system is typically represented by an etendue G-value, which is defined by its NA and the field of view. For microscope objectives, it can be defined as [3, 23]:

$$G = \frac{\pi}{4}\left(2y_{\mathrm{obj}} \cdot NA\right)^2 . \tag{2.3}$$

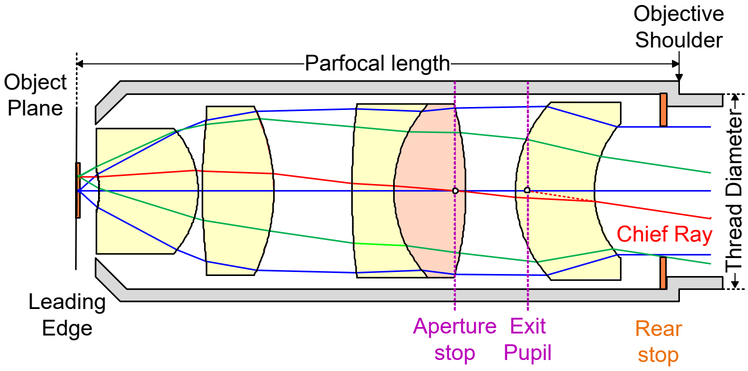

Figure 2.2.: Schematic drawing of microscope objective structure including housing. The aperture stop is fixed to realize telecentric path of the chief ray.

Figure 2.2 shows a typical microscope objective structure. The objective lens has a relatively sharp leading edge and a narrowed rear part with screw threads behind the objective shoulder. During the historical development of microscope objectives, two mechanical dimensions were standardized: the parfocal length and the thread diameter. The parfocal length is defined as the distance between the object plane and the objective shoulder, which limits the axial dimension of the objective lens. By designing objectives with identical parfocal length, the focus position could be fixed when changing the objectives with different magnifications on a turret by turning the nosepiece. The thread diameter determines the maximum size of the exit ray bundle, namely the exit pupil diameter D_{ExP} in infinite-conjugate setup. These two parameters were standardized early on to be relatively small, e.g., 45mm parfocal length and 0.8″ (20.32mm) thread diameter. However, when the required NA and etendue are extended, the short axial dimension is filled with lenses and the small thread size cannot match the large exit pupil size. Therefore, manufacturers have selected various larger values for their modern systems, e.g., 60mm parfocal length and 25mm thread diameter.

If the aperture stop of on optical system is placed at its rear focus, the entrance pupil is at infinity and the chief ray in the object space is parallel to the optical axis. This kind of system is called object-side telecentric system, which has great advantage for measurement applications. A varying distance of the object leads to a defocusing in the fixed detection plane and thus to a lack of focus, but the center of mass of the bundle does not change and there is no change in the magnification detected [24]. In both the finite-conjugate and infinite-conjugate setups, the microscope objectives are usually designed object-side telecentric. The rear stop of the lens coincides with the back focal plane to enforce this arrangement. However, in practice, according to Figure 2.2, the exit pupil usually locates inside the objective lens. Although the aperture stop can still be set to realize object space telecentricity, the rear stop deviates from the exit pupil position. This can cause some problems in the connected optical system, e.g., the scanning lens for the confocal microscopy [3].

2.2 Aberration Theory of High NA Systems

The main purpose of this work is to extract the lens modules from patented systems to aid the synthesis of new structures. Therefore, it is necessary to understand the aberration behavior of each surface and element. The tools to calculate the primary and higher-order monochromatic aberration contributions are introduced in Section 2.2.1, whereas the chromatic aberration and spherochromatism are illustrated in Section 2.2.2. The raytracing methods will be introduced in Section 2.2.3 and Appendix I to achieve reliable and comparable surface aberration contributions when the rays are traced from the reversed direction (high NA to low NA and low NA to high NA), particularly for the high NA systems fulfilling the sine condition.

2.2.1 Primary and Higher-order Monochromatic Aberrations

Concerning the monochromatic aberrations, in geometrical optics, the ray aberrations are the primary quality criteria, which can be represented as transverse aberration. If the transverse aberrations are expanded in a Taylor power series in terms of the aperture and field, the aberrations with different orders can be obtained. Historically, the optical aberrations are analyzed by 3rd-order Seidel terms as primary aberration [25]. In this approximation, a surface decomposition is additive and allows for hints to correct optical systems. Five primary monochromatic aberrations: spherical aberration, coma, astigmatism, field curvature and distortion can be characterized with five Seidel coefficients, where $\delta\left(\frac{u}{n}\right)=\frac{u'}{n'}-\frac{u}{n}$ and $\delta\left(\frac{1}{n}\right)=\frac{1}{n'}-\frac{1}{n}$:

$$\begin{cases} \textit{Spherical Aberration} & S_I = -A^2 h\delta\left(\frac{u}{n}\right) \\ \textit{Coma} & S_{II} = -A\bar{A}h\delta\left(\frac{u}{n}\right) \\ \textit{Astigmatism} & S_{III} = -\bar{A}^2 h\delta\left(\frac{u}{n}\right) \\ \textit{Field Curvature} & S_{IV} = -\Omega^2 c\delta\left(\frac{1}{n}\right) \\ \textit{Distortion} & S_V = \frac{\bar{A}}{A}\left(S_{III}+S_{IV}\right) \end{cases} . \tag{2.4}$$

The spherical aberration coefficient can be simply represented as:

$$S_I = nhi\left(i'-i\right)\left(i'-u\right). \tag{2.5}$$

In these formulae, u and n are the paraxial marginal ray angle and refractive index in the object space. h is the height of the incidence point of the marginal ray with the reference to the optical axis. $A = ni$ is the refraction invariant, where i is the angle of incidence of the paraxial marginal ray. Ω is the Lagrange invariant and c is the curvature of the surface. The primed quantities refer to the image space. Any quantity associated with the chief ray is denoted by a bar, e.g., $\bar{A} = n\bar{i}$. Based on these surface contributions, the Seidel diagram can be plotted, illustrating the surface contribution of each aberration intuitively. Thus, the functionality of each surface and element can be understood.

However, in the microscope objectives, due to the high NA, the primary aberration is not sufficient to evaluate its performance and aberration behavior. Higher-order aberrations, particularly the higher-order spherical aberration, must be considered. Unfortunately, although several analytical descriptions of 5th-order spherical aberration have been found in literature, the definition, variables and results are not consistent and reliable for all the systems [26]. Nowadays, the Zernike coefficients are useful tools to evaluate the higher-order aberrations. Nevertheless, they are difficult to be decomposed to the surface contributions to assist optical design.

Owing to the physical nature and correction strategy of the aperture-dominant systems, the Seidel aberration contributions are sufficient to evaluate the field aberrations (only except some extremely high NA cases). To evaluate the correction of the axial field, the Delano formula [25] is utilized to calculate the exact full-order spherical aberration $\Delta s'_{\mathrm{SPH}}$ and its surface contribution:

$$\begin{aligned}\Delta s'_{\mathrm{SPH}} &= \Delta s_{\mathrm{SPH}} \cdot \frac{n_1 u_1 \sin U_1}{n_k u_k \sin U_k} + \sum_j \frac{n_j}{n'_k} \cdot H_j \cdot \sin\frac{I'_j - I_j}{2} \cdot \frac{2 i_j \cdot \sin\frac{I'_j - U_j}{2}}{u'_k \sin U'_k} \\ &= \Delta s_{\mathrm{SPH}} \cdot \frac{n_1 u_1 \sin U_1}{n_k u_k \sin U_k} + \sum_j \frac{S_{\mathrm{FSPH}j}}{2 n'_k u'_k \sin U'_k},\end{aligned} \tag{2.6}$$

where the $S_{\mathrm{FSPH}j}$ is the full-order spherical aberration contribution coefficient of the surface No.j. The quantities denoted with subscript “1” indicate the properties of object space, while the quantities with subscript “k” show the properties of the image space. Both the real and paraxial raytracing data are used to calculate the aberration contributions, which are schematically demonstrated in Figure 2.3.

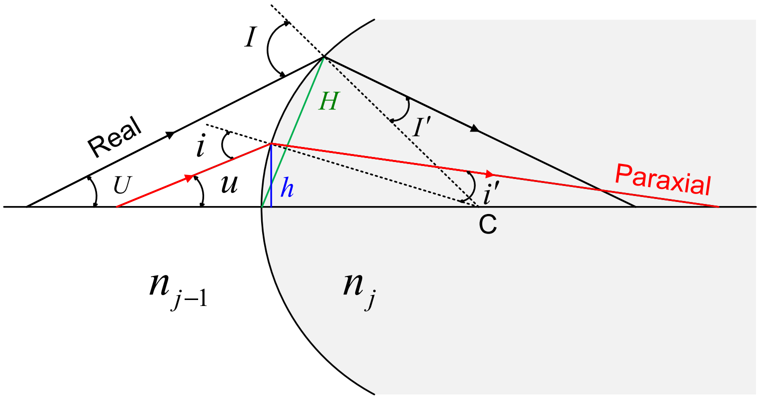

Figure 2.3.: Raytracing data for spherical aberration contribution calculation. The capital letters refer to the real ray data, while the small letters refer to the paraxial ray data.

Thus, the critical higher-order spherical aberration contribution coefficient S_{HSPH} resulting from the high NA can be determined by subtracting off the Seidel contribution S_I from the full-order contribution S_{FSPH} [27]:

$$S_{\mathrm{HSPH}}=S_{\mathrm{FSPH}}-S_I=4nHi\sin\frac{I'-I}{2}\sin\frac{I'-U}{2}-nhi\left(i'-i\right)\left(i'-u\right). \qquad (2.7)$$

When the spherical aberration is well corrected, the residual error at aperture zones is defined as zonal error or zonal spherical aberration. Conventionally, if the zonal error is not very large, the performance of objectives mostly depends on the spherical aberration correction at the full aperture. However, for recent fluorescence microscopy with laser excitation, if the light source has apodization, e.g., Gaussian distribution, the effective NA would be narrowed. The spherical aberration (and chromatic aberration) would increase tremendously if the zonal error (and spherochromatism) is not corrected. Regarding the special objectives with adjustable iris, this problem is more critical. Therefore, correcting zonal error is necessary for recent developed high NA objectives with excellent performance. Illustrative introduction will be given in Section 2.2.2 together with spherochromatism.

It is notable that during the propagation of aberrations, the 3rd-order aberrations of the prior surface can generate different ray heights and angles at the next surfaces from the paraxial intrinsic ray heights. Consequently, the perturbed ray heights induce 5th-order aberrations [28, 29]. When the primary aberrations are dominant, the induced effect is usually negligible. However, in the high NA systems, since the higher-order aberrations are tremendous, the induced aberrations are often utilized for correction.

It is well known that microscope objectives are conventionally designed inversely, namely regarding the object plane as the image and the intermediate image as the object. The advantages of this method are the straightforward evaluation of system resolution and easy raytracing from low NA space to high NA space. However, in the modern microscope systems, particularly with epi-illumination, the light beam passes through the objective lens from both directions. The optical performance of both side propagation should be consistent. To check both side performance and to avoid the possible negative impact of the higher-order induced aberrations, the raytracing and aberration evaluating method should be robust to handle both the tracing from high NA to low NA and from low NA to high NA, which will be introduced in Section 2.2.3.

2.2.2 Chromatic Aberrations and Spherochromatism

Due to the dispersion of optical materials, the refractive optical systems usually suffer from chromatic aberrations when they work for a wide spectrum. Regarding the typical visible range correction, it is common to select F(blue), d (yellow) and C(red) spectral lines for design and analysis of visual systems. Following the trend of using digital sensors, the F' (blue), e (green) and C'(red) spectral lines are also widely used for microscope objective design. For simplicity, in this thesis, the d-line is used as the reference and the F, d, C spectrum is considered for visible correction, because they are used in most of the patents.

The chromatic focal shift of the C-line with reference to the F-line is defined as the axial (longitudinal) chromatic aberration, while the difference between the C-line's and F-line's chief ray height on image plane is defined as lateral color to show the chromatic change of magnification. The d-line Abbe number ν_d can be defined to express the F-C dispersion:

$$\nu_d = \frac{n_d - 1}{n_F - n_C}. \tag{2.8}$$

Using a graph (Abbe diagram) in which the Abbe number ν is plotted as abscissa and refractive index n as ordinate, the main properties of optical materials can be well sorted. Figure 2.4 gives an Abbe diagram, where the glass labels from three often used vendors (Schott, Ohara and Hoya) are marked in the corresponding zones [27]. Some important glass types with specific advantages are pointed out, and these shall be discussed in Section 6.3 in detail. The "Middle Glasses" are defined by the d-line Abbe numbers between 50 and 57, whereas the "KZFS Short Flint" gives the region of the short flint glasses with the glass label of KZFS or KZFH.

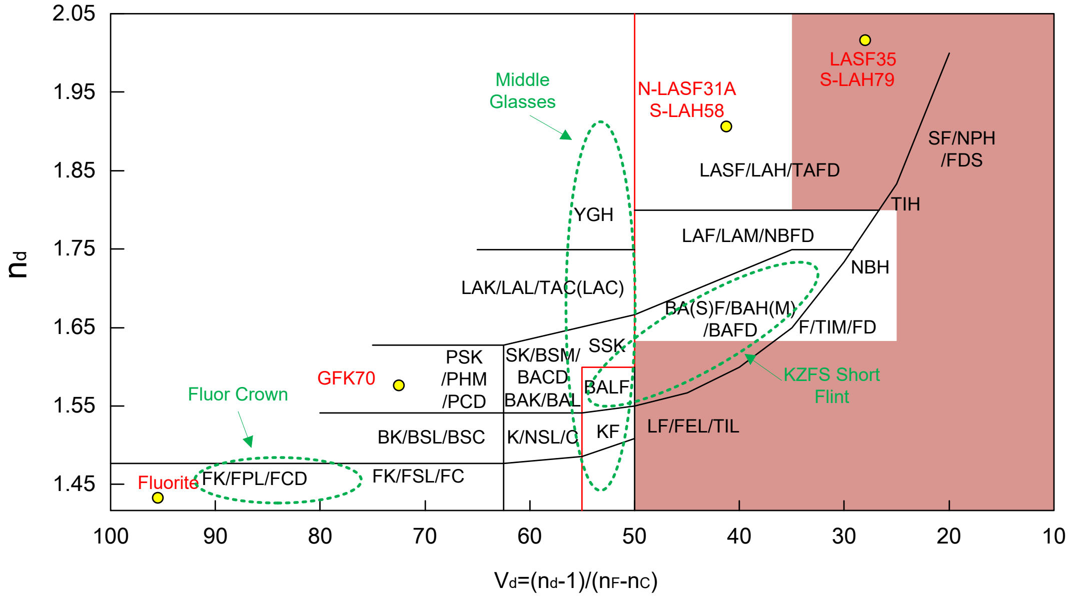

Figure 2.4.: Abbe diagram with the glass labels from three often used vendors. The red line separates the crown and flint glasses and the read area indicates the forbidden zone of material selection for high-contrast fluorescence imaging, which is quantitative defined in Appendix VII. The green encircled areas demonstrate the region of Middle Glasses, Long Crown and KZFS Short Flints, which are useful for microscope objective design.

It is well known that the basic surface contributions of axial chromatic aberration and lateral color can also be analyzed with the Seidel approach [25], where $\Delta\left(\frac{\delta n}{n}\right)=\frac{n'_{\lambda_1}-n'_{\lambda_2}}{n'_d}-\frac{n_{\lambda_1}-n_{\lambda_2}}{n_d}$:

$$\begin{cases} \textit{Axial Chromatic Aberration} & C_I=-Ah\Delta\left(\frac{\delta n}{n}\right) \\ \textit{Lateral Color} & C_{II}=-\bar{A}h\Delta\left(\frac{\delta n}{n}\right) \end{cases}, \tag{2.9}$$

When the typical F-C chromatic aberrations are considered, $\lambda_1=F, \lambda_2=C$. When the axial chromatic aberration is corrected for two wavelengths, the residual error of another spectral line is defined as the secondary spectrum. When the microscope objective should have apochromatic correction or the corrected spectrum is extended, the secondary spectrum must be analyzed. Under this circumstance, the secondary and higher-order spectrum is evaluated by calculating the additional λ_1 and λ_2.

In the recent developed high NA objectives, the spherochromatism, which is defined as the chromatic variation of the spherical aberration, sometimes significantly affects the system performance as well. The longitudinal aberrations of microscope objectives with different levels of spherochromatism correction are compared in Figure 2.5.

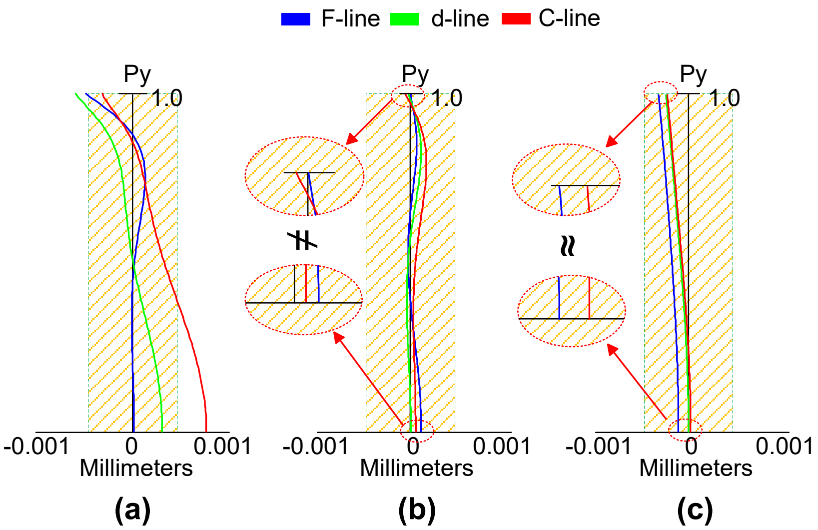

Figure 2.5.: The longitudinal aberrations of different correction levels, where P_y is the relative pupil height and the shaded region indicates the depth of focus of d-line. The spherochromatism is measured as the difference between the red and blue light for paraxial case and full aperture. (a) Achromatic color correction with spherochromatism correction for green and red light. (b) Apochromatic color correction with certain zonal error and spherochromatism control. (c) Apochromatic color correction with excellent spherochromatism and zonal error correction. The three systems have identical NA=0.8. Only the F, d, C correction is compared, without g-line performance demonstration for the apochromatic systems. Achromatic: two-color axial chromatic correction (usually F-line to C-line). Apochromatic: axial chromatic correction including secondary spectrum (usually g-line to C-line). Quantitative definitions are given in Section 4.2.1.

The longitudinal aberration (a) represents the typical performance of the conventional Achromate objectives, where the axial chromatic aberrations of red and blue light are well corrected near the full aperture, but the residual secondary spectrum of the d-line exists. To control the longitudinal aberration of d-line, the spherochromatism between the d-line and the C-line is corrected. Thus, the focal shift through the full spectrum is controlled within 2.5×DoF (Depth of focus). When it comes to the Apochromate system (b), the axial chromatic aberration and secondary spectrum are perfectly corrected for the three colors near the full aperture. The spherical aberration of the d-line is also cancelled for centroid green light. However, concerning the zonal error and spherochromatism, although they are controlled within the DoF, the performance at different zones are slightly different. The correction is not as perfect as the state-of-the-art system (c), in which nearly identical performance is achieved for the whole aperture with excellent spherochromatism correction.

As introduced in Section 2.2.1, in the advanced fluorescence microscope objectives and objectives with adjustable iris, it is necessary to correct the zonal error and the spherochromatism. To analyze the functionality of the lens modules in correcting spherochromatism, the 3rd-order spherochromatism surface contribution coefficients are utilized, with the used quantities demonstrated by Figure 2.6 [30]:

$$\begin{aligned} S_{SC} &= \Delta y\left(u-u'\right)\left(-4n'i'^2-nu^2+3nuu'\right)+\Delta uy\left(u-u'\right)\left(-4i'n'+nu-3nu'\right) \\ &+\Delta niy\left(i'^2-i'u+2i'u'-u^2+uu'\right)+\Delta n'i'^2y\left(u'-i'\right). \end{aligned} \tag{2.10}$$

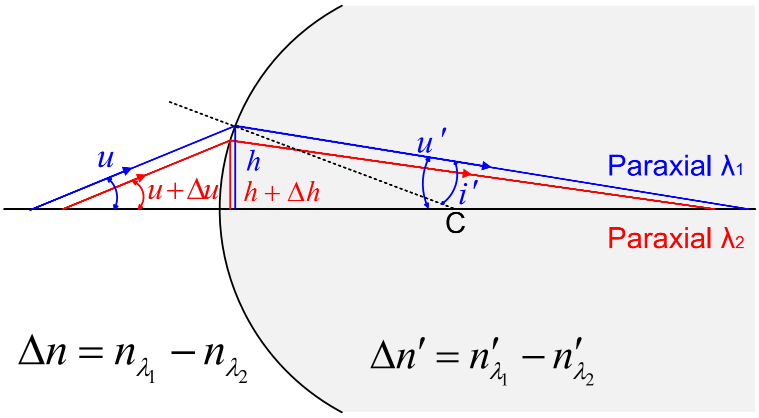

Figure 2.6.: Quantities defining spherochromatism. The blue rays and parameters refer to the primary wavelength λ_1 and red rays and parameters to the second wavelength λ_2.

2.2.3 Sine Condition and Modified Raytracing Method

In the Fourier optical model, the object can be expanded into single spatial frequencies. For each frequency an angle is determined by the grating equation for the light diffracted from the relevant object structure. Since the grating equations are based on the sine values of the angles, for finite angles, the sine values are transferred linearly through the optical system. Only if the diffraction orders have the right sine-equidistant sampling in the exit pupil, the image can be reconstructed correctly. This leads to the famous sine condition:

$$\frac{\sin U}{u} = \frac{\sin U'}{u'} \left(\text{Abbe's Presentation}\right). \tag{2.11}$$

In the high NA systems, due to the large finite object angle, it is necessary to consider the sine condition fulfillment, which requires pupil shape as spheres instead of planes. Under the precondition of zero spherical aberration, the fulfillment of sine condition is a necessary and sufficient requirement for zero linear coma. A system is called aplanatic (aplanatism) when the spherical aberration and linear coma are eliminated. However, in practice, the spherical aberration cannot be perfectly corrected as zero in high NA microscope objectives to satisfy sine condition. But it can be controlled small and the sagittal linear coma can be corrected. Thus, the system can be well corrected for the offence against sine condition (OSC) and realizing isoplanatism. The significance of isoplanatism is the stationarity of the aberration regarding a small shift in the field. This means that when the object point is shifted by a small amount, the aberration at the new image point will be the same as it was before the shift [29]. In the aperture-dominant systems, such as microscope objectives, the OSC should be corrected to assure a good performance of the small field. It is also notable that, if the optical system suffers from large pupil aberrations, the equidistant pupil sampling is also violated. Therefore, they should also be well corrected, particularly for the very-low-magnification microscope objectives.

In the conventional analysis of optical systems, the pupil is typically simplified to a pupil plane for raytracing. However, when the object space NA is larger than 0.5, the raytracing error resulting from the pupil shape cannot be neglected. To achieve accurate real ray data for aberration calculation in the analysis, the raytracing method should be able to find the real shape and size of the pupil. Popular commercial optical design software utilized different methods to find the real pupil. In Zemax/OpticStudio™, for high NA systems, the "real ray aiming" should be activated, which utilizes iterative raytracing to match the edge of the aperture stop and the real pupil [31]. A more general method to accurately scale and normalize the object and image space aperture is to define the canonical pupil coordinates [32]. In OSLO®, as the default setting, the "aplanatic ray aiming" is utilized to specify he real rays, which is based on the canonical coordinates [33]. CODE V® also implemented the canonical coordinates, thus defining the energy conserved object and image space for the optical systems that fulfills the sine condition [34]. When either of these two methods is applied in the analysis of microscope objectives, real ray data can be accurately obtained. Apart from the slight influence of higher-order induced aberration, the real ray data are nearly consistent when the rays are traced from different directions, namely from high NA object space to low NA image space or from low NA image space to high NA object space. However, when it comes to the paraxial ray, the paraxial marginal ray angle is determined by the pupil edge instead of the pupil sphere. Consequently, the paraxial raytracing, which is also important in aberration calculation, cannot be operated under the spherical pupil settings mentioned above. Regarding the microscope objectives, when the rays are traced from the low NA image space to the high NA object space, due to the small deviation at the edge of the planar and spherical entrance pupil, the paraxial raytracing is rather accurate. However, when the raytracing direction is reversed, the paraxial object space NA becomes too large, resulting in unrealistic or inconsistent paraxial ray data. This is also one of the reasons why the microscope objective lenses are conventionally designed inversely.

To solve this problem, a special iterative paraxial raytracing method in Zemax/OpticStudio$^{\text{TM}}$ is proposed [27]. Detailed mechanism of the method is described in Appendix I. When the microscope objectives are analyzed in Zemax/OpticStudio$^{\text{TM}}$, to calculate the aberrations, the real ray aiming is activated for accurate real raytracing, and the iterative paraxial raytracing is operated to achieve the paraxial ray data. A similar approach can also be applied in OSLO® and CODE V®, where the canonical pupil coordinates are implemented to trace the real ray. By operating an additional paraxial raytracing with the ideal pupil setting and combing the paraxial ray data with the real ray data to calculate the aberrations, the realistic and quasi-consistent aberration behavior of the microscope objectives can be determined.

2.3 Diffraction Theory of Resolution

Regarding a single radiant point as the object, the emitted spherical wave would be transversely limited by an imaging optical system. The aperture limitation has a diffraction effect resulting in a point spread function. In the lateral sectioning plane, the point spread function for a circular and homogeneous illuminated aberration-free aperture can be described as the Airy distribution function in the Fraunhofer approximation [24]:

$$I(r)=\left[\frac{2J_1\left(\frac{2\pi ar}{\lambda f}\right)}{\frac{2\pi ar}{\lambda f}}\right]^2=\left[\frac{2J_1(x)}{x}\right]^2, \tag{2.12}$$

where a is the radius of the circular aperture, λ is the wavelength, f is the focal length of the optical system and x is the normalized coordinate in the image plane. The first zero of the Airy distribution can be found at $x = 3.832$,

$$2r = D_{Airy} = \frac{1.21976\lambda}{n' \cdot \sin U'}, \tag{2.13}$$

which is defined as the diameter of Airy disk, shown in Figure 2.7(a).

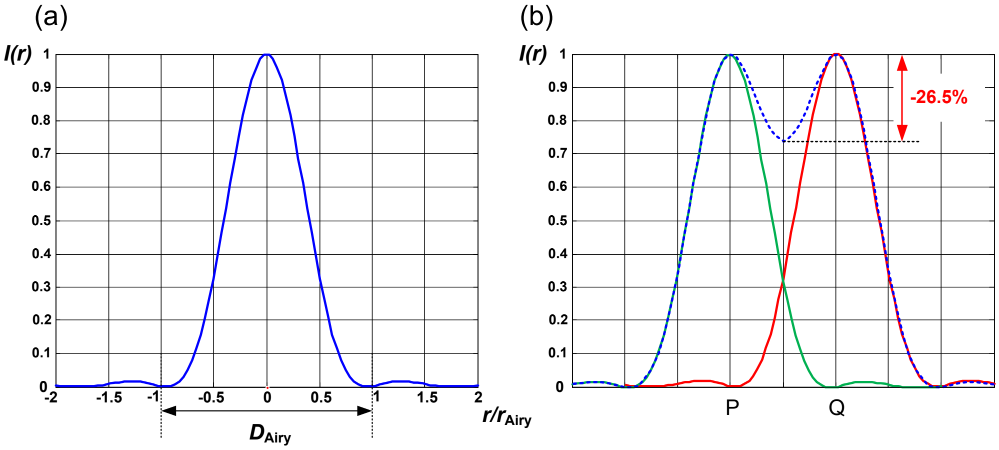

Figure 2.7.: (a) Point spread function with Airy distribution. (b) Rayleigh resolution criterion with 26.5% central dip of intensity.

The famous Rayleigh criterion defines the incoherent 2-points resolution. It states that two points are resolved if the maximum of the Airy disk of one point lies exactly with the first zero of the second point's diffraction pattern. Hence the resolution with incoherent light is defined as:

$$y = \frac{0.61\lambda}{NA}. \tag{2.14}$$

Regarding two Airy disks centered at P and Q, under the diffraction limit, at the center between P and Q, the intensity has a dip of 26.5%, demonstrated in Figure 2.7(b).

Concerning the same circular fully illuminated homogeneous pupil. The intensity distribution along the axis is given by:

$$I(z) = I_0 \cdot \left[\frac{\sin\left(\pi \cdot \frac{n' \sin^2 U'}{2\lambda} \right)}{\pi \cdot \frac{n' \sin^2 U'}{2\lambda}} \right]^2. \tag{2.15}$$

The depth of focus DoF is then defined as:

$$\mathrm{DoF} = \pm \frac{1}{2} \cdot \frac{\lambda}{n' \sin^2 U'} = \pm \frac{1}{2} \cdot \frac{n'\lambda}{NA^2} = \pm \frac{1}{2} \cdot R_E, \tag{2.16}$$

where R_E is the Rayleigh length and corresponds to an intensity drop to 80% along the axis.

When it comes to the coherent case, considering the object as a diffraction element itself, the diffraction at the aperture creates multiple maxima. These maxima can be considered as a source of another spherical wave. The interference of these spherical waves creates the image at the image plane. If the same central intensity dip of 26.5% as the incoherent case is considered, the resolution with coherent light is:

$$y \approx \frac{0.82\lambda}{NA}. \tag{2.17}$$

In microscopes, the state of coherence can be changed by modifying the ratio σ of the numerical apertures of the illumination NA_{ill} versus the observation NA_{obs}. The optimal resolution:

$$y = \frac{0.56\lambda}{NA} \tag{2.18}$$

can be obtained when $\sigma = 1.46$. In this thesis, since only the normal imaging performance are analyzed, for simplicity, only the incoherent case is considered.

3. Historical Development and State of the Art

To build up a bridge between the large amount of patented data and the systematic analysis, in this chapter, the microscope objective patents are first sorted in Section 3.1 to show the trend of the historical development. The well-known correction schemes for microscope objectives are also summarized in Section 3.2. These can be considered as the state-of-the-art design methods, which are understood by optical designers.

3.1 Overview of the Patents

To review the historical development of microscope objectives, 448 entries have been collected from patents of the United States, Germany and Japan. Although some individual entries can also be found from Russian, Chinese and Korean patents, they are mostly designed for a specific setup, not for standardized applications. Thus, they are excluded from the collection. Designed for different setups, some systems with identical structures were reported in multiple patents from different countries. These systems are combined with the reference to the US patents. The remaining German and Japanese patents indicate that the systems are only patented in the corresponding countries. Owing to the distinctive complexity, optical disk objectives and recent *in vivo* endoscopic microscope objectives are not considered during the patent collection. The collected entries are patented for various research and routine applications (same settings for mass measurement) and mostly focus on the field of biomedical research and semiconductor industry. Furthermore, reflective and catadioptric objectives are excluded.

From the first apochromatic objective patented by Boegehold in 1926 [35] to the latest released high etendue immersion objective in May 2018 [36], the trend of patents is illustrated in Figure 3.1, which is sorted by the release dates of the patents.

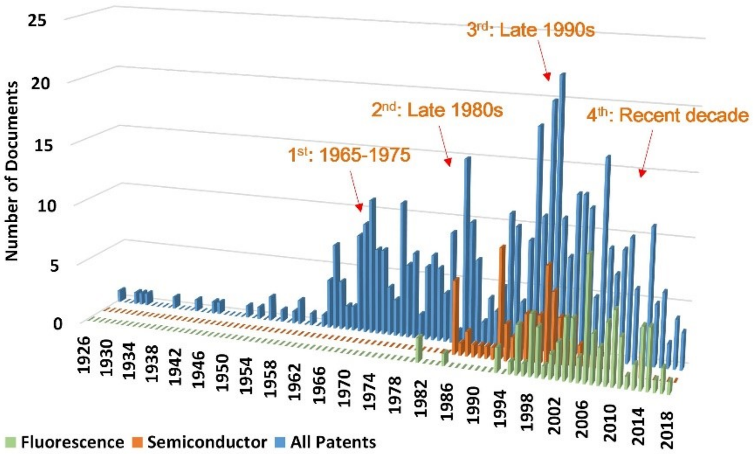

Figure 3.1.: Number of modern microscope objective patents from 1926 to 2018.

Except the early developments in Carl Zeiss before World War II, the major development of microscope objectives mostly started in the 1950s, and there are four peak periods of publications:

1. From 1965 to 1975, most of the basic objective structures were invented for biomedical and metallurgical applications. During this time, there were an increasing number of systems designed for infinite-conjugate instead of the conventional finite-conjugate system with standardized tube length.
2. From the mid-1980s, following the flourishing demand from the semiconductor industry, the working distance and corrected spectrum were extended, corresponding to the requirements from semiconductor fabrication operation. From the 1980s, the application segmentation happened. The objective series for research and routine applications are clearly separated. The advanced objectives for semiconductor industry significantly changed the routine applications, whereas applying fluorescence microscopy to biology and material science led to a revolution of objective design for research application.
3. In the 1990s, various advanced objectives with excellent fluorescence contrast were further invented. Therefore, the highest peak period of microscope objective patenting was found around 2000, which results from the development for both the research and routine applications.
4. Coming into the 21st century, there are two reasons that led to the recent peak period of development: use of digital sensors and advanced fluorescence microscopy

methods, such as nonlinear microscopy (e.g., multiphoton microscopy), total internal reflection fluorescent microscopy (TIRFM) and super-resolution localization microscopy. For one thing, utilizing digital imaging and post-magnification, it is possible to obtain high-resolution image with large visual field. Therefore, objectives with low/medium magnification and high NA are preferred instead of the high magnification objectives, thus extending the etendue of the objective lenses. For the other, owing to the essential requirement of high contrast, high resolution and special system parameters (working spectrum, working distance, etc.), the structures of objectives designed for advanced fluorescence microscopy should be modified. Hence, combining these two effects, a series of objectives with highest complexity was reported in the recent decade.

Due to the limit of space, the concrete lens evolution during the historical development is not given in this section, which is demonstrated in Appendix II.

3.2 Well-described Correction Schemes

Before the application segmentation in 1980s, most of the microscope objectives share common design principles focusing on the correction of spherical aberration, field curvature, axial chromatic aberration and lateral color. These corrections schemes were well described in the literature and utilized by some systematic design approaches [14] for low NA systems.

Utilization of aplanatic surfaces is the most well-known scheme for spherical aberration correction. According to Equation (2.6), the spherical aberration vanishes under three conditions ($H = 0, I' = I, I' = U$), which correspond to the following three cases: the marginal ray has zero height at the surface, the marginal ray has no refraction on the surface and the marginal ray fulfills aplanatic condition. The three cases are named as vertex (v), concentric (c) and aplanatic (a), respectively. Fulfilling these three conditions, the surface can generate an image that is free of all orders of the spherical aberration and linear coma. Combining two of these conditions, three lens setups are widely used in the front group of the microscope objectives as shown in Figure 3.2.

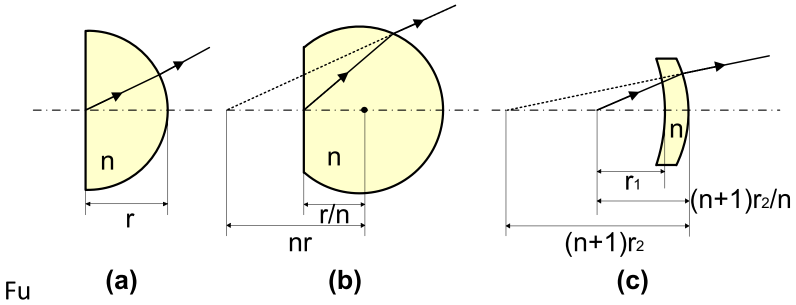

Figure 3.2.: Typical aplanatic lenses with refractive index n. (a) vertex-concentric (v-c). (b) vertex-aplanatic (v-a). (c) concentric-aplanatic (c-a).

According to the object and image distance shown in Figure 3.2, the respective magnifications of these three aplanatic lenses can be calculated as follows:

$$\begin{gathered} M_{v-c} = \frac{r}{r/n} = n,\ M_{v-a} = \frac{(n+1)r}{(n+1)r/n^2} = n^2, \\ M_{c-a} = \frac{(n+1)(2n-1)r_2^2 - 2n^2 r_1 r_2}{n r_1 (r_2 - r_1)}. \end{gathered} \tag{3.1}$$

The type (a) v-c lens, which is typically used as a contact magnifier, has a magnification same as its refractive index. The type (b) v-a lens, which is also known as the Amici lens, has an important functionality, that is, the magnification of the lens is the square of its refractive index, which means the large NA from the object could be lowered down with a factor of n^2 after the aplanatic lens. Hence, the v-a lens, which is typically made of a high-index material, is often used as the front lens of microscope objective and significantly reduces the complexity of following groups for aberration correction. However, the v-a lens has a major drawback in terms of system assembly under high NA, that is, the hyper-hemispherical lens cannot be mounted to the leading edge of the objective. When the type (c) c-a lens is applied, the working distance can be enlarged, which is identical to the radius of the front surface. However, for typical cases, $M_{c-a} < M_{v-a}$, the NA collection is less effective.

When it comes to the field flattening, there are three well-known correction schemes:

1. Utilizing the field lens close to the image or intermediate image;
2. Utilizing the thick meniscus lens with positive Petzval curvature and arbitrary optical power;
3. Petzval's theorem, utilizing positive and negative elements spaced widely apart from

each other.

The first method is typically only used in the very-low-magnification objectives, which can also significantly shift the pupil and realize object-side telecentricity. The second and third methods are widely used in the rear groups of modern microscope objectives. It is also well known that the total field curvature should be understood with a combination of Petzval curvature and astigmatism. According to Petzval's theorem, when the third method is applied, the astigmatism can be corrected by the remote rear lenses. However, when the second method is used, the thick meniscus lens cannot correct astigmatism by itself.

The correction principles for axial chromatic aberration including secondary spectrum are also well known. According to the achromatism condition:

$$\frac{\Phi_1}{v_1}+\frac{\Phi_2}{v_2}=0, \tag{3.2}$$

where Φ_1 and Φ_2 designate the powers of the two thin elements, whereas v_1 and v_2 are their Abbe number, to correct the axial chromatic aberration, the optical power of the two elements should have different signs. Furthermore, the two Abbe numbers should be different. The further their ratio is away from 1, the smaller the individual refractive powers of the two elements are, which can relax the element's sensitivity. The corresponding material pairs are called achromatic material selections. When a third element and the correction of secondary spectrum are further considered, according to the apochromatism condition:

$$\frac{\Phi_1}{v_1}+\frac{\Phi_2}{v_2}+\frac{\Phi_3}{v_3}=0, \frac{P_1\cdot\Phi_1}{v_1}+\frac{P_2\cdot\Phi_2}{v_2}+\frac{P_3\cdot\Phi_3}{v_3}=0, \tag{3.3}$$

where P_1, P_2, P_3 are the relative partial dispersion of the materials (e.g., the relative partial dispersion of the g-line is specified as P_{gF}=(ng-nF)/(nF-nC)), to correct the secondary spectrum, the materials should be selected with identical partial dispersion or forming a large area on the relative partial dispersion diagram shown in Figure 3.3. The corresponding material pairs are called apochromatic material selections.

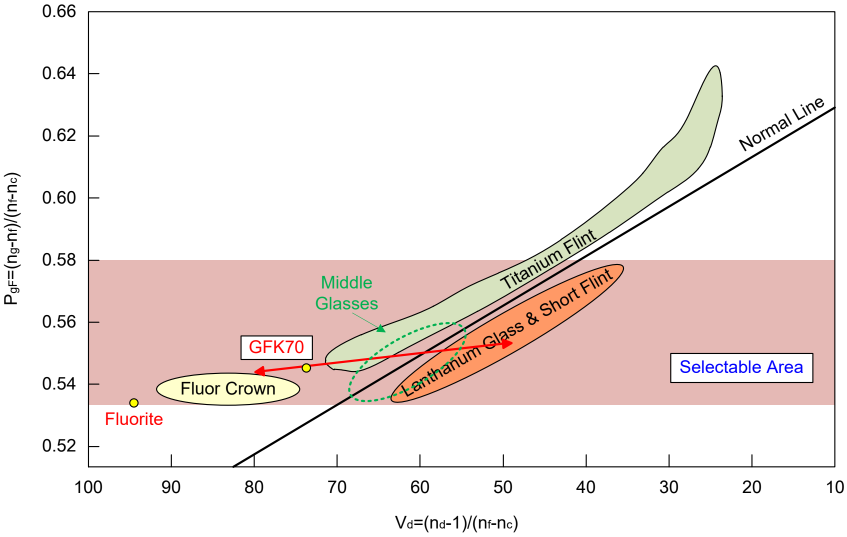

Figure 3.3.: Partial dispersion diagram for g-line and F-line. The normal line is defined by K7 and F2 glasses (Schott convention). In microscope objective design, the materials are often selected from the “Selectable Area” and the “Fluor Crown”, “Middle Glasses” and “Short Flint” have extraordinary functionality for secondary spectrum correction, which will be discussed in Section 6.3.

Based on the strategies of different manufacturers, the lateral color of an objective should be fully corrected or controlled around a fixed value, e.g., 1.5%. Mostly, the rear group plays a key role in the lateral color control. To increase its contribution, Takenaka [13] introduced that thick elements and positive dense flint elements should be used in a comparatively rear part of the objective. This structure is widely used in various systems, but the reason and principles of these two schemes have not been discussed in literature.

In Chapter 6, to realize an entire systematic analysis of lens modules, these well-known design schemes are also discussed. Their functionalities for other aberration correction or application requests addressing are systematically analyzed and compared. They are marked with red color to be differentiated from the new-found lens modules.

4. Objective Database and Classifications

In this chapter, the basic information of the microscope objective database is introduced in Section 4.1. Focusing on the color correction, field flattening, system etendue, working distance, CORR function and parfocal length, new system classifications are proposed in Section 4.2, which are useful for system complexity analysis. By the end of this chapter, an example is given to demonstrate the relationship between the system parameters and system complexity.

4.1 Microscope Objective Database

To extract the lens modules or the building blocks for microscope objective design, the collected systems should be systematically analyzed and compared. An objective database can be built up from the collected patents. 75 patents are excluded from the collection, which are only corrected for UV or IR spectral range, and therefore have different considerations of chromatic aberration correction. It is also notable that typically there are many embodiments included in one patent. When the system database is built up, the maximum etendue objectives with each basic structure are selected. Eventually, from the remaining 373 patents, 484 systems with different structures are built up within Zemax/OpticStudio^{TM} as a database. To realize the excellent resolution, the design of microscope objectives is specified with diffraction-limited performance, at least on the optical axis. Wave aberrations or Strehl number are often used to describe the system performance. In this work, to match the patented performance, the longitudinal aberration curves, which are usually given in the patents, are used as the criterion to construct the systems. Based on these systems, the structural and aberration behaviors of the patented systems can be analyzed, but the performance is sometimes not perfectly diffraction-limited.

The systems can be sorted with their NA and object height as shown in Figure 4.1(a). The general throughput of conventional microscope objectives can be demonstrated by two boundary constant-etendue curves, G=0.0243 mm^2 and G=0.9503 mm^2. More than 90% of the collected objectives, with only 38 exceptions, locate within the area formed by these two curves. Assuming identical intermediate image size of 22 mm, these two G-values represent a 50×/0.40 and a 20×/1.00 objective, respectively. The maximum etendue value of the collected systems is achieved by a 10×/0.90 objective with intermediate image size of 25 mm [37], which is used for virtual slide microscopy. When it comes to the assignees, according to Figure 4.1(b), the four major vendors of microscope objectives: Olympus, Nikon, Leica and Carl Zeiss, hold 85% of all patents, but the Japanese companies patented much more than the German companies. The other two main assignees are American Optical Corporation (AO) and Mitutoyo. AO was the first assignee that patented a series of "clear three group" objectives with infinite conjugate in 1970s, whereas Mitutoyo is the major assignee of long working distance objectives especially for semiconductor industry. A list of the systems in the database is given in Appendix III.

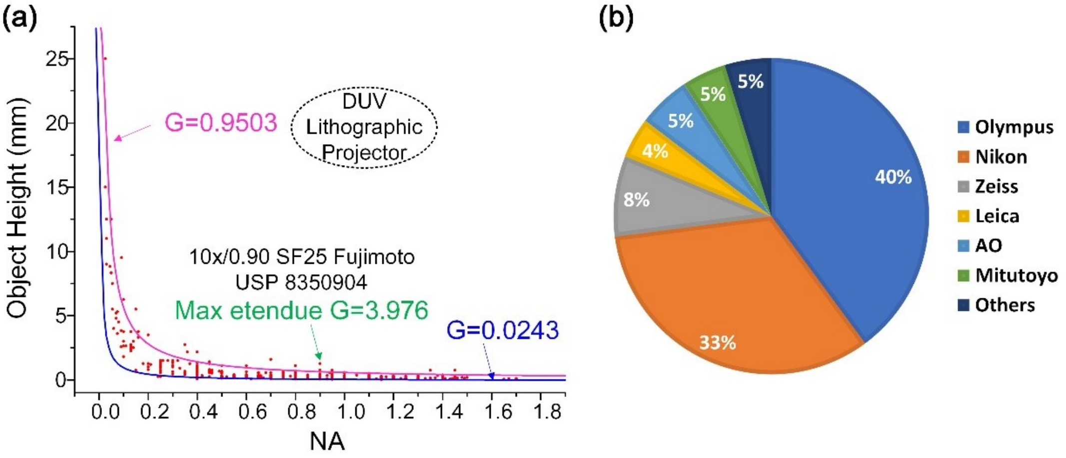

Figure 4.1.: (a) The diagram of collected objective lenses as a function of numerical aperture and field size. The blue and pink curves indicate the boundary G-values (mm^2) of conventional microscope objectives. Position of typical DUV lithographic projectors is plotted as a reference. (b) Share of different assignees in the database.

4.2 Classification of Microscope Objectives

To analyze the objectives and extract the lens modules, the collected objectives should be classified into several classes. Thereby, the structure of individual objective lenses from each class can be compared considering their functionality resulting from aberration correction, application and manufacturing requests. The most conventional classification method is based on the system performance, which mostly focuses on the correction of chromatic aberration and field curvature. Correction of these two most important aberrations can partly indicate the complexity of the objectives. However, the conventional classes are too simple to describe the advanced systems. Thus, new classifications are required. Furthermore, when the microscope objectives are corrected for different NA and field size, namely etendue, the system complexity can be significantly different. It is only possible to analyze the impact of aberrations on the lens modules by combining an etendue classification and a performance classification. The new performance-based classifications are introduced in Section 4.2.1, whereas the etendue-based classification is demonstrated in Section 4.2.2. Other important parameters are discussed in Section 4.2.3.

4.2.1 Performance-based Classification

The traditional quality classes of microscope objectives are defined based on the longitudinal chromatic aberration correction and field flatness, which is briefly demonstrated in Table 4.1. They are quantitatively defined with respect to the DoF, which is given in Equation (2.16).

Table 4.1.: Conventional classification of microscope objectives based on performance.

Field correction		Color correction improved→		
←Improved	None	Achromate	Fluorite	Apochromate
	Plan-	Plan-Ach		
			Plan-Fluor	
				Plan-Apo

- **Achromate**: Red-blue two colors' longitudinal chromatic aberration corrected within 2×DoF. The secondary spectrum is also limited within 1.5×DoF. *Class (a)*
- **Fluorite (Semiapochromate)**: Red-green(yellow)-blue at least three colors' longitudinal chromatic aberration corrected within 2.5×DoF. *Class (b)*
- **Apochromate**: Red-green(yellow)-blue at least three colors' longitudinal chromatic aberration corrected within DoF. Typically, the Apochromate is corrected from g-line to C-line. *Class (c)*
- **Plan**: Best focus position at the field edge deviates from the axial focus position within 2.5×DoF [38].

The higher level of correction is achieved by combining better chromatic and field correction. The Plan-apochromate class typically represents the best performance systems. However, from 1980s, there were an increasing number of objectives corrected for extended spectral range, even reaching IR and UV spectrum. For instance, Carl Zeiss claimed that their APOCHROMATS are fully color-corrected for up to 7 wavelengths from UV through to IR. There is not a standardized class for these systems with superb performance. Different vendors named these advanced features in distinctive way. Therefore, apart from the traditional Ach-/Fluor-/Apo- classification, the wavelength dependence of the objectives should be further carefully analyzed. Furthermore, the classical “Plan” definition is also insufficient to evaluate the field correction. Many systems applied extra complexity to fully correct coma and astigmatism, which must be classified into additional field correction classes.

Color Correction

The corrected spectrum of modern microscope objectives is summarized in Figure 4.2. Beside the conventional three classes: Achromate, Fluorite and Apochromate, four new classes are introduced regarding their spectrum extension in the visible range (VIS), UV and IR:

- **Improved VIS Apochromate**, which extends the corrected spectrum over the full visible range, typically corrects longitudinal chromatic aberration from g-line to A-line. In some special examples, the corrected spectrum can be further extended to h-line approaching NUV and s-line reaching NIR. *Class (d)*
- **IR Superapochromate** extends the corrected spectrum to t-line, which is often required by multiphoton microscopy and IRDIC applications. It is notable that in the Raman microscopy, IR superapochromatic correction from the VIS to SWIR around 2000 nm is also required. *Class (e)*
- **UV Superapochromate** maintains full-spectrum correction from NUV to VIS. It is sometimes well corrected from i-line to C-line, which assures the common focus of UV excitation and visible observation. This is also widely used for semiconductor inspection systems. *Class (f)*

- **UV-IR Superapochromate** is the state-of-the-art chromatic correction class, which can be corrected from i-line to t-line. Only a few objectives can reach this class, and they are used for multiphoton microscopy. *Class (g)*

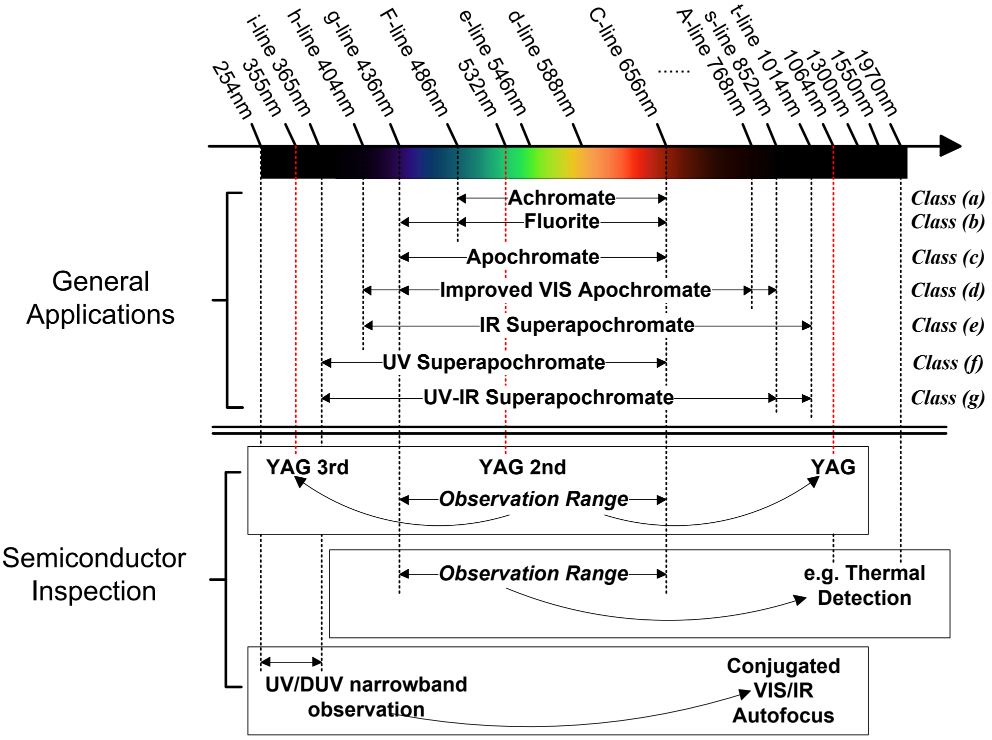

Figure 4.2.: Spectrum of various chromatic correction classes.

When it comes to the semiconductor inspection systems, despite the visible range for observation, correction of specific wavelengths in UV and IR range is often required, instead of a full spectrum correction.

- **YAG laser (1064 nm) and its harmonics** are widely used for semiconductor repairing. To assure the repairing, laser beam is focused onto the observation plane, achromatism of the visible range (including second harmonic 532nm), 1064 nm and/or third harmonic 355nm should be realized.
- **Longer wavelengths in NIR and SWIR, such as 1300, 1550 and 1970 nm**, are often used to test the thermal behavior of high frequency circuits.
- **UV/DUV observation** is mostly used in the modern semiconductor industry instead of the traditional visible observation. Due to the limited choice of materials, which has good transmittance in DUV, this type objectives can only be achromatic corrected for a narrow-band of spectrum. However, they should also be corrected

for a conjugated wavelength in VIS or IR, which is used for autofocusing. Since the correction of this type objective is different from the broadband systems, they are excluded from discussion.

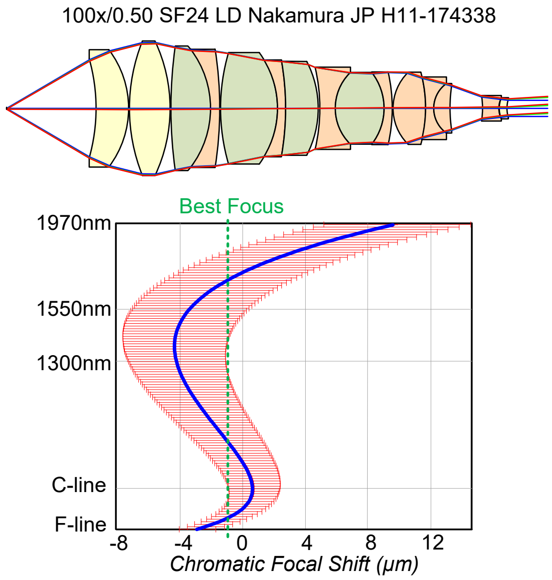

Figure 4.3.: Chromatic focal shift of a 100×/0.50 objective, which is measured in the object space. The blue curve shows the paraxial focal shift, and the red area indicates the DoF of each wavelength.

Considering the applications using YAG laser, since 1064 and 355 nm are not far away from the visible spectrum, the design principle is similar to that of IR/UV Superapochromate systems. Thus, the corresponding systems are classified into *class (e)/(f)*. When it comes to the second case, it is impossible to perfectly correct the longitudinal chromatic aberration for full spectrum from VIS to SWIR. Nevertheless, since the depth of focus of SWIR light is far larger than that of visible light, it is possible to realize the best focus plane within the DoF of both spectra. An example 100×/0.50 objective is shown in Figure 4.3, where the best focus plane can be found within the DoF of F-line thorough to 1800 nm, which means “Apo”. The boundary wavelength 1970 nm is also corrected within 2.5×DoF, which means “Semiapo”. The complexity of this system type is not critical, but the design only works for medium and low NA cases. Concerning its visible correction, these systems are classified into *class (d)*. Longitudinal aberration and chromatic focal shift of seven example systems from these seven color correction classes are compared in Appendix IV to demonstrate their distinctive chromatic performance and complexity.

Field Correction

Conventionally, the field correction classification is only related to the field flatness. Apart from the field curvature correction, in high-performance systems, correction of other field aberrations, especially coma, should also be considered. The new field correction classification consists of the following seven classes shown in Table 4.2.

Owing to the small field, coma and astigmatism in low NA systems are usually not critical, which are well corrected in the Plan objectives *class 2*. However, because the primary transverse coma increases linearly with field size and quadratically with NA, it would be tremendous at the boundary field of high NA systems ($NA \geq 0.50$). Some high NA systems only utilize a small field with corrected field curvature and sagittal coma to fulfill isoplanatism. Although the tangential coma is not well corrected, because of the small field, it is still acceptable (*class 3*).

Table 4.2.: Seven field correction classes of modern microscope objectives.

		Field curvature	**Field aberration**	**NA**	**Etendue**
Non-plan (*Class 1*)		No correction	No correction	Arbitrary	Arbitrary
Plan-	*Class 2*	Corrected	Corrected	Low	Medium/low
	Class 3	Corrected	Not well corrected	High	Medium/low
	Class 4	Corrected	Corrected with vignetting	High	Medium/low
	Class 5	Corrected	Corrected without vignetting	High	Medium/low
	Class 6	Corrected	Corrected with vignetting	High	High
	Class 7	Corrected	Corrected without vignetting	High	High

When it comes to the high NA systems with relatively large field (high magnification system with medium etendue), vignetting is a useful tool to control the field deviation by shrinking the effective NA of the field boundary (*class 4*). Coma can also be well corrected without vignetting, but special lens modules must be introduced, particularly to the rear group, resulting in tremendous complexity (*class 5*). Microscope objectives with extremely high etendue were invented recently for virtual slides application ($G \geq 0.9503\ mm^2$). Utilizing similar intermediate image size (SF20-SF30), the magnification is very low (10×~20×) and the NA is extremely high (dry 0.90-0.95, oil immersion 1.40-1.45). Consequently, with standardized infinity optics, the exit pupil size is 5-10 times larger than that of high magnification high NA systems. Hence in *class 6* systems, lens modules in *class 5* must be utilized, and the vignetting is inevitable. As the state-of-the-art *class 7*, in the high etendue systems, field aberration can also be fully corrected without vignetting. However, the dimension of the objective is enlarged, and/or the standardized infinity optics should be abandoned. The representative systems of these seven classes and their field performance are demonstrated in Appendix V.

As a conclusion, seven color correction classes and seven field correction classes are defined to classify the modern microscope objectives more detailed. As a combination, there are 49 new microscope objective types instead of the 6 conventional types given in Table 4.1. In Appendix III, all the systems are marked with these classes. An overview table with the number of systems that belong to the 49 types is also given.

4.2.2 Etendue-based Classification

According to the NA vs. field plot in Figure 4.1(a), the general behavior of microscope objectives can be seen, but the different complexity of the structures corresponding to different correction level cannot be distinguished. The systems can be further classified into six zones, demonstrated in Figure 4.4:

- **Zone 1:** typical ach/apochromate two-group systems.
- **Zone 2:** typical Plan-ach/apochromate clear-three-group systems.
- **Zone 3:** novel three-group systems with special correction lens modules.
- **Zone 4:** systems with extremely high NA or etendue, which sacrifice other system parameters, such as parfocal length and immersion liquid type.
- **Zone 5:** very low magnification parfocal telecentric systems.
- **Zone 6:** very high magnification systems.

There are three solid boundaries in Figure 4.4: (a) magnification of 4, (b) magnification of 100 and (c) NA of 1.50, which defines Zone 5, Zone 6 and partly defines Zone 4, respectively. Below the boundary (a), nearly all the Zone 5 systems are designed with “PNP” structure to fulfill the requirements of parfocality and telecentric object space. In the Zone 6, only with few TIRF objectives as exceptions, most of the very high magnification systems are designed with long working distance for semiconductor-related or metallurgical applications. Additional complexity should be introduced to control the more severe chromatic aberration resulting from the reduced focal length and increased working distance. The design principles utilized in most of the Zone 6 systems are similar. The boundary condition (c) gives the limit of normal oil immersion, under which circumstance the oil index is typically around 1.515 at d-line. To realize the extremely high NA, special oil must be used. For instance, the oil with d-line index 1.78035 is used by Olympus (100×/1.65-1.70) [39, 40], and 1.80914 is used by Nikon (100×/1.65-1.67) [41, 42].

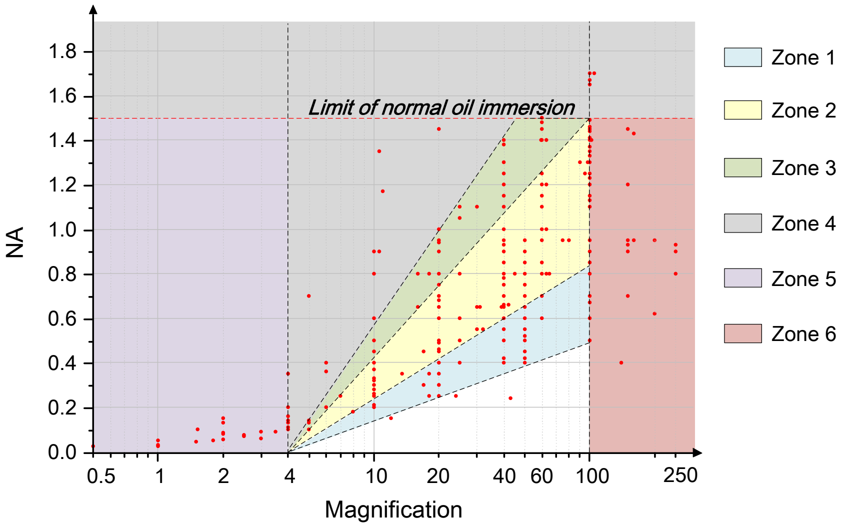

Figure 4.4.: 6-zone classification of microscope objectives based on etendue.

Most of the conventional microscope objectives, which hold an 86% share in the database, are classified into Zone 1, Zone 2 and Zone 3. On the semi-log coordinate in Figure 4.4, these zones are defined by four lines, which can be relatively represented by the etendue. With respect to 22 mm intermediate image diameter, the four lines approximately represent G=0.025 mm^2, G=0.051 mm^2, G=0.086 mm^2, G=0.950 mm^2. In each zone, most of the systems are designed with similar structural complexity from basic two groups to sophisticated three groups. In Zone 4, except the extremely high NA region defined by NA=1.50 boundary, the other systems have extremely large etendue, which are also the exceptional systems in Figure 4.1(a).

4.2.3 Other Important Parameters

Apart from the color correction, field correction and system etendue, there are three other important parameters influence the complexity of objectives. Furthermore, the pupil fixation is also necessary to be considered. It determines the telecentricity and it is also important for microscope systems applying contrast methods.

Working Distance (W.D.)

The W.D. of an optical system mostly depends on its focal length and NA. Since microscope objectives are designed for a standardized optical tube length, the magnification can be considered instead of the focal length. Typically, the W.D. reduces with increasing NA and decreasing focal length, namely increasing magnification. To extend the working distance for easy operation, except the Zone 5 systems and a few exceptions in Zone 4, retrofocus and double-Gauss structure are used in most microscope objectives.

The relative working distance factor κ can be defined as the ratio between the free working distance (W.D.) and the effective focal length of the objective f_{obj}:

$$\kappa = \frac{\mathrm{W.D.}}{f_{\mathrm{obj}}}. \tag{4.1}$$

The normal retrofocus structure can extend the relative working distance factor κ to 0.5, whereas the double-Gauss structure can realize up to 2.0. In the modern objectives, particularly for semiconductor inspection applications, extended W.D. is required with high magnification. To meet this demand, quasi-aplanatic shell lenses are inserted into the front group to form a strong retrofocus structure, but trade-off between extended W.D. and reduced NA for correction must be made [22]. These long working distance retrofocus lenses usually reach $\kappa = 1.0 \sim 8.0$ for medium NA (0.50~0.70) and $\kappa = 0.5 \sim 2.0$ for high NA (0.70-0.90). The state-of-the-art system even realized $\kappa = 13.0$ with magnification 200 and NA=0.62 [43].

The illustration above only considers the dry lenses. However, when it comes to the high NA immersion objectives, there is a different philosophy to control the working distance. Owing to the requests from applications, the front lens of immersion objectives is usually designed with an embedded structure. The smaller component is made of index matching material and has a planar front surface. According to its layout demonstrated in Figure

4.5(a), to reduce the spherical aberration, the cemented surface is designed quasi-concentric to the object plane. Since the thickness of the cover glass is standardized, the W.D. not only depends on the NA and focal length, it is also influenced by the thickness of the small embedded component, which usually has a standard value due to critical manufacturability. Therefore, for fixed NA, the W.D. of the high NA immersion objectives is usually set around a nominal value and thus nearly independent of the magnification. Figure 4.5(b) gives a comparison of the immersion objectives with different NA, with reference to the typical NA=0.90 dry objectives. The selected systems all have *class (c)* color correction and *class 6* field correction. It is also notable that during the recent development, for live cell observation, water dipping objectives were invented. These high NA immersion objectives are designed with long working distance but without the front planar surface. The design principle used in these systems is similar to that utilized in the dry lenses.

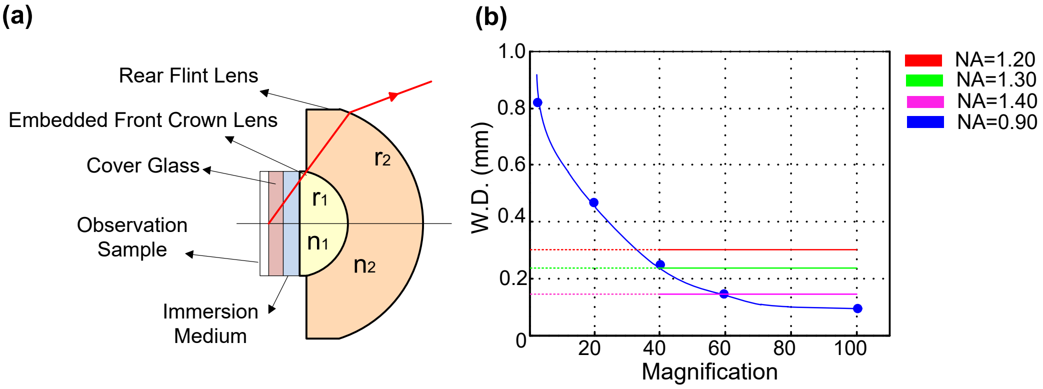

Figure 4.5.: (a) Embedded front lens in high NA immersion objectives. Detailed design principle will be discussed in Section 6.4.1. (b) The W.D. dependence on magnification of dry and oil-immersion objectives. The nominal W.D. of NA=1.20, NA=1.30 and NA=1.40 objectives are 0.3, 0.24, and 0.15 mm, respectively.

The systems with different κ and different W.D. extension strategies can be classified into six classes summarized in Table 4.3:

Table 4.3.: Six classes of working distance of modern microscope objectives.

W.D. Classes	System type	κ
Class I	Normal W.D. microscope objectives	0.0-0.5
Class II	Immersion high NA objectives	-
Class III	Medium NA, long W.D. double-Gauss objectives	0.5-2.0
Class IV	Medium NA, long W.D. retrofocus dry objectives	1.0-8.0 (13.0)
Class V	High NA, long W.D. retrofocus dry objectives	0.5-2.0
Class VI	Long W.D. immersion objectives (water dipping)	0.5-1.0

CORR Function

When designing the microscope objectives, the system correction is based on certain assumptions about the environmental conditions. However, in practical use, these assumptions are often violated because of environmental change or bias use of supplies (e.g., cover glass and immersion liquid). Therefore, a correction collar is often used in the high-performance microscope objectives to adjust these changes with correction (CORR) function. Correction and adjustment should be realized for four most crucial parameters:

1. Thickness of the cover glass (CG),
2. Immersion liquid type,
3. Operation temperature, and
4. Imaging depth for Z-stack scanning (Confocal setup).

The design methods for CORR function will be discussed in Section 6.5 and Appendix IX. Movable groups are usually used. Although the general system complexity is not significantly changed, special optical power distributions are applied, which should be considered during the systematic analysis.

Parfocal Length and Tube Lens Arrangement

The fundamentals of parfocal length definition and tube lens arrangement have been illustrated in Section 2.1. Each vendor selects their own parfocal length and tube lens focal length for their standardized microscope system, which is summarized in Table 4.4:

Table 4.4.: Combinations of parfocal length and tube lens focal length as they are realized by the most common vendors.

Manufacturer	Parfocal length	Tube lens focal length
Carl Zeiss	45 mm	164.5 mm
Leica	45 mm	200 mm
Nikon	60 mm	200 mm
Olympus	45 mm	180 mm
Mitutoyo	95 mm	200 mm
AO	34/45 mm	182 mm

Owing to these different selected values and based on different technology roadmaps, objectives from different manufacturers have distinctive structures under the same magnification and NA. The parfocal length basically determines the amount of space for integrating lens elements. With a longer choice, it is possible to design the objective with more relaxed arrangement of the components. However, as a drawback, increasing the parfocal length would lead to an adverse effect on ergonomics that the viewing port of upright microscopes and the specimen stage position of inverted microscopes are raised in proportion to the increase of parfocal distance [44]. When it comes to the tube lens arrangement, despite the consideration of lateral color correction, selecting a longer focal length, the chief ray angle of the off-axial field can be reduced, thus relaxing correction, but the mechanical dimension of the whole microscope is enlarged. Taking the advantage of the relaxed mechanical dimension and longer focal length, Nikon objectives are usually designed with a less sensitive structure. Furthermore, it is also feasible to design 1× objective and even 0.5× macro-objectives using a special two-part structure [45] for the standardized microscope system.

It is notable that to realize the extended etendue and W.D., all the vendors extended their parfocal length in the recent development. 75 mm parfocal length is often used by Nikon and Olympus. Some 105 mm parfocal systems are patented by Carl Zeiss. To realize the extremely high etendue for virtual slides application, the parfocal lengths of some systems are far beyond the conventional limit, which can reach 300 mm.

Pupil Fixation

In most of the collected patents, information about aperture stop is not given. However, in microscope objectives, selecting an appropriate stop position is crucially significant, because it determines the telecentricity and fixes the pupil position. According to Figure 2.2, a rear physical stop is often placed at the exit of the microscope objectives to filter the stray light, but it is deviated from the real aperture stop position and exit pupil position, which is usually located inside the objective. Therefore, the exit pupil is not accessible for accurate manipulations. It is feasible to shift the pupil position outside the system behind the glasses, but two to three lenses should be added.

In the collected database, most of the collected systems have an exit pupil inside the system, mostly located between the middle and rear group. The criteria of telecentricity is used to fix its position for analysis.

4.3 Complexity Analysis Example

Utilizing the new classifications and considering the important parameters, a practical example is given in this section to illustrate the comparison of the system complexity. 54 oil-immersion microscope objectives with *class 4* and *class 5* field correction are selected from etendue Zone 2 and Zone 3. The number of elements is compared regarding the color correction and system etendue, which is demonstrated in Figure 4.6:

The following conclusions can be drawn:

1. Compared with the Plan-apochromate *class (c)*, the Plan-achromate *class(a)*, which typically has low cost, requires three to four less elements for correction.
2. For medium etendue systems, the difference of element number between Plan-fluorite *class (b)* and Plan-apochromate *class (c)* cannot be clearly distinguished, because the major difference is the material selection but not additional element utilization. Comparing the Plan-apochromate *class (c)* systems with the Plan-superapochromate *class (e)/(g)* systems, to correct the extended spectrum, only the material selection is more sophisticated, but the number of elements is similar.
3. The parfocal length significantly influences the number of elements. Most of the 45 mm parfocal systems utilize 13-15 elements, whereas the Nikon 60 mm parfocal systems utilize 15-18 elements. The 40×/1.40 SF20 system [46] realizes the maximum etendue of standardized parfocal length system as $G=0.385\ mm^2$. The 40×/1.40 SF30 system [47] uses a conventional structure with 25 elements but extends the parfocal distance to 150 mm, and thus it nearly reaches the boundary etendue of conventional system as $G=0.866\ mm^2$.

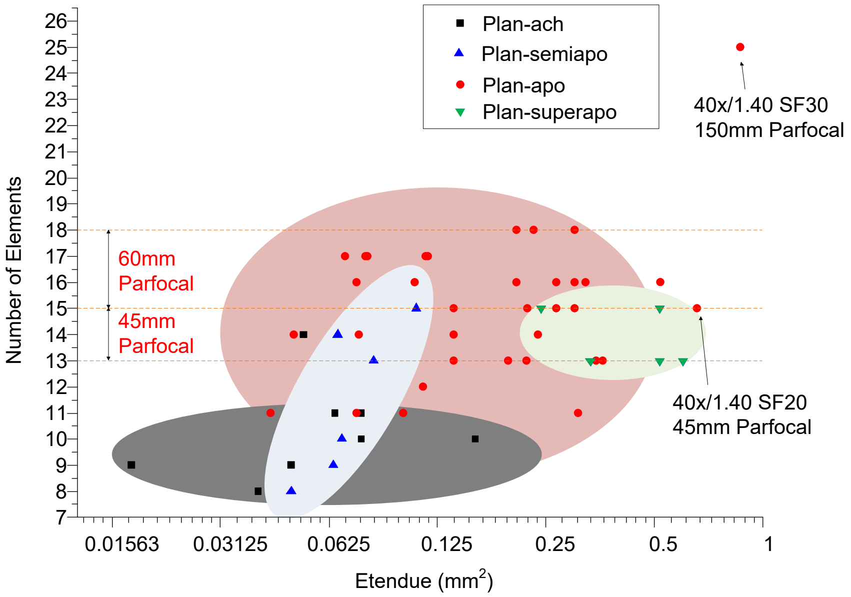

Figure 4.6.: Number of elements vs. etendue of selected oil-immersion objectives.

Thereby, with the systematic classifications of microscope objectives, the design complexity can be better understood. By selecting appropriate systems for comparison, the detailed functionalities of lens modules for aberration correction can be then understood, which are demonstrated in Chapter 6.

5. Addressing Application and Manufacturing Requests

After the application segmentation in 1980s, the development of microscope objectives became strongly application-oriented. Each new application brought with it specific requirements of etendue (NA and magnification), working spectrum, color correction, field correction, working distance and CORR function. According to the new classifications based on these parameters (see Section 4.2), in this chapter, the impacts of application requests on the objective design are first summarized in Section 5.1. Impacts of some common manufacturing requests are then discussed in Section 5.2.

5.1 Impact of Applications

Conventional Inverted Setup vs. Upright Setup

An inverted microscope (IM) is a microscope with its light source and condenser on the top, above the stage, while the objectives are below the stage pointing up. From the 1980s, owing to the interest of cell culture observation, IM became popular in biomedical research. A comparison of the conventional inverted setup and upright setup is shown in Figure 5.1(a)(b). The upright microscope objective images the specimen between the cover slip and slide glass. The thickness of the cover slip is standardized, which is typically 0.17 mm. But the thickness of the slide glass is not standardized and usually varies between 1.2 mm to 1.7 mm. In the IM, the objective images the cell, which floats in the culture medium, through the bottom of the cell culture dish. However, the cell does not perfectly locate at the bottom surface, leaving a variable distance. The bottom thickness of the dish is also not standardized, varying between 0.5 to 1.5 mm. Furthermore, the inverted objectives often work with slide glass or without substrate. Consequently, the conventional inverted microscope objective with NA>0.40 must be designed with correction collar for 0-2 mm CG correction.

Since the correction range is large, the objective must be flexible for a large scale of working distance. Thus, the conventional inverted objectives are designed with relatively long working distance $\kappa = 0.5 \sim 1$, which results in the more challenging correction of longitudinal aberration, spherical aberration and coma. Consequently, the maximum etendue of the IM objectives is limited to G=0.1 mm^2. Figure 5.1(c) gives an overview of the off-the-shelf objectives with long working distance and long CORR range (>0.6 mm) from the major vendors. 20×/0.40, 40×/0.60, 60×/0.70 are the typical magnification and NA combinations.

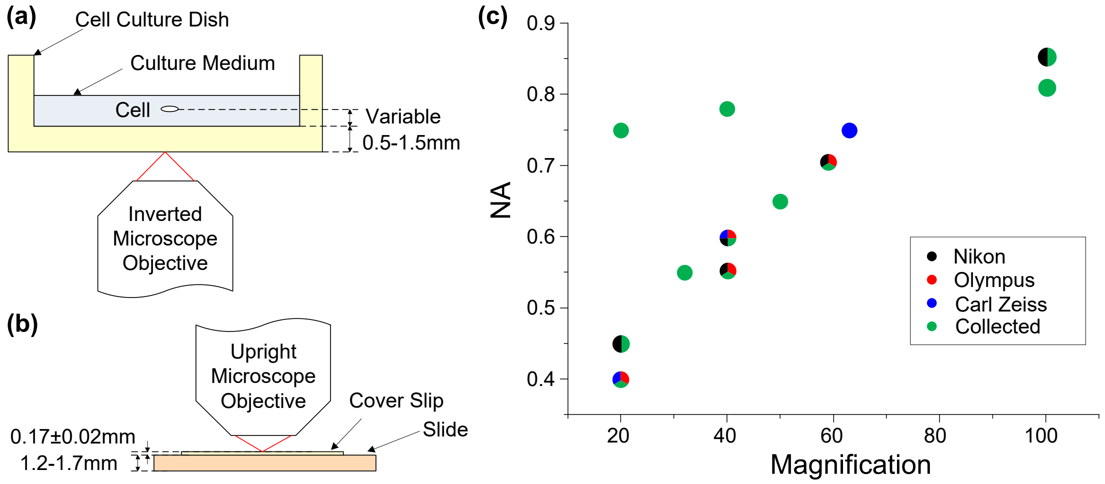

Figure 5.1.: (a) Conventional inverted microscope observation. (b) Conventional upright microscope objective observation. (c) Overview of the off-the-shelf objectives with long working distance and large range CORR from major vendors and the corresponding examples in the database.

Confocal Setup

The use of laser illumination in the 1970s made the confocal imaging realistic for microscopy. In the middle of 1980s, the confocal laser-scanning microscope (CLSM) was invented and the confocal setup was incorporated into the standardized microscope systems used for biomedical applications [48]. Utilizing pinhole filtering, better axial and radial resolution are realized and it is feasible to operate 3D volume imaging with optical sectioning [49, 50].

For optical sectioning, there are three requests for CORR function. First, similar to most common objectives for biomedical confocal imaging, water-immersion objectives with NA larger than 1.10 must be designed with CG correction collar. Second, high NA objectives should also work with silicone oil, glycerin and oil immersion, and advanced objectives were designed with immersion correction. Third, to realize a fast and robust scanning, recently developed objectives were designed with a lightweight simple moving group for depth correction.

When it comes to the impact of confocal setup on the basic properties of microscope objectives, to achieve more efficient 3D reconstruction of the object with high resolution, particularly with the help of post-magnification, objectives with high NA and large observation field are preferred. Furthermore, since laser scanning is used to obtain the image, better field flatness is required. The field aberrations should also be controlled, and the relative illumination at the image edge should be improved with less vignetting. Therefore, advanced objectives are designed with medium etendue and excellent field correction (at least *class 4/5*) for confocal setups.

Fluorescence Microscopy

Most of the current fluorescence microscopes are implemented with reflected light fluorescence setup (epifluorescence), which utilizes the epi-illumination setup consisting of a light source, an excitation mirror to filter the operating wavelength, a dichroic mirror letting the longer wavelength fluorescence pass and an emission filter for further filtering. The epifluorescence setup has a great advantage in analyzing the opaque material with higher fluorescence intensity, and it is possible to be combined with other transmitted light methods. Generally, based on the epi-illumination setup, epifluorescence microscopy has the following six requirements for the objective design:

1. High NA in the object space,
2. Relatively large NA in the image space,
3. High transmittance over a wide spectrum,
4. Favorable chromatic correction over a wide spectrum *class (d)/(f)/(g)*,
5. Favorable field correction *at least class 4*, and
6. Low autofluorescence.

To intensify the fluorescence, the intensity of the excitation illumination light should be enlarged. Therefore, under the epi-illumination setup, the corresponding object space NA is required to be high. The resolution is improved simultaneously for more detailed observation. Furthermore, since the fluorescence emitted from the specimen is typically weak, to increase the brightness of the image for more efficient observation, a larger image space NA is also required. Due to these two effects, the optimal magnification of the objective should be reduced.

When it comes to the system performance, first the specific excitation and emission wavelength for fluorescence significantly change the system requirements regarding working spectrum. For one thing, the working spectrum of popular fluorescent dyes and proteins covers a wide range. For instance, Fura^{-2} for Ca^{2+} detection is excited at 340 and 380 nm in UV; Kaede and PAFP are excited around 400 nm; and CFP, GFP, YFP have their peak excitation wavelengths at 430, 488 and 514 nm, respectively. To assure the high intensity of illumination, the objective lens must have high transmittance over a wide spectrum from UV to VIS. Furthermore, since the peak emission wavelengths of the fluorescent dyes and proteins also cover a wide range from UV to VIS, to realize fluorescent observation for multicolor imaging with multicolored fluorescent tag, the chromatic aberration must be superapochromatic corrected to *class (d)*/*(f)*/*(g)* level. Second, to improve the operability of the microscope and observe large field at the same time, improved field correction is also required, typically as *class 4*. The low autofluorescence is the last requirement in the advanced fluorescence microscopy to further improve the contrast. To reduce the intrinsic autofluorescence generated by the optical elements in the objective lens, optical materials with low autofluorescence should be selected.

Live Cell Observation and Multiphoton Microscopy

In the conventional microscopic observation for biological applications before 1950s, the cells must be stained. The invention of phase contrast microscopy then made it feasible to observe the structure of live cells. However, when the behavior of molecules in the live cells became the major interest, despite the general considerations of fluorescence microscopy, special requirements were involved in the design of live cell and specimen observation apparatus. Moreover, to obtain the 3D image of the live tissues, since it is difficult to use the confocal setup for Z-stack scanning, utilization of multiphoton excitation is becoming popular. This nonlinear microscopy approach also imposed several new requirements on the objective design.

When the fluorescence observation is performed on live cells, the fluorescent substance is used to stain the living specimen. According to the general requirements of fluorescence microscopy, the objectives should be designed with large object space NA, which is also required by live cell observation to detect as much information from the cells at a time. Furthermore, it is also desired to keep a state of live cell behavior in the sight for a longer time observation. Therefore, a wider object field size is required. Consequently, the etendue of the live cell observation objectives should be large.

A special requirement of live cell fluorescence observations is to reduce the cell toxicity. When some stimulus, such as the excitation light, is given to the live specimen, there is the possibility that the stimulus itself adversely affects an active state of the cell, e.g., phototoxicity of UV light. Therefore, IR light is usually used for live cell observation with various new approaches: multiphoton, CARS, SHG, IRDIC and optical tweezers. The IR excitation has three major advantages:

1. Owing to the longer wavelength, the scattering and absorption of IR light in the live specimen is reduced. Consequently, a longer penetration depth can be realized for depth imaging;
2. Less phototoxicity;
3. It is comparably easier to achieve excellent transmittance in IR range.

A series of microscope objectives have been specifically corrected only for IR. Due to the different material selection strategy, they are excluded from the systematic analysis. The other IR objectives, particularly for IRDIC and multiphoton microscopy, are corrected for VIS-IR or UV-IR, corresponding to *class (f)/(g)* color correction level.

It is notable that regarding the environmental condition of the live cell observation, particularly for a special water dipping lens [22], it is necessary to design the objective to be capable of working under both the room temperature 23°C and body temperature 37°C. Typically, the high-performance high etendue systems are designed with correction collar for temperature adjustment [51].

During the multiphoton excitation, a fluorescent object is illuminated with a light beam with wavelengths of integral multiples of an inherent absorption wavelength. Thereby, the resulting excitation is nearly equivalent to that caused by the light with wavelength of the inherent absorption wavelength. Based on this nonlinear phenomenon, the IR light can be used for excitation for deeper penetration and less phototoxicity, and the fluorescence emission is generated as typical UV or VIS excitation with higher efficiency. For instance, serotonin is excited at the wavelength of 260 nm and produces emission at 300-380 nm. It is complicated to design such a UV-capable system. However, utilizing three-photon excitation, it can be exited at 750 nm, thus realizing fluorescence observation in normal system [52].

The multiphoton excitation only occurs in the vicinity of the focal point, and the fluorescence is only emitted from the focal plane. Advantageously, fluorescence in samples is subject to less discoloration, and the confocal setup with confocal pinholes is no longer necessary to realize the depth imaging. However, due to this effect, the design of multiphoton microscope objectives became more challenging. First, to reduce the area of excitation and emission, larger NA is preferred to achieve better resolution. Second, since the excitation (IR) and emission (UV/VIS) with different wavelengths occurred at the same position, the chromatic aberration for wide spectrum from UV to IR must be well corrected, as the *class (f)/(g)*. The objective should also have excellent transmittance through the full spectral range. Third, although the IR excitation light has low scattering, the emission light, which lies within UV and VIS, may become diffused in the specimen. Therefore, to collect the scattered fluorescence without loss, the objective should be designed with large field. Lastly, for a large depth imaging, the working distance should also be comparably enlarged. For different depths, to reduce the spherical aberration induced by the index change of specimen and realize fast auto-scanning, the objective should be designed with a moving group for depth correction.

Total Internal Reflection Fluorescent Microscopy (TIRFM)

TIRFM utilizes total internal reflection (TIR) in a prism or cover glass and thus can be classified as trans-TIRFM (prism- and lightguide-based TIRFM) and cis-TIRFM (through-objective TIRFM), respectively. Only the cis-TIRFM with high NA objectives is considered in this work. To realize TIR at the cover glass, the NA of TIRF objective should be larger than 1.38, which is the typical refractive index of cells. The practical TIRF objectives are usually designed with NA>1.42. Utilizing some special oil, the NA can exceed 1.65, reaching 1.70, but the strong autofluorescence of the oil hampers the image contrast. TIRF objectives utilizing typical Type A oil with NA between 1.45 and 1.49 are favorable.

Different from the requirements of typical high NA objectives for confocal fluorescence microscopy, the TIRF objectives are usually designed with high magnification. When a small area is illuminated, the signal-to-noise ratio can be improved. Another special requirement of TIRF objectives is the CORR function for CG thickness and temperature. Owing to the application principle of TIRF, the excitation laser beam should be perfectly focused onto the front surface of the cover slip. Therefore, when the CG thickness is deviated from the nominal value, the induced spherical aberration must be corrected. Furthermore, immersion oil always suffers from critical index thermal change and thermal expansion. When the TIRF is used under body temperature, the corresponding error should also be corrected.

Virtual Slide Microscopy

Adopting the new digital image sensors with a great number of pixels, the virtual slide microscope gets a wide field of view and high resolving power in observation and became the state-of-the-art research tool for brightfield and fluorescence microscopy. The basic idea of a virtual slide microscope is a combination of the wide field fluorescence observation and confocal Z-stack scanning, but the magnification of the objective is significantly reduced to 10×-20× achieving an object diameter of 1.5-2.5 mm. The NA is further enlarged, reaching 0.90-0.95 for dry lens and 1.35-1.45 for oil-immersion objectives. Thereby, an extreme etendue of microscope objectives is required.

To realize an efficient field scanning, the same as conventional confocal setups, all the field aberrations must be corrected. The objective should also be apochromatic corrected at least for VIS and with excellent transmittance from UV to VIS. However, due to the tremendous etendue, it is challenging to correct both the axial aberrations and the field aberrations. To achieve the *class (c)/(d)* color correction and *class 6/7* field correction, trade-off between vignetting, parfocal length and entire microscope size are usually made. The virtual slide microscope was invented to achieve high scanning speed. However, to operate the Z-stack scanning, the conventional method, which moves the entire objective, would induce vibrations and the speed is low. Introducing special optical elements with zooming effect, such as adaptive elements and Alvarez plate, brings with necessity of pupil arrangement and increases system complexity. Thus, a light weight moving group is usually used in the virtual slide microscope objectives for efficient depth adjustment.

Semiconductor Industrial Applications

From the 1980s, following the flourish of semiconductor industry, a series of microscope objectives were specifically designed for industrial inspection, repairing and fabrication. Except some very low magnification objectives for positioning, the typical semiconductor inspection lenses require large magnification (50×-100×) and high NA without immersion. Moreover, a long working distance is also required for repairing and fabrication. However, it is well known that with an increasing magnification, the chromatic aberration gets more critical and with the increasing working distance the spherical aberration, field curvature, coma and chromatic aberration get more severe [53]. Combining these two effects, trade-off between the NA and working distance should be made, which can be seen from the difference between the W.D. *class IV* and *class V*.

According to the introduction in Section 4.2.1, regarding the operation spectrum, except the DUV objectives, the semiconductor inspection objectives should work for VIS with possible extension to UV or IR, which are mostly based on the wavelengths of YAG laser and its harmonics for laser repairing. Therefore, color correction levels *class (d)/(e)/(f)* are applied. Comparing the semiconductor objectives with biomedical objectives with similar etendue and color correction, the semiconductor systems usually require better field correction. For one thing, to achieve excellent illumination uniformity, the vignetting cannot be accepted. In addition, higher-order field aberrations, including the chromatic variation of coma, can also influence the precise inspection. The *class 5* field correction is usually required for these systems.

The conventional semiconductor objectives were mostly designed without CORR function. However, in the recent two decades, there is an increasing demand for the inspection under glass plates, particularly for the inspection of liquid crystal substrate. The variable thickness of the substrate is typically around 2-5 mm. The corresponding inspection lenses should be designed with large-range CG correction.

Overview of the impacts of the discussed applications on the design of microscope objectives is given in Appendix VI.

5.2 Impact of Manufacturing and Technology

Compared with the impact of applications, the impact of manufacturing and technology requests is more difficult to summarize systematically. Most of the requests originated from the technique roadmaps and process details of the manufacturers, which are typically kept as trade secrets. The most important four aspects are considered in this work:

1. Manufacturing accuracy of the optical elements,
2. Element mounting and air gaps alignment,
3. Dimensional restriction, and
4. Stray light control.

Two examples are used in this section to illustrate the consideration 1&2 and 3&4, respectively.

Example I

Figure 5.2 shows three different front group structures of high magnification oil-immersion objectives from practical patented systems.

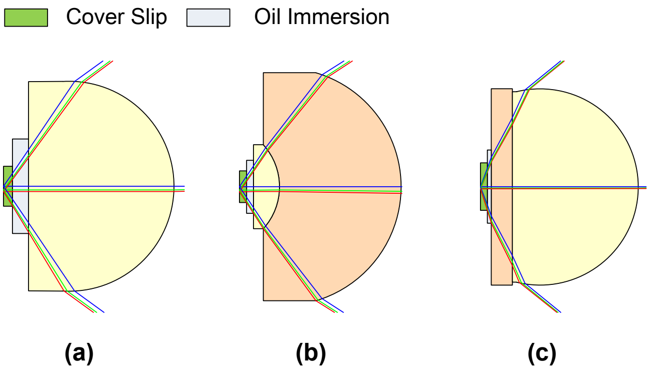

Figure 5.2.: Front groups of high magnification oil-immersion microscope objectives. (a) 100×/1.25 Shi [54] (b) 100×/1.25 Shoemaker [55] (c) 160×/1.43 Bauer [56].

The front group (a) utilized a simple hemisphere made of crown glass with matched refractive index to the immersion oil. The front group (b) has the most popular structure, utilizing an embedded small crown lens with matched index, which is cemented with a meniscus flint lens with strong power. The front group (c) is based on the new technique "optical contact bonding". The strong positive crown lens is designed as a hyper-hemisphere and bonded to a plane plate.

Considering the manufacturing accuracy of the optical elements, in the popular front group (b), although the embedded lens has great advantage in field curvature correction and spherical aberration restraint, it is difficult to produce due to the small clear aperture (~1 mm). "Ball technology" is usually used for the production, but the cost is relatively high. Therefore, for the cost-driven systems, the front lens is designed as a single lens. However, for index matching, the lens material should have similar refractive index as the immersion liquid, which is typically low. If the refractive index of the lens is not large enough, to achieve high NA, the shape of the lens tends to be hyper-hemispherical, which cannot be mounted to the leading edge of the objective. The front group (a) nearly reaches the maximum NA, which can be achieve by single hemispherical lens with d-line refractive index around 1.52 (type A oil matched).

In the recent super-resolution localization microscopy, owing to the strong illumination intensity at the front group, the cementing surface in the (b) type front group is vulnerable. However, if a single lens is used, the maximum NA cannot fulfill the required strong excitation. Utilizing the front group (c), the NA can be further enlarged with the hyper-hemisphere, and the optical contact bonding is not sensitive to the strong UV illumination. Furthermore, the mounting of the front group can be fixed at the edge of the thick plane plate, thus assuring the feasibility of system assembly. The only risk is the robustness of the "optical contact bonding" technique.

According to this comparison, to determine the shape of the front group, all three design concepts are involved: the functionality in aberration correction determines the basic shape; the application request fixes the boundary condition; and the final trade-off is associated with the consideration of manufacturing and technology.

Example II

Figure 5.3 gives a comparison of two 60× TIRF objectives with different parfocal lengths. Both systems have *class (c)* color correction and *class 4* field correction.

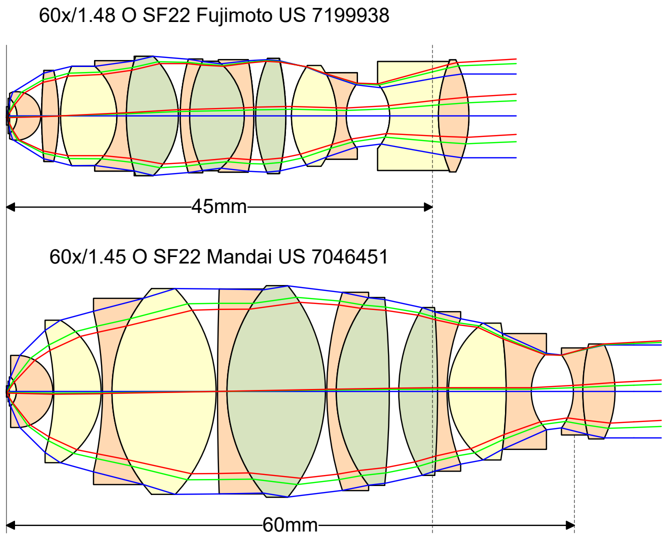

Figure 5.3.: Layouts of a 45 mm parfocal and a 60 mm parfocal 60× oil-immersion TIRF objectives from Olympus [57] and Nikon [58].

The parfocal length determines the mechanical dimension to fill lenses. The 60×/1.48 45 mm parfocal objective from Olympus uses two cemented triplets in the middle group, whereas the 60×/1.45 60 mm parfocal objective from Nikon utilizes four doublets. These two setups have similar functionalities in spherical and chromatic aberration correction, but the triplet setup can save space.

The selection of cemented doublets or triplets also highly depends on the manufacturers' coating technique. Due to the strong veiling glare generated by the air-glass interface, if excellent anti-reflection cannot be realized by the coating, the air-glass interface with strong curvature should be avoided. Consequently, except for the functionality of aberration correction, the cemented triplets utilized in the high-performance objectives are typically designed with stronger inner cemented surfaces and flatter outer surfaces. On the contrary, if the veiling glare can be controlled by coating, utilization of more cemented doublets can introduce additional degrees of freedom for correction, which is advantageous in relaxing the system sensitivity.

6. Design Principles and Lens Modules

In this chapter, the systematic analysis results are introduced. Overview of aberrations and their correction strategies are illustrated in Section 6.1. For the systems from different zones with different aberration correction strategies, the corresponding optical power distribution methods are discussed in Section 6.2. As the most important aspect of color correction, the general material selection strategies are demonstrated in Section 6.3. Finally, the detailed lens modules in the common three-group objectives are systematically summarized in Section 6.4. Special structures for CORR function are briefly introduced in Section 6.5 with the detailed discussion given in Appendix IX.

6.1 Aberration Correction Strategies

The five monochromatic and two primary chromatic aberrations as well as the higher-order spherical aberration and spherochromatism can be compared in terms of their distinctive correction strategies. The aberrations correction in Zone 1-4 common systems is first considered, in which the distortion is not critical due to the small field. The special aberration correction strategies used in the Zone 5/6 systems will be discussed together with their optical power distributions in Section 6.2.

Before the invention of Plan-objectives, the general aberration correction strategy has been well described [59] and classified into two basic types:

1. Spherical aberration, coma and axial chromatic aberration should be corrected at the source, where they are generated;
2. Astigmatism and lateral chromatic aberration should be compensated by remote lens groups, e.g., a remote rear group, the eyepiece or the tube lens.

After Boegehold created the Plan-objective with a thick meniscus lens as the rear group [60], the correction strategy of the field curvature also belongs to the second type.

However, when the system etendue increases, particularly due to the high NA, it is no longer feasible to correct the tremendous spherical aberration and axial chromatic aberration within a single element or single lens group. The residual errors should also be compensated by different lens groups. Moreover, due to the increasing field, the coma should be corrected by compensation as well. Another specific effect induced by the high NA and large field is the large higher-order contribution, but its correction strategy for spherical aberration and coma are different. The higher-order spherical aberration is inevitable when the NA is larger than approximately 0.5. To correct the full-order spherical aberration, the higher-order contribution should compensate the lower order contribution. When it comes to the coma, on the contrary, its higher-order contribution should by restrained at the source, whereas the primary contribution is compensated by different groups [61]. This is realized by the appropriate selection of a rear group structure, where the chief ray height is large, thus tending to generate higher-order coma. Table 6.1 presents a comparison of five representative objectives belonging to the Zone 1 two-group system, Zone 2 double-Gauss type system, Zone 2 clear-three-group system, Zone 3 novel three-group objective and Zone 4 extremely high etendue system, respectively. The group contributions of full-order spherical aberration, primary spherical aberration, coma, astigmatism, field curvature, axial chromatic aberration (ACA) and lateral color (LCA) are demonstrated with their aberration coefficients, which are calculated in the image space.

The correction strategy of the **spherical aberration** is the most complicated, which can be classified into three types:

1. The middle group compensates nearly all of the spherical aberration introduced by the front group. System (a)/(d);
2. The middle group and rear group correct the spherical aberration together. System (b)/(c);
3. The rear group corrects most of the spherical aberration. System (e).

Concerning the **higher-order behavior**, in the Zone 1/2 systems (a) and (b), due to the relatively small NA, the primary contribution dominates the spherical aberration. In the Zone 2 objectives with high NA, such as the system (c), although a larger higher-order spherical aberration is introduced by the large aperture, it is compensated between the middle and rear groups, which is identical to the primary behavior. When it comes to the high etendue systems, the higher-order contribution should be used to correct the high aperture, particularly to restrain the zonal error. Thus, the full-order compensation is distinctive to the primary behavior, which can be seen from system (d) and (e).

Table 6.1.: Representative objectives from each etendue zone with comparable correction strategy.

Objective system	Spherical aberration	Field and chromatic aberrations
(a) Zone 1 two-group 40×/0.65 SF18 Uetake USP 3623792 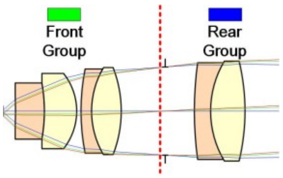	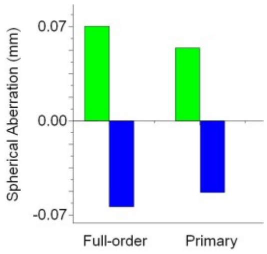	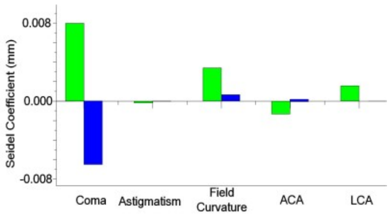
(b) Zone 1/2 double-Gauss 20×/0.40 SF31 Matsubara USP 3925910 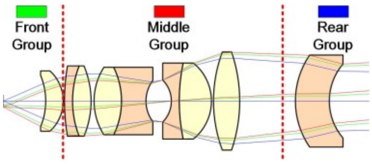	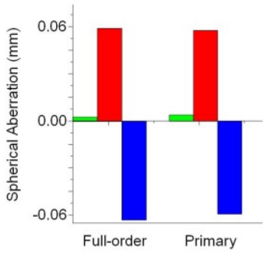	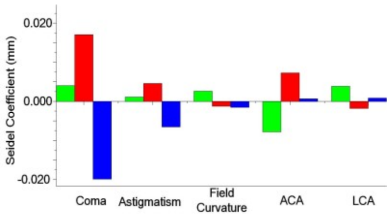
(c) Zone 2 clear-three-group 100×/1.30 O SF12 Shoemaker USP 3700311 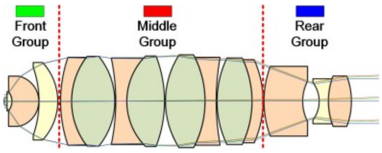	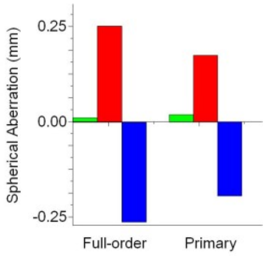	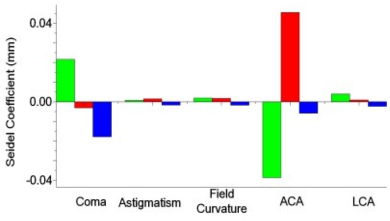
(d) Zone 3 novel three-group 40×/1.20 W SF23 Okuyama USP 2003-0043473 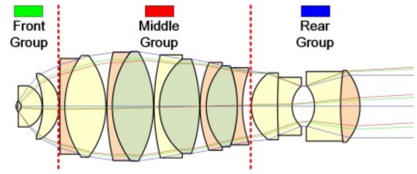	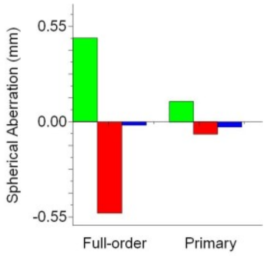	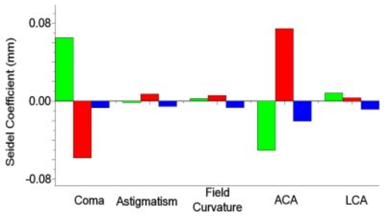
(e) Zone 4 extremely high etendue 10×/0.90 SF25 Fujimoto USP 8350904 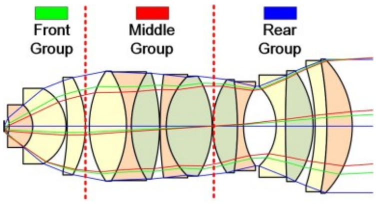	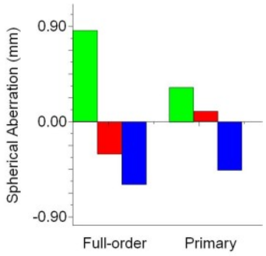	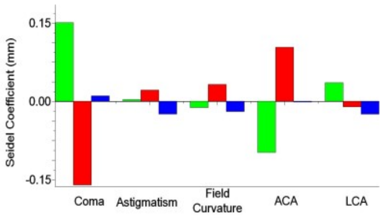

The chromatic aberrations are calculated from F-line to C-line.

There are also various coma correction strategies, which can be basically classified as two types: correction in the rear group and correction in the middle group. When the system etendue is relatively small (Zone 1-2), given that the chief ray height at the rear group is large, it is feasible to compensate the coma with a lens group with strong optical power, particularly with thick meniscus lenses, which is also beneficial to field curvature correction. This compensation behavior can be found in systems (a), (b) and (c). However, when the etendue increases, the exit pupil size is enlarged, resulting in the large coma ray height in the rear group. To avoid the tremendous coma introduced by the asymmetric coma rays, especially to vanish the higher-order contribution, one method is to introduce vignetting to reduce the off-axial effective NA by cutting off the coma rays. Another method for complete coma correction is to design the rear group with relatively small optical power and quasi-symmetric structure. Due to the high NA, although the chief ray height is low in the middle group, it can still generate a significant contribution for coma compensation. The systems (d) and (e) use both vignetting and quasi-symmetric rear group to restrain coma.

According to Table 6.1, the **astigmatism** is not difficult to correct in microscope objectives. It is slightly introduced by the front and middle groups and compensated by the rear group.

In the conventional microscope objectives, to achieve the large magnification, the front and middle groups are designed with strong positive optical power, resulting in a negative Petzval curvature. To compensate this **field curvature**, one method based on Petzval's theorem is to use a remote negative lens group for compensation. Boegehold introduced another method, which utilizes thick meniscus lens with appropriate curvatures to generate a positive Petzval curvature (negative Seidel contribution) with arbitrary optical power. In modern microscope objectives, both methods are utilized to generate a rear group for field curvature compensation. But there are two exceptions. First, in the double-Gauss structure, such as system (b), the field curvature is controlled by its symmetric thick meniscus structure. Second, the embedded front lens used in immersion objectives can also generate significant positive Petzval curvature.

In almost all the systems, the correction strategies of the **axial chromatic aberration** are the same. The front group always introduces a certain amount of axial chromatic aberration, which must be corrected by the middle group. In the conventional systems, the rear group is nearly free of axial chromatic aberration. But when the thick lenses are used in the rear group, particularly containing high dispersive dens flint glasses with large marginal ray height, the rear group can also contribute to axial chromatic correction.

In the standardized microscope systems, different vendors have different strategies to correct the **lateral color**. System (a) and (b) are finite-corrected systems, in which the lateral color should be compensated by the eyepiece. Therefore, a significant residual lateral color can be seen. The systems (c)/(d)/(e) are infinite-corrected systems from AO, Nikon and Olympus, respectively. All the three vendors fully correct the lateral color in both the objective and tube lens, which is mostly realized by a great compensation effect in the rear group. Leica and Zeiss leave a certain amount of lateral color in the objective and compensate it in the tube lens. Under this circumstance, the rear group is utilized to control the lateral color to the standardized value instead of eliminating it.

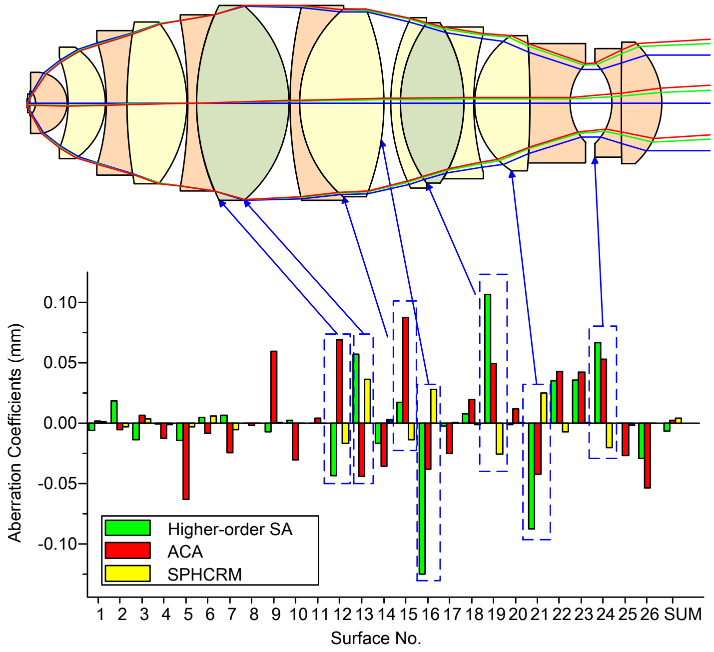

Figure 6.1.: Surface contribution of higher-order spherical aberration, axial chromatic aberration (F-line to C-line) and spherochromatism (F-line to C-line) of the 55.9×/1.40 oil-immersion objective [62] with perfect spherochromatism correction.

When it comes to the spherochromatism correction strategy, it can be understood by an induced effect. Generally, the significant spherochromatism contribution comes together with a large contribution of higher-order spherical aberration (SA) and axial chromatic aberration (ACA), which can be seen from the 55.9×/1.40 oil-immersion objective [62] with perfect spherochromatism correction in Figure 6.1. The spherochromatism is mostly corrected in the middle and rear groups by lens modules with extraordinary higher-order aberration behaviors.

Based on the structural behaviors and the aberration correction strategies, the functionality of the two or three groups in Zone 1-4 systems can be summarized:

- **The front group**, with great positive optical power, consists of several quasi-aplanatic meniscus lenses. It helps the system collect a large aperture angle. However, since the aplanatic condition cannot be perfectly fulfilled in practical systems, there is usually large residual spherical aberration and coma. Field curvature, axial chromatic aberration, lateral color and slight astigmatism are also introduced by the front group.
- **The middle group** (rear group in the two-group), which is composed of several cemented doublets and triplets, provides great contribution to spherical aberration, coma and axial chromatic aberration. Spherochromatism can be corrected by extraordinary higher-order effects. However, due to its strong positive power, it always generates a significant negative Petzval curvature.
- **The rear group** is usually designed with negative optical power or weak optical power for field curvature correction. Thick meniscus lenses are often used with possible quasi-symmetric structure to flatten the field for several colors. The residual astigmatism can also be corrected by this structure. In the low etendue systems, it often contributes to coma correction, while it reduces the coma contribution and turns to spherical aberration correction in the high etendue systems. With appropriate selection of materials, the rear group also corrects or controls the lateral color.

6.2 Optical Power Distributions

Among the six zones of the microscope objective classification based on etendue, the optical power distribution has four basic types:

1. Double-Gauss objectives in Zone 1 and Zone 2. (medium/low NA, medium/low magnification)
2. Zone 1-4: basic optical power distribution with a positive front group, a positive middle group and a negative rear group, forming a "PPN" structure as an overall retrofocus system. According to the relative marginal ray heights in each group, it can be further classified. The optical power of the middle and rear group can be fine adjusted for special correction strategy or application requests. (medium/high NA, medium/high magnification)
3. Zone 5: very-low-magnification objectives (low NA) with a positive front group, a negative middle group and a positive rear group, forming a "PNP" structure.
4. Zone 6: very-high-magnification long working distance objectives (high NA) having a "PPN" retrofocus structure with stronger retrofocus factor. Special subgroups are inserted between the middle and rear group.

The correction principle of the double-Gauss system is well known, which is adopted from the classical photographic objective design. The coma is well controlled by the quasi-symmetric structure and the field curvature is corrected by the two thick meniscus cemented lenses. But this structure typically cannot correct the spherical aberration introduced by NA>0.5. Therefore, it can only be used to extend the working distance for the low NA systems with low/medium etendue, which are found in Zone 1/2.

The optical power distribution of most modern Zone 1-4 systems can be generally understood as the "PPN" retrofocus structure shown in Figure 6.2, which is widely used for the working distance extension. The retrofocus system is conventionally characterized by a ratio between the working distance and effective focal length. However, as introduced in Section 4.2.3, the working distance of microscope objectives does not only depend on the optical structure, but it is also significantly influenced by the environmental condition and application requests. Therefore, a retrofocus factor:

$$r = \frac{h_{\text{exit}}}{h_{\text{max}}} \tag{6.1}$$

is utilized as a measure to quantitatively classify the various practical retrofocus-like optical power distributions, where h_{exit} is the marginal ray height of the exit ray bundle and $h_{\max}$ is the maximum marginal ray height in the middle part of the objective.

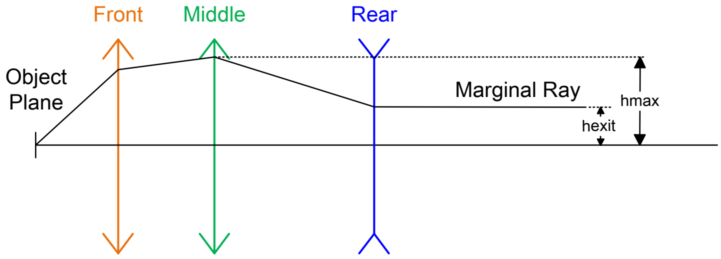

Figure 6.2.: “PPN” retrofocus structure of most Zone 1-4 microscope objectives.

The majority of the collected systems have a “PPN” structure with the retrofocus factor $r = 0.25{\sim}0.80$. To further extend the working distance, the retrofocus factor should be reduced. The PPN objectives with retrofocus factor below 0.25 are named as “PPN strong retrofocus” to show the extraordinary retrofocus effect. With increasing etendue, the h_{exit} is extended and can even be larger than the $h_{\max}$. Although this system may not have the retrofocus effect, they can still be characterized by the retrofocus factor larger than 0.8. According to the retrofocus factor and application requests, the various power distributions of Zone 1-4 systems can be classified into the seven types in Table 6.2.

The type (a) PPN is the most commonly used power distribution in the microscope objectives with medium and high magnifications. The positive middle group mainly corrects the axial chromatic aberration introduced by the front group, but generates large residual spherical aberration, which should be compensated by the negative rear group with large marginal ray height. The negative power of the rear group is also beneficial to the field curvature compensation. Furthermore, given that the chief ray height in the rear group is high, associated with the large marginal ray height and large optical power, the rear group also contributes to coma correction.

The type (b) PPN strong retrofocus is usually used for high magnification objectives with long working distance. According to the retrofocus principle, to enlarge the working distance, the rear group should be designed with great negative power and low marginal ray height, while the middle and front groups have strong positive power and large marginal ray heights. Consequently, the rear group typically contributes only a small amount of

Table 6.2.: Representative objectives belonging to seven types of optical power distributions.

Power distribution type	Example system	Retrofocus factor
(a) "PPN" 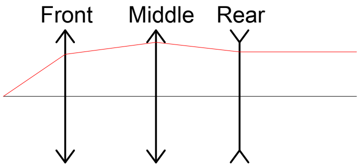	100×/1.25 O SF12 Shoemaker USP 3700311 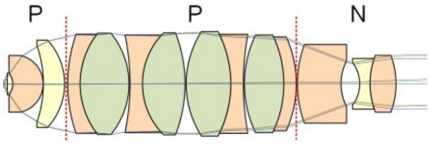	0.25-0.8
(b) "PPN strong retrofocus" 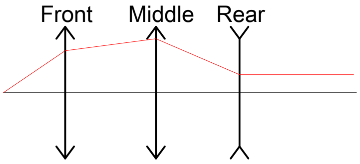	100×/0.90 LD SF25 Hiraga JP 2000-241710 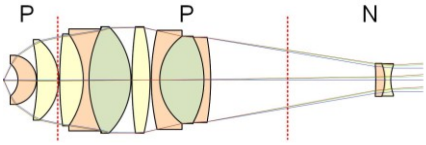	<0.25
(c) "PP(NP)" 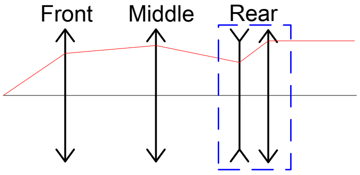	10×/0.90 SF25 Fujimoto USP 8350904 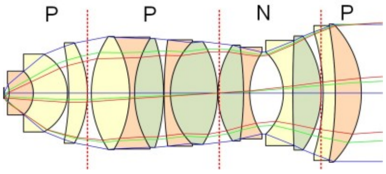	>0.8
(d) "P(PN)0" 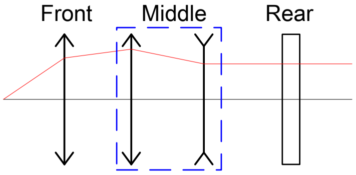	100×/1.40 O SF22 Konishi USP 5739957 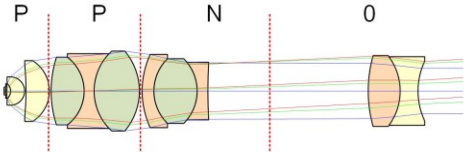	Typically, 0.5-0.8
(e) "P(P0)N" 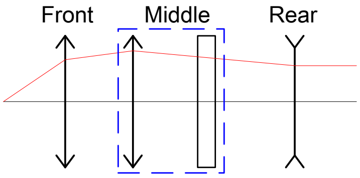	40×/1.20 W SF23 Okuyama USP 2003-0043473 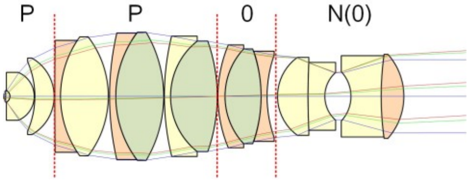	Corresponding to (a)(b)(c)(d)
(f) "(P0)PN" 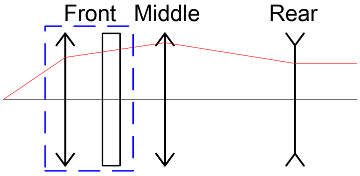	20×/0.90 W SF18 Nobis USP 9696536 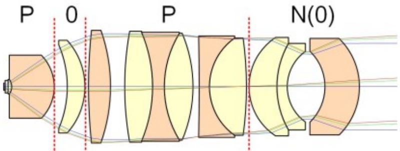	Corresponding to (a)(b)(c)(d)
(g) "P(P0P)N" 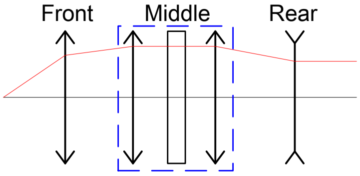	60×/0.70 LD SF18 Shimizu USP 4666256 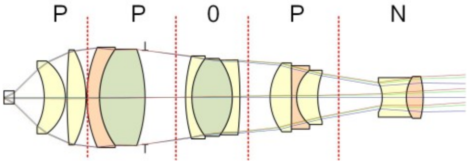	Corresponding to (a)(b)(c)(d)

spherical aberration and coma compensation. Due to its negative power and special material selection, it still has the functionality for field curvature and lateral color correction. However, since the rear group does not compensate spherical aberration and coma, the complexity of the middle group typically increases to correct these two aberrations.

If the optical power of the entire rear group is considered, the general power distribution of the type (c) is also PPN. However, the h_{exit} is usually larger than the h_{max}. The rear group is often designed with weak negative power and quasi-symmetric structure, which consists of a negative sub-group and another positive subgroup forming the magnification of the rear group larger than 1. This structure is helpful in fulfilling the conditions for field curvature correction and avoiding generation of higher-order coma. Owing to the large marginal ray height, although the overall power is small, this type rear group has large contribution to spherical aberration correction.

Type (d) adopts a similar idea to type (c) by designing the rear group with weak negative power (marked as “0” in Table 6.2). To realize this power distribution, the middle group should have a strong positive subgroup and another strong negative subgroup. The afocal rear group can be designed nearly free of spherical aberration. Since the marginal ray height is large, if a single or cemented meniscus lens is used, it can also contribute significantly to coma compensation. If a quasi-symmetric structure is utilized, the rear group can be designed free of coma, thus leaving a great degree of freedom to compensate the field curvature and lateral color.

Type (e) through (g) are applied to the microscope objectives with CORR functions. As an important requirement of the CORR objectives, when movable lens groups are used, the system’s overall focal length cannot be significantly changed, and the chromatic correction cannot be violated during the moving process. Consequently, the movable group is usually designed to be nearly afocal and free of axial chromatic aberration. To correct the spherical aberration, it is typically put in the front or middle group with large marginal ray height. In the type (e) system, which is often used by Nikon, in order to adjust the CG thickness, a weak power cemented triplet, which well corrects the axial chromatic aberration, is inserted between the middle and rear group. The triplet is very sensitive to spherical aberration. When it comes to the type (f) example, the movable meniscus lens between the front and the middle group is designed with weak power to realize the depth adjustment for automatic Z-stack scanning. The element is made of glass with low dispersion to avoid hampering the chromatic correction. The type (g) example utilizes an afocal movable cemented triplet with low dispersion in the center of the middle group. Compared with type (e) and type (f), the element is less sensitive to spherical aberration, but has a wider range of movement, which can correct the environmental change with a larger range. Notably, these special optical power distributions are only fine adjustments within one individual group, whereas the overall power distribution like type (a)-(d) can be applied depending on the system NA and magnification. For instance, the type (e) and (f) examples have general distribution like type (d), while the type (g) example is similar to type (b).

The very-low-magnification Zone 5 is defined by a magnification below 4×. To fulfill the requirements of telecentric object space and parfocality, nearly all the systems within this zone are designed with the "PNP" power distribution shown in Figure 6.3. The middle and rear group form a typical telephoto structure. The additional front group plays the role of a field lens, which does not affect the telephoto structure but significantly shifts the pupil for telecentricity and corrects the field curvature.

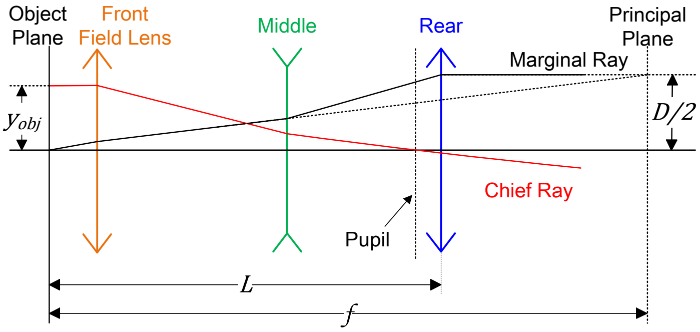

Figure 6.3.: "PNP" telephoto structure of Zone 5 very-low-magnification microscope objectives.

Conventionally, the telephoto system can be characterized by the telephoto ratio:

$$t = \frac{L}{f}, \tag{6.2}$$

where L is the overall length of the system and f is the effective focal length. In photographic systems, it typically lies between 0.6 and 0.9 [24].

In the microscope objectives, the overall length is limited by the parfocal length. Assuming the microscope objectives are corrected for infinite-conjugate with 200 mm tube lens, the effective focal lengths of 1×, 2×, 3× objectives are 200, 100 and 66.7 mm, respectively. Telephoto ratios of 0.225, 0.45, 0.675 and 0.3, 0.6, 0.9 are required to match 45 mm (Leica) and 60 mm (Nikon) parfocal length, respectively. It is self-evident that it is relatively simple to design 2× and 3× objectives, because the telephoto ratios match the typical values. Although the field lens is helpful to reduce the telephoto ratio, it is nearly impossible to reach a value below 0.3, namely 1× objectives, with sufficient W.D. Based on the telephoto structure, despite the aberration correction burden, the maximum feasible NA is limited by the standardized thread diameter D_{Thread}. The diameter D of the exit marginal ray bundle should be smaller than the thread diameter:

$$NA < \frac{D_{\mathrm{Thread}}}{2f} = M\,\frac{D_{\mathrm{Thread}}}{2f_{\mathrm{tube}}}. \tag{6.3}$$

Under the Royal Microscopical Society standard thread diameter of 20.32 mm with 200 mm tube lens, the maximum NA of a 1× objective is 0.05. To extend the feasible NA and relax the optical design, manufacturers selected larger thread diameters, e.g., 25 mm by Nikon and 27 mm by Carl Zeiss.

The aberration behavior of the Zone 5 system is field dominant, which is distinct from the aperture-dominant Zone 1-4 and Zone 6 systems. In the conventional photographic telephoto systems, to achieve quasi-telecentric object space, the aperture stop should be located behind the rear group. The external pupil introduces critical distortion and large pupil aberration, which should be avoided in microscope objectives, particularly for uniform illumination under epi-illumination setups. Furthermore, when the telephoto ratio reduces, the lateral color and field curvature become critical. Combining these two effects, the front field lens is used to compensate the field curvature and shift the pupil for distortion correction. Thick meniscus lenses are also utilized in the front and middle group to correct field curvature. The overall “PNP” structure also fulfills Petzval’s theorem for better field curvature correction. When it comes to the lateral color, to correct or control it, achromatic glass pairs and dense flint glasses are used in both the front and rear groups.

Apart from the telephoto ratio, the structure of the Zone 5 systems also depends on a symmetry factor:

$$s = \frac{D}{2y_{\mathrm{obj}}} = \frac{2f_{\mathrm{tube}} \cdot NA}{D_{\mathrm{img}}}, \tag{6.4}$$

where D_{img} is the intermediate image size (SF). Table 6.3 shows three representative "PNP" objectives with low t/low s, high t/high s and high t/medium s, respectively.

Table 6.3.: Representative Zone 5 systems with different telephoto ratios and symmetry factors.

System Parameters	System Layout	Telephoto Ratio *t*	Symmetry Factor *s*
1×/0.03 SF25 Yamaguchi Nikon JP 2009-294518 60mm parfocal length	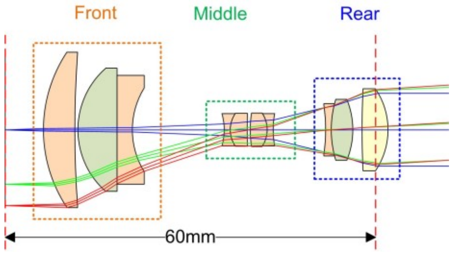	0.30	0.48
2×/0.10 SF25 Otaki Nikon USP 6128128 60mm parfocal length	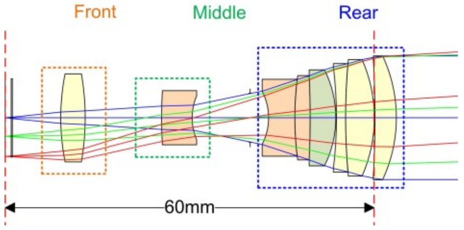	0.60	1.60
3×/0.06 SF24 Klein Leica USP 3176583 45mm parfocal length	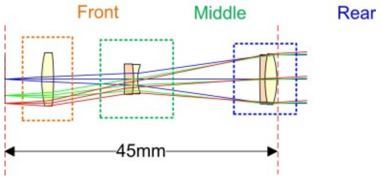	0.675	1.00

When $s = 1$ the general geometrical structure of the "PNP" is nearly symmetric. Thus, both the front and rear groups can be designed rather simple. When $s > 1$, the axial correction is dominant. Hence, the rear group is designed with complicated structure for spherical aberration correction. Typically, special materials are used in the rear group for lateral color correction. When $s < 1$, the field ray bundles are significantly separated at the front group. Therefore, dense flint glasses and achromatic glass pairs are used in the front group with strong bent meniscus lenses for better pupil shift, field curvature correction and lateral color compensation.

Except for two systems designed for TIRFM, the other 18 collected Zone 6 objectives are designed for semiconductor inspection with long W.D. (*Class IV/V*). All the systems have "PPN strong retrofocus" power distribution. Compared with the Zone 1-4 systems, with the increased magnification, the focal length of the system reduces. Thus, the axial chromatic aberration becomes more critical. Moreover, due to the requirement of long W.D., to further reduce the retrofocus factor, the optical power of the negative rear group should be enlarged, while the positive front groups should have less power. The axial chromatic aberration becomes excessive in proportion to the increase of focal length of the positive subgroup [63]. Because of the enlarged diameter of the positive subgroup, the spherical aberration, field curvature and coma also become more severe under high NA [53]. Consequently, compared with the Zone 1-4 systems, the Zone 6 systems are designed with more compound rear groups shown in Figure 6.4, which consists of a negative front subgroup, a positive middle subgroup and a negative rear subgroup with strong power, which steadily narrows the ray bundle and significantly corrects the chromatic aberration.

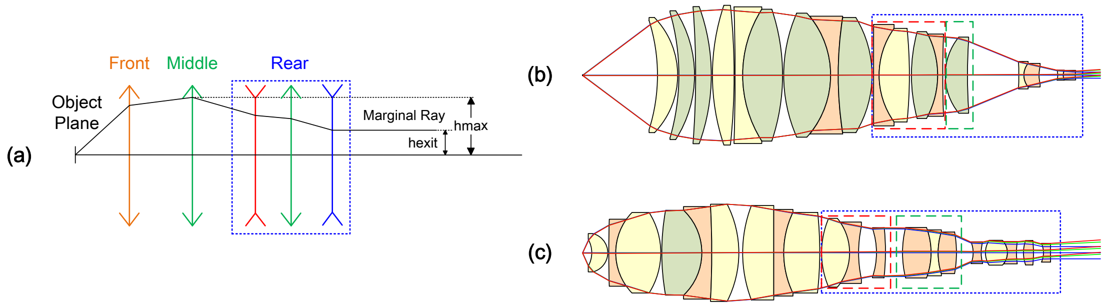

Figure 6.4.: (a) Optical power distribution of Zone 6 systems. (b) 200×/0.62 SF30 objective [43] with *Class IV* W.D., $\kappa = 13$, $r = 0.05$. (c) 250×/0.90 SF26.5 objective [53] with *Class V* W.D., $\kappa = 0.53$, $r = 0.13$.

6.3 Material Selection Strategies

There are four major material selection considerations in microscope objective design:

1. Transmittance,
2. Refractive index and dispersion,
3. Relative dispersion for secondary spectrum correction, including the extended spectral range, and
4. Autofluorescence and manufacturing consideration.

The transmittance of the optical material is the most basic consideration for material selection in refractive optical systems. Figure 6.5 demonstrates the transmittance of the 438 glasses from three glass vendors, which are measured with a 10 mm glass sample under the wavelengths of 2000, 1000, 400, 360, and 340 nm. The specified wavelengths cover the spectrum of typical microscope objectives from UV to IR. For the conventional microscope objectives corrected for visible spectrum, except for some SF dense flint glasses with high refractive index, which have low transmittance in blue, most of the optical glasses can be used and they have excellent transmittance ranging from 400 to 1000 nm. However, the number of selectable materials is reduced when the working wavelength is extended to the UV and IR, which spectrum is important for fluorescence microscopy and semiconductor inspection applications.

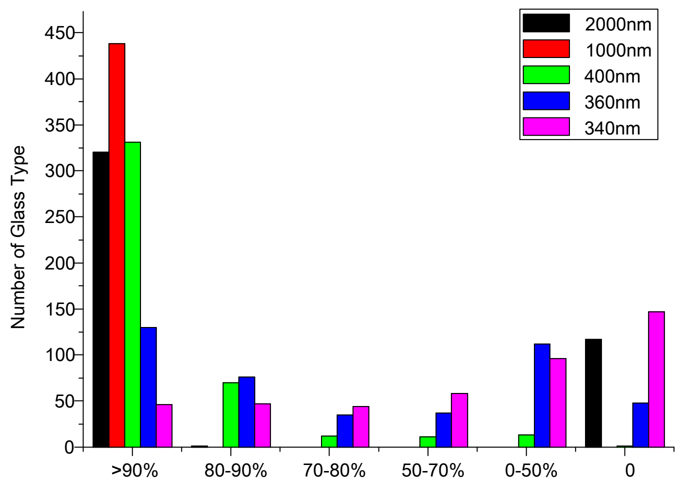

Figure 6.5.: Number of glasses from Ohara, Hoya and Schott with six levels of transmittance at five specific wavelengths from UV to IR, which is measured with a 10 mm-thick glass sample.

The second and third considerations are associated with the achromatic and apochromatic material selection methods, which were discussed in Section 3.2. Besides, axial chromatic aberration generated from other groups should be restrained. For instance, optical materials with large refractive index can relax the surface bending to achieve greater optical power with less spherical aberration. Particularly in the front group, if the aplanatic lenses are made of high-index materials, the high NA can be collected more efficiently. However, according to Figure 2.4, high index materials often suffer from critical dispersion. To reduce the chromatic impact, in practice, optical materials towards the top-left on the

Abbe diagram is preferred. The N-LASF31 A or L-LAH58 are typically used instead of LASF35 or L-LAH79 in front lenses of high NA systems, whereas the GFK70 is preferred in the medium NA systems. Generally, the LAK, LAF and LASF glasses are better choices compared with the SF glasses.

Generally, several cemented doublets and triplets are used in the middle group of microscope objectives. The positive components of cemented doublets are often made of crown glasses, whereas the negative components are made of flint glasses. The materials have large difference of Abbe number (ratio) and relatively small index gap. Thereby, the arbitrary chromatic aberration contribution can be generated by appropriate power distribution of the components, while the bending of the cemented surface is relaxed to avoid critical sensitivity. To correct the secondary spectrum and higher-order axial chromatic aberration, in the conventional Apochromate, such as cemented triplet, three materials forming a large area on the partial dispersion diagram are selected, including the anomalous dispersive fluor crown (FK/FPL) or fluorite, short flint and dense flint glasses. However, when it comes to the design of microscope objectives, typically the dense flint glasses with large dispersion are not used in the middle group for axial chromatic aberration correction. The g-line and F-line partial dispersion of the selected materials mostly lie in the range between 0.535 and 0.58 (the optimal area is within 0.535 to 0.56). All the favorable glasses for transmittance consideration and achromatism consideration are included within this range. Selecting materials from this narrowed region, the optical power of the components could be relaxed to correct secondary spectrum.

When the corrected spectrum is extended, to realize super-apochromatism, additional spectral lines approaching UV and IR should be considered, e.g., i-line, s-line, t-line. Figure 6.6 shows the partial dispersions of all the Schott glasses with both P_{gF} and P_{Cs}.

According to Figure 6.6, the fluor crown and short flint have anomalous partial dispersion in both the blue side (g-F) and the red side (C-s), while the “Middle Glasses” have normal dispersion on both sides. In contrary, the dense flint only has anomalous dispersion on blue side. Therefore, typically utilizing the glasses in the “Selectable Area” on Figure 3.3 could also correct secondary spectrum for extended spectral range, but the dense flint glasses cannot be used.

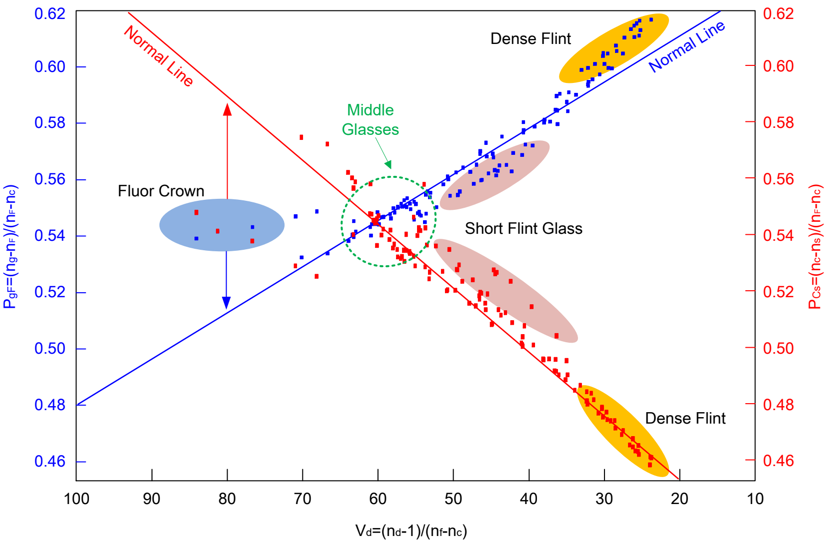

Figure 6.6.: Partial dispersion diagram for both the g-F-line and C-s-line of the Schott glasses. The normal line is defined by the K7 and F2 glasses.

The last aspect is less considered in conventional system design. Only in the microscope objective for high-contrast fluorescence imaging, the reduction of autofluorescence is with concern. Materials containing Nb_2O_5 or Ta_2O_5 as constituents, e.g., NBH-class from Ohara, are widely used because of the advantageous feature of excellent UV and VIS transmittance and low autofluorescence. According to the patents [64-68], materials cannot be selected from the forbidden zone, which is shown on the Abbe diagram in Figure 2.4. The materials with large dispersion typically induce great autofluorescence under high illumination intensity.

As a conclusion, according to the four considerations, based on the philosophy of aberration compensation by different groups, the materials with anomalous dispersion and the materials with medium refractive index and medium dispersion are widely used in the modern microscope objectives with high performance. Generally, glasses from the FPL, YGH and NBH series of Ohara, the FK, LAK, LASF and KZFS series of Schott, and the GFK series of Sumita are selected by most of the vendors.

6.4 Lens Modules in the Three Groups

According to the aberration correction strategies and optical power distributions introduced in Section 6.1 and 6.2, all of the microscope objectives can be divided into two or three functional groups. In this section, the concrete lens modules utilized in the front, middle and rear groups are summarized. They are used in the major Zone 1-4 systems, which have 443 entries (91.5%) out of the database with 484 microscope objectives. Each summarized lens module is valid in more than 80% of applicable examples. The well-described correction schemes, which have been introduced in Section 3.2, are also analyzed and compared with the other new-summarized lens modules. The special lens modules used in the Zone 5 systems have been discussed in Section 6.2 together with its power distribution. Despite the complicated rear group, the lens modules used in the front and middle groups of the Zone 6 systems are nearly the same as Zone 1-4 systems. Therefore, Zone 5 and Zone 6 are not further discussed in this section.

6.4.1 Front Group

Table 6.4 shows the lens modules used in the front group. Their functionalities for spherical aberration (SA), field curvature (FC) and axial chromatic aberration (ACA) are summarized. Special considerations from application and manufacturing requests are also illustrated.

The first two lens modules utilize the aplanatic surfaces, which have been introduced in Section 3.2. In practical systems, there are popular setups introducing the quasi-concentric-aplanatic shell-lenses into the front group to overcome the drawback of single v-a lens and c-a lens, which are shown in Figure 6.7.

The solution (a) utilizes a series of c-a lens to realize the high NA with sufficient free working distance. The strong power for NA collection is well distributed to the shell lenses. Therefore, the decentering sensitivity of each element also reduces compared with a single element. This setup is usually used for the medium/high NA objectives with large magnification and long working distance, particularly for semiconductor inspection applications. The remaining high NA systems with short working distance mostly use the solution (b), which is a combination of the c-a shell-lenses and the v-a lens. Therefore, the high NA is effectively collected, while the hyper-hemispherical shape can be avoided under high NA. It is notable that the spherical aberration is very sensitive to the axial shift of the meniscus elements in the shell-lens group. Corresponding to the power distribution type (f) in Table 6.2, by reducing its optical power, which might slightly violate the aplanatic condition, it is possible to realize the depth CORR by moving the meniscus lens.

Table 6.4.: Summary of lens modules in the front group. The well-described correction schemes are marked with red color. The "Coma" in the SA cells indicates the linear coma elimination with aplanatic surfaces.

No.	Lens modules	Aberration restraint			System parameter		Application/ Manufacturing requests
		SA	FC	ACA	NA	W.D.	
1	Aplanatic v-a lens	🟥 Coma	🟦	🟩	🟥	🟦	Hyper-hemisphere hard to mount
2	Aplanatic c-a lens	🟥 Coma	🟦	🟩	🟪	🟥	-
3	Aplanatic shell-lenses	🟥 Coma	🟦	🟩	🟥	🟥	Possible CORR
4	Thick meniscus front lens in dry objective	🟪	🟧	🟩	🟥	🟧	-
5	High refractive index material	🟥	🟦	🟦	🟥	🟩	Large autofluorescence
6	Medium refractive index material with medium Abbe number	🟥	⬜	🟧	🟪	🟩	Low autofluorescence
7	Low refractive index material in shell-lenses	🟥	⬜	🟧	⬜	🟩	Low autofluorescence
8	Embedded front lens with index-matched material	🟥	🟥	⬜	🟧	⬜	Epi-illumination, immersion
9	Monolithic front lens with index-matched material	🟥	🟦	🟧	🟦	🟩	Easy to produce, low cost, epi-illumination, immersion
10	Front lens with optical contact bonding	🟥	🟪	🟩	🟧	🟩	Localization microscopy, low autofluorescence, capable to mount hyper-hemisphere

🟥	Great positive effect	🟧	Significant positive effect	⬜	Slight positive effect
🟪	Slight negative effect	🟦	Significant negative effect	🟩	Negligible effect

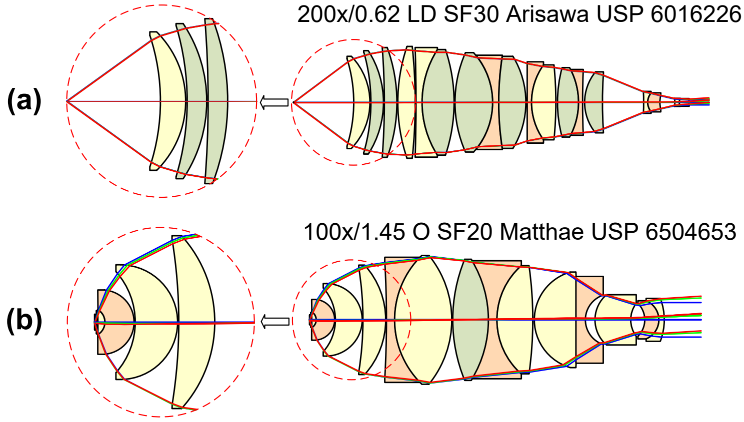

Figure 6.7.: Practical front group with aplanatic shell-lenses (a) purely concentric-aplanatic shell-lenses. (b) vertex-aplanatic lens associated with concentric-aplanatic shell-lenses.

Lens module No. 4 is applied to the dry objectives with extremely high NA, e.g., NA=0.95. To achieve sufficient free working distance, the front surface should be designed concave, which typically cannot fulfill aplanatic condition. Therefore, the ray bending on the front surface is usually large, which introduces tremendous spherical aberration. As a consequence, special lens modules must be used in the middle group for compensation, particularly for higher-order spherical aberration. However, the thick meniscus front lens can generate positive Petzval curvature with positive optical power, which can relax the rear group for field curvature compensation.

The lens module No. 5-7 are associated with the material selection for the aplanatic lenses. According to the discussion in Section 6.3, although the high refractive index materials, which locate at the top-right, can significantly enlarge the NA, due to its large dispersion and strong autofluorescence, they are not preferred in some advanced systems. Medium index materials with medium dispersion are useful as the front lens, whereas the low index materials with extremely low dispersion can be used for the shell lenses. The most popular glass choices are demonstrated in Appendix VII.

In the immersion microscope objectives, the front lens is usually designed with an embedded structure (lens module No. 8) consisting of a front small embedded plano-convex crown lens and a rear large meniscus flint lens, which was shown in Figure 4.5(a). In the immersion objectives, the immersion liquid is used between the objective front surface and the specimen (or cover glass). If the front surface of the first lens has a strong curvature, which is typically used in the high NA dry objective, this can lead to the generation of air bubbles on the surface during observation. It is also difficult to clean the front surface when the observation is finished or when the specimen is changed. Therefore, the front surface in most immersion objectives is designed as a plane. However, since the rear large meniscus lens is often made of high index material for NA enlargement, to avoid total internal reflection at the front surface under epi-illumination, the embedded small plano-convex lens must be designed with materials with refractive index matched to the immersion liquid. Some examples are listed in Table 6.5.

Table 6.5.: Low refractive index glasses selected for the embedded front lens.

Glass Type	Refractive Index (n_d)	Abbe Number (ν_d)	Immersion Liquid
N-K5	1.522	59.48	Oil
N-BK7	1.517	64.17	Oil
N-FK5	1.487	70.41	Water
Quartz	1.458	67.83	Water

Apart from the functionality for application requests fulfillment, the embedded lens also has great advantage in field curvature restraint. Owing to the shape and index difference of the two components, this embedded front lens always generates a positive Petzval curvature with great positive power, which can relax the complexity of the rear group for field curvature correction:

$$\frac{1}{R_{Ptz}}=0-\frac{n_2-n_1}{n_1 n_2 r_1}-\frac{1-n_2}{n_2 r_2}=-\frac{1}{n_2}\left(\frac{n_2-n_1}{n_1 r_1}+\frac{1-n_2}{r_2}\right)>0, \tag{6.5}$$

where the refractive indices n_1, n_2 and surface radii r_1, r_2 are marked on Figure 4.5(a). However, due to the special technology and high requirement of the manufacturing accuracy of the cemented surface, the embedded front lens is costly. Furthermore, the cemented surface is vulnerable to the strong illumination intensity under epi-illumination for super-resolution localization microscopy. Therefore, simple monolithic front lens (lens module No. 9) and “optical-bonded” front lens (lens module No. 10) have been created to address the manufacturing requests, which have been discussed by example I in Section 5.2. Regarding the functionality for aberration correction, the front lens of typical high NA dry objective, typical embedded front lens for immersion objective, monolithic front lens for immersion objective and the novel front lens utilizing optical contact bonding technology are compared in Appendix V with practical examples.

6.4.2 Middle Group

Table 6.6 shows the lens modules used in the middle group. Their functionalities for spherical aberration (SA), zonal spherical aberration/zonal error (ZSA), axial chromatic aberration (ACA) and spherochromatism (SPHCRM) correction are summarized. Considerations resulting from application and manufacturing requests are also illustrated.

Table 6.6.: Summary of lens modules in the middle group. The well-described correction schemes are marked with red color.

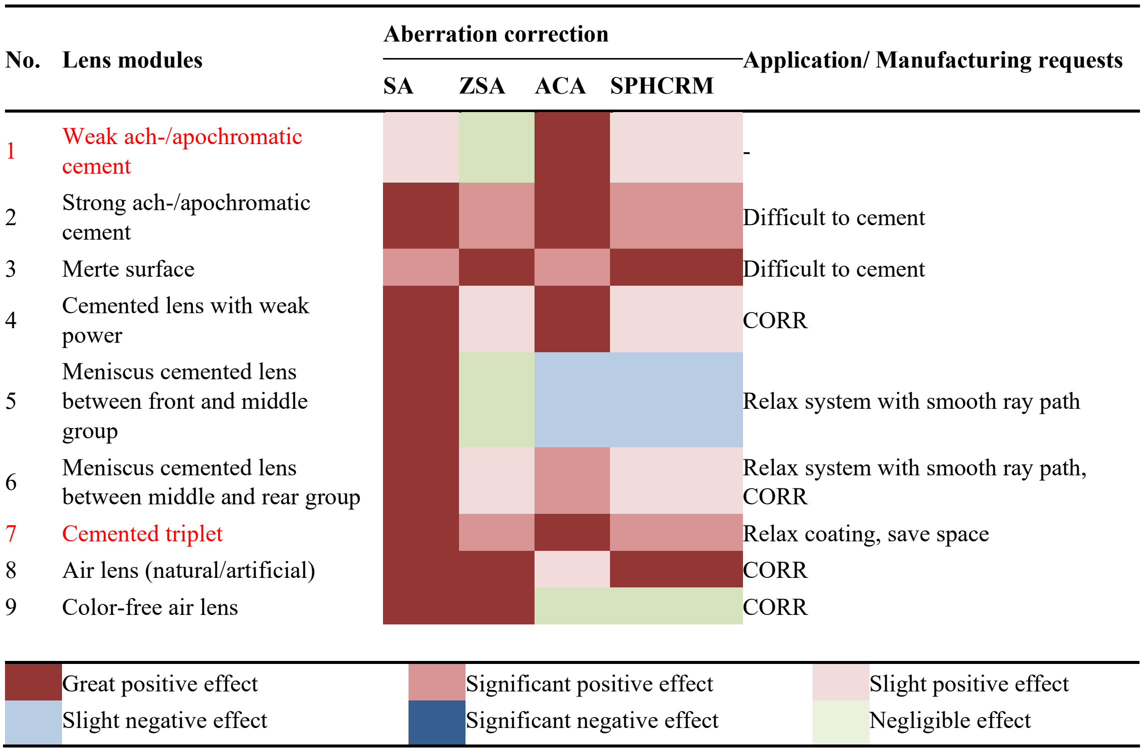

No.	**Lens modules**	**Aberration correction**				**Application/ Manufacturing requests**
		SA	**ZSA**	**ACA**	**SPHCRM**	
1	Weak ach-/apochromatic cement	🟨	🟩	🟥	🟨	-
2	Strong ach-/apochromatic cement	🟥	🟧	🟥	🟧	Difficult to cement
3	Merte surface	🟧	🟥	🟧	🟥	Difficult to cement
4	Cemented lens with weak power	🟥	🟨	🟥	🟨	CORR
5	Meniscus cemented lens between front and middle group	🟥	🟩	🟦	🟦	Relax system with smooth ray path
6	Meniscus cemented lens between middle and rear group	🟥	🟨	🟧	🟨	Relax system with smooth ray path, CORR
7	Cemented triplet	🟥	🟧	🟥	🟧	Relax coating, save space
8	Air lens (natural/artificial)	🟥	🟥	🟨	🟥	CORR
9	Color-free air lens	🟥	🟥	🟩	🟩	CORR

🟥	Great positive effect	🟧	Significant positive effect	🟨	Slight positive effect
🟦	Slight negative effect	■	Significant negative effect	🟩	Negligible effect

The middle group plays the key role in correcting the spherical aberration and axial chromatic aberration. As a common layout, several cemented doublets and triplets constitute the positive middle group with relatively large optical power. According to Section 3.2 and 6.3, to correct the axial chromatic aberration and higher-order spectrum, the materials are selected with distinctive Abbe number but similar partial dispersion.

The first three lens modules for the middle group are based on the different choices of cementing surface radius and refractive index gap between the two cemented components. The element cementing used in the middle group can be classified into four types:

1. Typical achromatic material selection with weak surface cementing (weak surface bending),
2. Typical achromatic material selection with strong surface cementing (strong surface bending),
3. Special material selection with Merte surface cementing, and

4. Cemented element with weak optical power.

When the achromatic materials are selected with appropriate power distribution, the cemented lens can contribute significantly to axial chromatic aberration contribution. With stronger curvature, the higher-order spherical aberration contribution on the cementing surface increases, thus contributing more significantly to the zonal error and spherochromatism correction. Furthermore, with the heavily curved cementing surface, if the two cemented materials have a small index gap in the range of 0.05-0.15, a Merte surface [29, 69, 70] is created, which has extraordinary higher-order spherical aberration behavior. Table 6.7 summarizes the Merte material pairs with distinctive Abbe number but similar partial dispersion, which are useful in the middle group of modern objectives.

Table 6.7.: Popular glass pairs for Merte cementing.

Glass Pair	**Refractive Index Difference (Δn_d)**	**Abbe Number Difference/ Ratio ($\Delta \nu_d$)**	**Partial Dispersion Difference (ΔP_{gf})**
GFK70, E-F2	0.051	35.05/1.95	0.042
GFK68, N-KZFS11	0.047	25.80/1.62	0.015
N-PK51, N-KZFS4	0.087	32.31/1.73	0.019
N-PK51, N-KZFS11	0.111	34.41/1.82	0.021
S-FPL51, N-KZFS11	0.143	38.83/1.92	0.023
Fluorite, S-NSL3	0.084	36.33/1.62	0.012
Fluorite, N-SK5	0.150	33.96/1.56	0.002
E-SK5, F9	0.031	23.08/1.61	0.054

All the four types of cementing are used in the example 60×/1.45 oil-immersion objective shown in Figure 6.8. The objective has *class (c)* level apochromatic correction from g-line to C-line. The first doublet (lens module No. 5) is realized by cementing the negative component made of E-F2 ($n_d = 1.620,\ \nu_d = 36.26$) and the positive component made of GFK70 ($n_d = 1.569,\ \nu_d = 71.31$). It forms a Merte cementing and generates nearly equivalent amount of primary and higher-order spherical aberration. The doublet 1 locates between the front group and middle group. To smoothen the ray path, the fast doublet is designed with quasi-concentric front surface. Thus, it also has similar functionality as the lens module No.3 of front group, which is an aplanatic shell-lens. However, to relax the design, typically the doublet is not used to compensate the chromatic aberration from the front group. The powers of E-F2 and GFK70 lenses are carefully selected to fully correct axial chromatic aberration within this element.

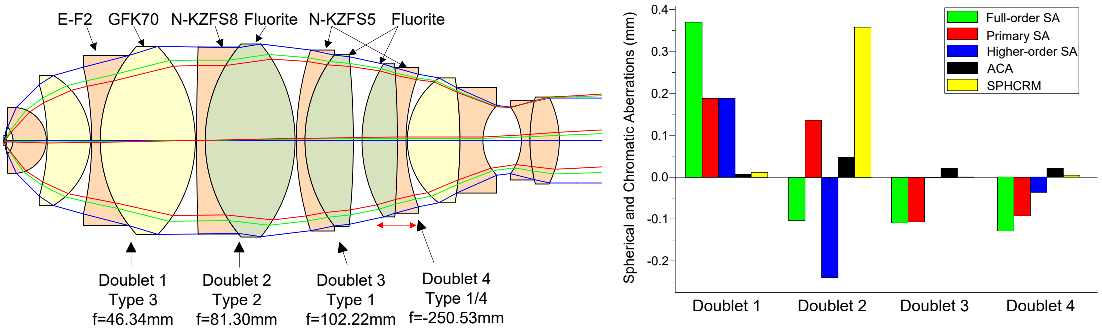

Figure 6.8.: 60×/1.45 oil-immersion objective utilizing all the four types of cemented doublet with their aberration contributions, including primary and higher-order of spherical aberration (SA), axial chromatic aberration (ACA, g-C) and spherochromatism (SPHCRM, g-C). The red arrow indicates the movable component for CORR functionality.

The material selection in the second and third doublet follows the basic achromatic and apochromatic consideration. The fluorite ($n_d = 1.434,\ \nu_d = 95.26$) is utilized in both doublets as the positive component, but doublet 2 selects N-KZFS8 ($n_d = 1.720,\ \nu_d = 34.70$) for the negative component, while the doublet 3 utilizes N-KZFS5 ($n_d = 1.654$, $\nu_d = 39.70$). The fluorite and the KZFS short flint glass have distinctive Abbe number, but similar partial dispersion within the selectable area (the g-line and F-line partial dispersion between 0.535 and 0.58). Therefore, the doublet 2 and doublet 3 can significantly introduce positive axial chromatic aberration contribution with suppression of secondary spectrum. Thus, the tremendous negative chromatic aberration introduced by the front group can be compensated. However, compared with type 1 doublet 3, due to the larger index gap between the two materials and the stronger curvature (associated with incidence angle), the type 2 doublet 2 has a critical marginal ray bending on the cemented surface, resulting in tremendous higher-order spherical aberration contribution, which is similar to the functionality of Merte surface. Doublet 2 introduces overcorrected higher-order spherical aberration that compensates the under-corrected primary contribution as well as the residual higher-order terms. On the contrary, although the height and incidence angle of marginal ray is nearly identical, the doublet 3 is almost free of higher-order spherical aberration due to the weak cemented surface.

The type 4 doublet 4 (lens module No. 6) is made of the same materials as doublet 3, but it has very weak negative optical power. Owing to the apochromatic material selection, doublet 4 has significant axial chromatic contribution. The element is sensitive to both the primary and higher-order spherical aberration. Thereby, the longitudinal movement of this component is utilized to realize CORR function of cover glass thickness, corresponding to the power distribution type (e) in Table 6.2.

All the four cementing types can be utilized to generate cemented triplets (lens module No. 7) with three basic setups shown in Figure 6.9. The "PNP" triplets typically have positive optical power, while the "NPN" triplets are negative.

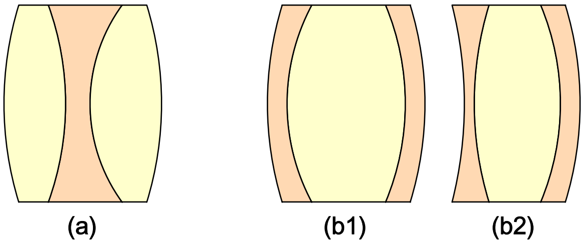

Figure 6.9.: (a) "PNP" cemented triplet (b1), (b2) "NPN" cemented triplet.

According to the example II in Section 5.2, the cemented doublets and triplets can achieve equivalent functionality for spherical aberration and axial chromatic aberration correction. But different from the correction strategy of the system only utilizing cemented doublets, when the triplet is used, optical designers usually create two cemented triplets with positive and negative power, respectively. These two cemented lenses compensate each other, and the residual difference is utilized to correct the aberration from other groups. Thereby, the type (d) power distribution in Table 6.2 can be realized to relax the rear group. Figure 6.10 demonstrates an example 63×/1.20 water-immersion objective [71], where this correction strategy is applied. In the middle group, a PNP positive triplet and an NPN negative triplet maintain spherical aberrations with different signs, while both chromatic contributions are positive. Compared with the strategy to fully correct aberrations within one triplet, simply using the residual error for compensation could achieve better results, which corresponds to the strain design consideration [72].

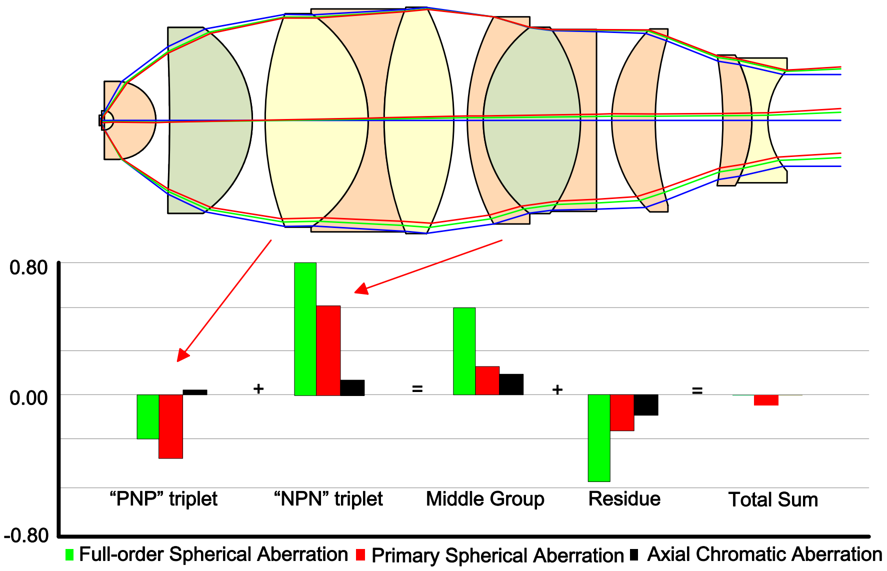

Figure 6.10.: 40×/1.20 water-immersion objective with a pair of PNP and NPN cemented triplets in the middle group. The axial chromatic aberration is calculated for F-line to C-line.

Notably, in some patented entries, the PNP triplet can also be designed with negative optical power. In the 40×/1.20 water-immersion objective [73] shown in Figure 6.11, the second triplet selects FPL53 ($n_d = 1.439,\ \nu_d = 94.96$) for the two positive elements and S-LAL59 ($n_d = 1.734,\ \nu_d = 51.47$) for the negative middle lens. To correct the spherical aberration, including the zonal error, the two inner cemented surfaces have strong curvatures, while the outer surfaces are weakly curved. Hence, the high index middle lens has great negative power (f=−6.87 mm) and the two low index positive lenses have relatively weak power (f=15.55 mm and f=22.82 mm). Consequently, the overall focal power of this PNP triplet is negative. According to the surface aberration contributions, the overall spherical aberration of the two PNP triplets have different signs, which is the same as the typical case with a pair of PNP and NPN triplets. However, the two cemented surfaces of the second triplet both generate negative spherical aberrations, which is different from the aberration behavior of a normal NPN negative triplet. The four cemented surfaces of the two PNP triplets generate larger higher-order spherical aberration, which is helpful in correcting the zonal error and spherochromatism.

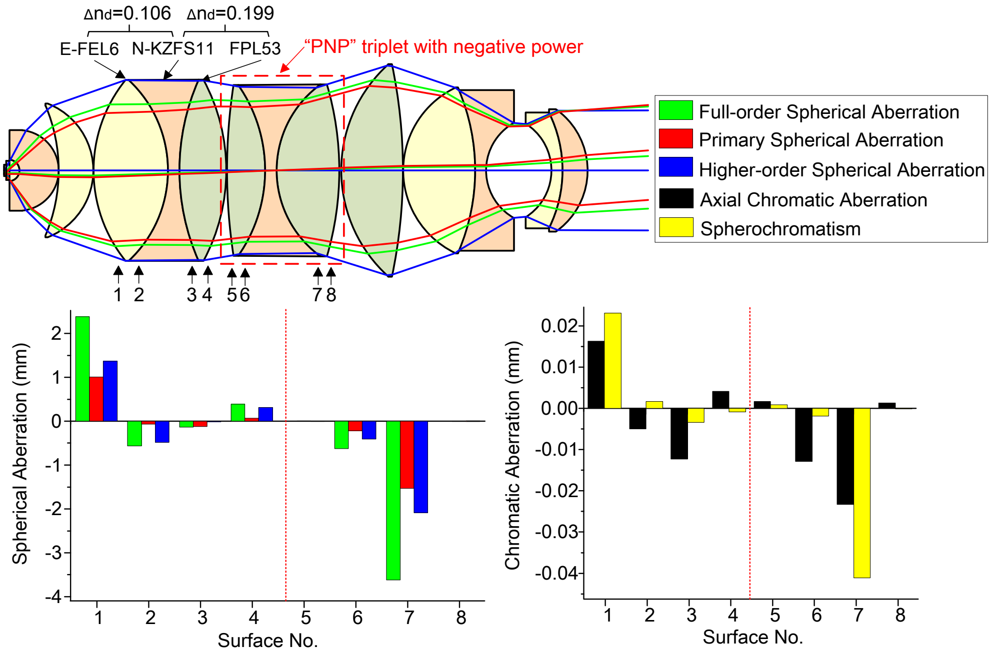

Figure 6.11.: 40×/1.20 water-immersion objective with two PNP cemented triplets in the middle group. The first normal PNP positive triplet uses both the normal cementing (type 1) and the Merte cementing (type 3), while the second PNP negative triplet only uses normal cementing (type 1 and type 2). The axial chromatic aberration and spherochromatism are calculated from g-line to C-line.

With four considerations: aberration compensation, ray path smoothening, optical power distribution and manufacturing consideration, the cemented doublets and triplets are arranged in the middle group to achieve excellent spherical and axial chromatic aberration correction with favorable sensitivity.

The consideration of the aberration compensation can be seen from the examples illustrated above. For one kind, systems like the example in Figure 6.8 suppressed the aberration contribution in each doublet. The element sensitivity can be reduced, but more components should be used. For another, according to the examples in Figure 6.10 and Figure 6.11, applying the strain design idea by using two cemented triplets with opposite aberration behavior, better correction can be realized with a smaller number of components, but the element sensitivity gets critical.

To restrain the unexpected aberration generated in the middle group due to large marginal ray height, the ray path should be smoothened. Therefore, the cemented elements between the middle group and the front group (or the rear group) can be designed with meniscus shape, which also provides similar functionalities as the adjacent group, e.g., the doublet 1 in the example shown in Figure 6.8. Furthermore, arranging the middle group with quasi-symmetric ray path, it is also feasible to correct the coma, which can relax the design of the rear group.

Regarding the special power distribution types, particularly for the CORR objectives, weak power type 4 cementing should be utilized to achieve the focal-length-invariant and chromatic-correction-invariant performance, when the objective is adjusted for environmental change.

The last consideration of manufacturing and technology has been discussed by example II in Section 5.2. In the systems shown in Figure 6.10 and Figure 6.11, since a smaller number of elements are used, the design can match the 45 mm parfocal length, while the system in Figure 6.9 should uses the 60 mm parfocal length. Furthermore, comparing one cemented triplet with two cemented doublets as equivalence, two strongly curved glass-air interfaces are removed. Thereby, the requirement of surface coating is relaxed.

The last two lens modules are associated with another structure: the air lens, which introduces extraordinary higher-order spherical aberration contribution. The utilization of air lenses is based on a new point of view of the narrow air gaps in microscope objectives, which are usually formed by surfaces with strong curvatures. Two conditions of an air gap should be fulfilled to correct the spherochromatism and zonal error:

1. Strongly curved surface and/or large index step, and
2. Ach-/apochromatic choice of materials.

When the first condition is fulfilled, the air lens contributes a lot to zonal error control. With the additional second condition, it is more beneficial to spherochromatism correction. In microscope objectives, it is easy to fulfill these two conditions, corresponding to the utilization of cemented lenses with appropriate glass choice and strongly curved outer surface. There are two types of air lens utilized in the middle group: the natural air lens and the artificial air lens.

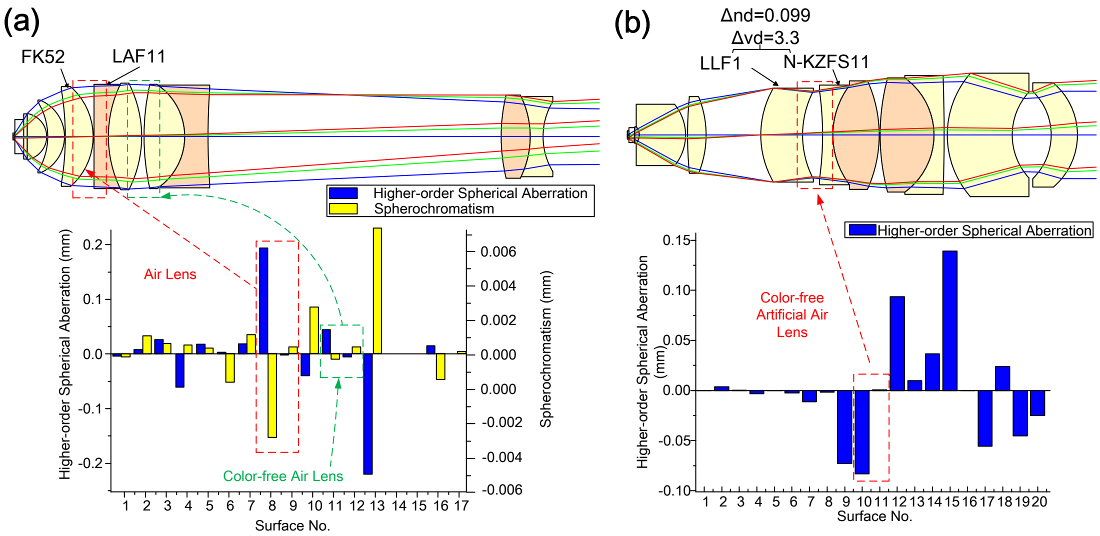

Figure 6.12.: (a) 98×/1.30 oil-immersion objective with two natural air lenses. (b) 25×/0.80 water-immersion objective with artificial air lens.

The natural air lens is formed by the small air space between the cemented lenses. Considering the 98×/1.30 oil-immersion objective in Figure 6.12 (a), the gap between the FK52 ($n_d = 1.486,\ \nu_d = 81.61$) lens and the LAF11 ($n_d = 1.757,\ \nu_d = 31.70$) lens forms an air lens generating enormous higher-order spherical aberration. Furthermore, the two materials with large difference of dispersion fulfill the achromatic condition, thus contributing to spherochromatism correction. On the contrary, another color-free natural air lens is formed by two doublets with FK52 glass. Since there is no index gap and dispersion difference, the air lens is free of chromatic aberration and has small higher-order contribution. In the recent decade, special artificial air lenses have been generated, which have special reverse bent structure in the middle group. Figure 6.12(b) gives a 25×/0.80 water-immersion objective with a reverse bent lens, which only has the functionality of spherical control. The two selected glasses LLF1 ($n_d = 1.548,\ \nu_d = 45.75$) and N-KZFS11 ($n_d = 1.638,\ \nu_d = 42.41$) have similar dispersion. Therefore, the air lens is free of chromatic aberration and only corrects zonal error. It is notable that the front surface of the reverse bent lens also holds significant higher-order spherical aberration contribution and the focal power of the lens is very small. Therefore, this element can be used to realize cover glass thickness CORR function for this objective with type (f) power distribution.

6.4.3 Rear Group

Table 6.8 shows the lens modules used in the rear group. Their functionalities for spherical aberration (SA), zonal spherical aberration/zonal error (ZSA), coma, astigmatism (AST), field curvature (FC), axial chromatic aberration (ACA) and lateral color (LCA) correction are summarized. Special considerations resulting from application and manufacturing requests are also illustrated.

Table 6.8.: Summary of lens modules in the rear group. The well-described correction schemes are marked with red color.

No.	**Lens modules**	**Aberration correction**							**Application/ Manufacturing requests**
		SA	**ZSA**	**Coma**	**AST**	**FC**	**ACA**	**LCA**	
1	Single meniscus element (possibly cemented)	🟩	🟩	🟧	🟦	🟥	🟩	🟩	Low/medium etendue, low cost, insensitive
2	Quasi-symmetric Gauss type	🟩	🟩	🟥	🟥	🟥	🟩	🟩	Critical sensitivity
3	Petzval type	🟩	🟩	🟦	🟥	🟥	🟩	🟩	Possible CORR, medium sensitivity
4	Long separation between the middle and rear group	🟩	🟩	🟩	🟩	🟩	🟩	🟥	Hampering parfocality
5	Thick lens	🟧	🟧	⬜	⬜	🟥	🟧	🟥	-
6	Dense flint principle	🟧	🟩	🟩	🟩	🟥	🟦	🟥	-
7	Achromatic cementing	⬜	🟩	🟩	🟩	🟩	⬜	🟧	-
8	Buried surface	🟩	🟩	🟩	🟩	🟩	🟥	🟥	-
9	Air lens	🟥	🟥	🟦	🟦	🟩	⬜	🟩	CORR
10	Additional lens with Gauss type	🟥	🟥	🟥	🟥	⬜	🟧	🟧	High etendue

🟥 Great positive effect	🟧 Significant positive effect	⬜ Slight positive effect
🟦 Slight negative effect	■ Significant negative effect	🟩 Negligible effect

The first three lens modules are associated with three basic structures of the rear groups, which are shown in Figure 6.13. The type (a) rear group with single meniscus element is the most classical rear group. It can be designed with negative or very weak power, which is composed with a single thick meniscus lens or two components cemented together. Since the chief ray height is relatively large on this element, it can significantly contribute to the coma correction. However, to avoid generating higher-order coma, the single element should be placed with its concave surface facing the image side [61]. However, to restrain spherical aberration the single element cannot be designed with strongly curved outer surfaces. Consequently, it is difficult to compensate astigmatism with this structure. Therefore, typically the type (a) rear group is not applied to the Zone 3 and Zone 4 systems with relatively high etendue, in which the astigmatism is critical. Owing to the excellent sensitivity and low cost, it is widely used in the Zone 2 systems with low or medium etendue. It is particularly useful in the high magnification long working distance objectives with strong retrofocus structure.

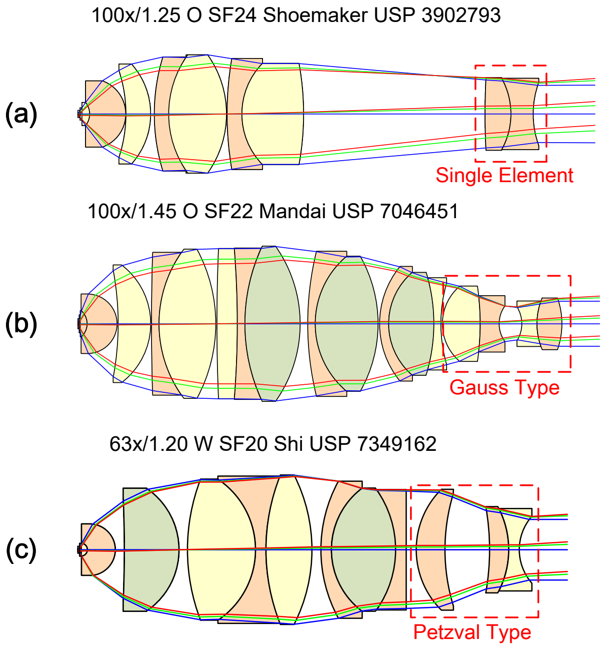

Figure 6.13.: Three basic rear group structures. (a) Single meniscus lens, including cemented meniscus lens. (b) Gauss type quasi-symmetric setup with two thick meniscus lenses. (c) Petzval type with separated positive and negative components.

The type (b) quasi-symmetric Gauss type rear group is the most popular setup in high NA modern microscope objectives, particularly for immersion application. Two single or cemented meniscus lenses with strongly curved outer surfaces are used, which is similar to the middle part of classical double-Gauss photographic objectives. Although the aperture stop cannot be located between the two groups for perfect symmetry, this setup is still able to finely adjust coma and lateral color according to the symmetry principle and control the astigmatism with the strong curvatures. However, due to the great ray bending in the air gap, the element is very sensitive to centering error. Besides, the strongly curved surfaces also require tight surface figure tolerance. The cost of the Gauss type rear group is relatively high.

The type (c) Petzval type rear group can balance the cost and correction level, which was first reported by Klein in 1967 [74]. This very early development utilized the conventional Petzval structure with two positive lenses and a negative lens forming a "PNP" structure, which well corrects both the astigmatism and Petzval curvature. However, since the three components should be placed remote to each other, the objective cannot be parfocalized. In the recent developments, advanced Petzval type rear group with separated positive and negative components are used, by which the field curvature and coma are well corrected. Compared with Gauss type, it is less sensitive. For some special cases, the Petzval type rear group can also be designed sensitive to spherical aberration by applying air lens effect, which is useful to realize CORR function. The drawback of this structure is that the higher-order coma is hard to control, thus it is not used in the Zone 4 systems with extremely high etendue.

The major functionality of the lens modules No. 4-8 is to correct lateral color. According to the condition of lateral color correction:

$$\sum_j \frac{\overline{\omega}_j}{\omega_j} \cdot \omega_j^2 \cdot \frac{\Phi_j}{\nu_j} = 0, \tag{6.6}$$

where ω_j represents the relative marginal ray height, while the $\overline{\omega}_j$ is the relative chief ray height. The Φ_j is the focal power and the ν_j is the Abbe number. The first term $\overline{\omega}_j/\omega_j$ can be regarded as the ray bundle separation contribution, and the second term $\omega_j^2 \cdot \Phi_j/\nu_j$ is considered as the axial color contribution. To generate a large contribution in the rear group for compensation, the ray bundle separation of fields should be as large as possible and the glasses should be carefully selected to introduce appropriate axial color. The well-known "thick lens" and "dense flint" principles, which were introduced in Section 3.2, manipulated these two terms respectively. Utilizing the lens modules No. 4 and No. 5, the first term's contribution can be increased, whereas the lens modules No. 6-8 select special materials to increase the contribution of the second term. Due to the limit of space, some practical glass selections will be illustrated in Appendix VIII with example systems.

When the system etendue is extended, the exit pupil size is enlarged and the marginal and coma ray heights in the rear group increase, resulting in inevitable spherical aberration and tremendous coma. To compensate the spherical aberration between the middle and rear group, especially concerning the higher-order contribution for zonal error correction, advanced lens modules should be utilized. The lens module No. 9 is similar to the lens module No. 8 used in the middle group. However, different from the middle group, the rear group lacks the natural air lens, which is usually formed by the cemented lenses with strong outer curvature in the middle group. Typically, only the artificial air lens can be found in the rear group. Figure 6.14(a) demonstrates a 40×/1.00 water-immersion objective [75] utilizing a natural air lens in the middle group and an artificial air lens in the rear group. The rear group belongs to the basic structure type (c), which is comprised of separated elements made of flint glasses, with weak positive and negative optical power. The S-FTM16 ($n_d = 1.593,\ \nu_d = 35.31$) meniscus lens and N-SF57 ($n_d = 1.847,\ \nu_d = 23.78$) meniscus lens forms a strong positive artificial air lens with large index gap, thus generating tremendous higher-order spherical aberration. The two cemented triplets in the middle group forms a natural air lens with smaller index gap, thus generating smaller higher-order contribution under similar marginal ray height and incidence angle. The artificial air lens in the rear group can also be used to realize CORR function of the objective. It is notable that, as a byproduct, the Petzval type rear group with air lens may also generates higher-order coma. Therefore, this type of air lens is seldom used in the objectives with extremely high etendue.

When the system etendue is extremely high, the power distribution must be changed to type (c), consisting of quasi-symmetric part and an additional positive component. To avoid generating tremendous spherical aberration and higher-order coma, a positive meniscus lens with quasi-concentric front surface is usually added behind the Gauss group. Three high etendue objectives are shown in Figure 6.14(b)-(d) under the same scale.

The system (b) has the smallest etendue, where only a single meniscus lens is added to smoothen the ray path. With nearly doubled etendue, the system (c) exploits greater bending of the additional lens and utilizes more complicated quasi-symmetric structure. When it comes to the system (d) with highest etendue, the additional lens is also designed as a cemented doublet, which is the common structure used in the state-of-the-art high etendue systems. The aberration correction functionalities of these complicated rear groups are very complicated. All the aberrations are involved and cannot be clearly decoupled. Designing the Zone 4 extremely high etendue objectives always requires special consideration.

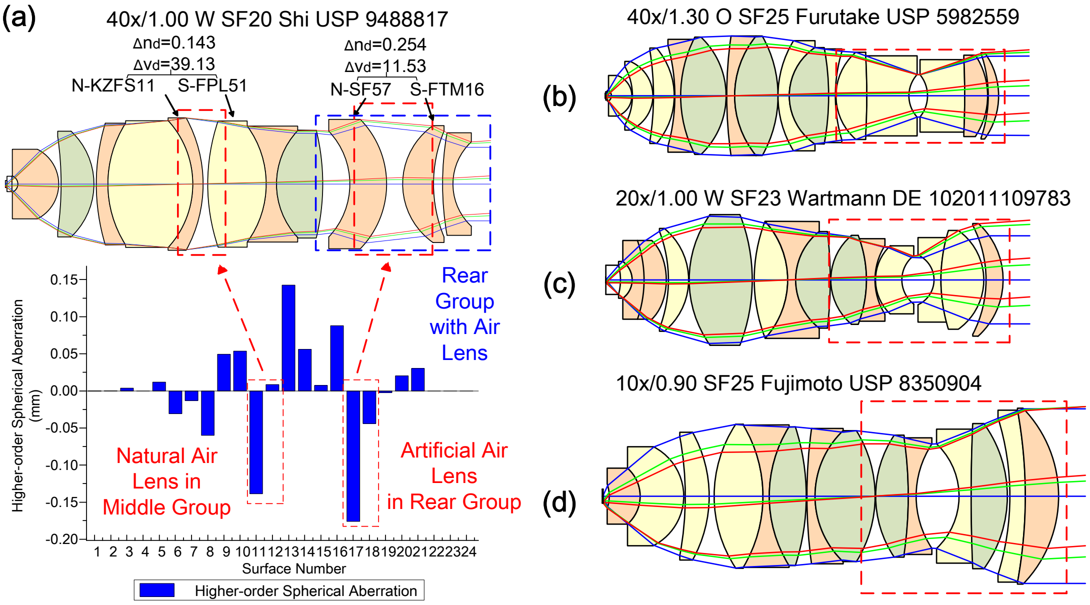

Figure 6.14.: (a) 40×/1.00 water-immersion objective with natural air lens in the middle group and artificial air lens in the rear group for spherical aberration and zonal error correction. (b) High etendue system with additional single meniscus lens behind the Gauss type rear group. (c) High etendue system with both additional meniscus lenses in front of the Gauss type rear group and behind the Gauss type rear group. (d) Extremely high etendue system with additional cemented meniscus lens behind the Gauss type rear group.

6.5 CORR Objectives

According to Section 4.2.3, to adjust four kinds of environment parameters, correction collars have been used in CORR objectives, which introduce significant system complexity both optically and mechanically. Generally, there are three types of solutions used to realize the correction function:

1. Removable/replaceable elements,
2. Moving components with various power distributions, and
3. Air lenses.

The lens module No. 3 of the front group, No. 4, 6 of the middle group belong to the second type. Lens modules No. 8 and No. 9 of the middle group and No. 9 of the rear group are associated with the third type. Due to the limit of space, comparison of practical CORR systems utilizing these three methods are demonstrated in Appendix IX.

7. Microscope Objective Synthesis

Through the six chapters, the building blocks and design principles utilized in most of the modern microscope objectives have been systematically sorted and analyzed. Three major aspects determine the lens modules selection, including aberration correction, application requests and manufacturing considerations. As a reverse process, the workflow of the system synthesis is shown in Figure 7.1, in which the utilized lens modules also originate from the three claimed aspects.

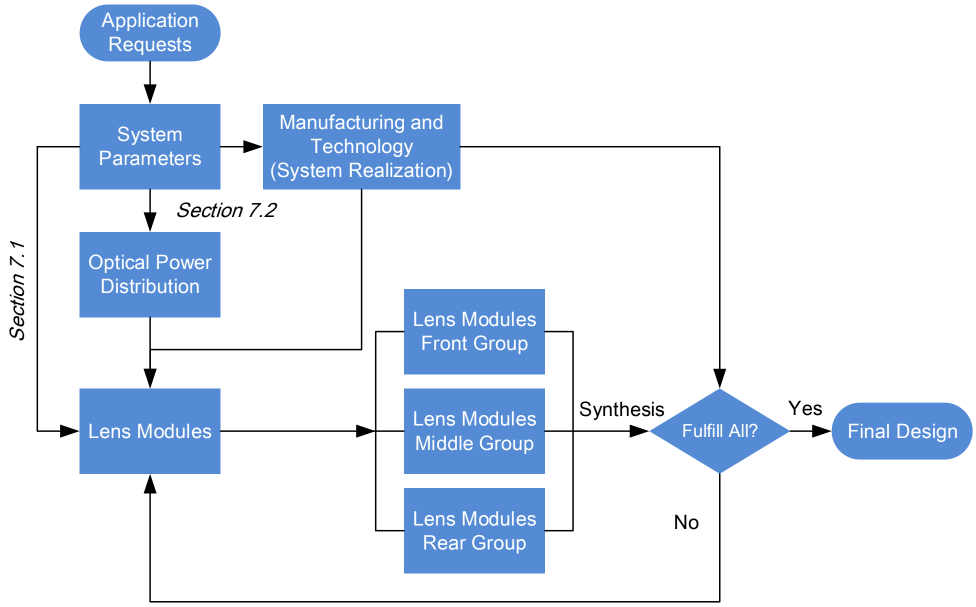

Figure 7.1.: Workflow of the microscope objective synthesis.

The microscope objective design is mostly application-oriented. The system parameters are determined by the applications and corresponding correction levels of chromatic aberration and field aberration. According to these parameters, several lens modules can be directly fixed, and the corresponding manufacturing and technology also set certain boundary conditions and predetermine some lens modules. As the major aspect of consideration, regarding the system parameters, the optical power distribution should be carefully selected out of the Table 6.2. Then synthesizing the lens modules from front, middle and rear group, the new objective structure can be achieved and then checked with the boundary conditions given by the manufacturing requests.

In this chapter, Section 7.1 illustrates the process of system modification for new application requests. When the application is slightly changed, without disturbing the basic structure of the objective lens by keeping the optical power distribution, several lens modules belonging to front, middle and rear group are introduced locally into the system to match the new system parameters. The combination of system parameters and correction levels in this example has not been reported in patents, which can be regarded as an extrapolation of the solution space of microscope systems. Section 7.2 illustrates the process of the synthesis of a new system structure from the basic lens modules, which can be considered as an interpolation of the conventional solution space. The optical power distribution is first fixed, and the lens modules are inserted step by step to gradually match the required system parameters.

7.1 Modification of an Available System for New Applications

A patented 40×/0.85 SF26.5 Plan-apochromate objective [76] is used as the initial system. The 45mm parfocal system is corrected for infinite-conjugate with 180mm tube lens. The new system parameters of the two steps system modification for new applications are listed in Table 7.1.

Table 7.1.: Applications and system parameters of the two-step modification. Before the step I, the surface curvatures of the initial system are first slightly adjusted to incorporate the extended spectrum. "Fluo-" indicates general fluorescence microscopy.

Parameters	Initial	Step I	Step II
Application	Fluo-	Multiphoton	Multiphoton
Magnification	40×	40×	40×
NA	0.85	0.85	0.95
Spectral Range	g-C	i-t	i-t
Color	Apo-	Apo-	Apo-
Correction	*Class (c)*	*Class (g)*	*Class (g)*
Field	Plan-	Plan-	Plan-
Correction	*Class 4*	*Class 4*	*Class 4*

The system layouts of each step system are shown in Figure 7.2. The longitudinal aberrations and RMS wavefront errors of each step system are demonstrated in Figure 7.3 and Figure 7.4, respectively.

In the first step, the working spectrum of the initial system, which was corrected for general fluorescence microscopy, should be extended from g-C to i-t, covering the spectral range from NUV to NIR for multiphoton microscopy. In the second step, to improve the resolution for more efficient excitation, the NA should be enlarged to 0.95. In the modified systems, correction of the Petzval curvature should be maintained, and the other field aberrations could be corrected by utilizing certain amount of vignetting as *Class 4*. Conventionally, *Class (e)* color correction with *Class 4* field correction was the highest correction level that achieved by the 40×/0.95 objectives. The modified system is out of the classical solution space.

Before applying the new lens modules to the two steps, the surface curvatures were slightly adjusted to incorporate the correction of i-line and t-line. However, according to Figure 7.3(a2) and Figure 7.4(a), although the t-line correction is acceptable, the NUV i-line is out of control and the field correction of g-line is hampered.

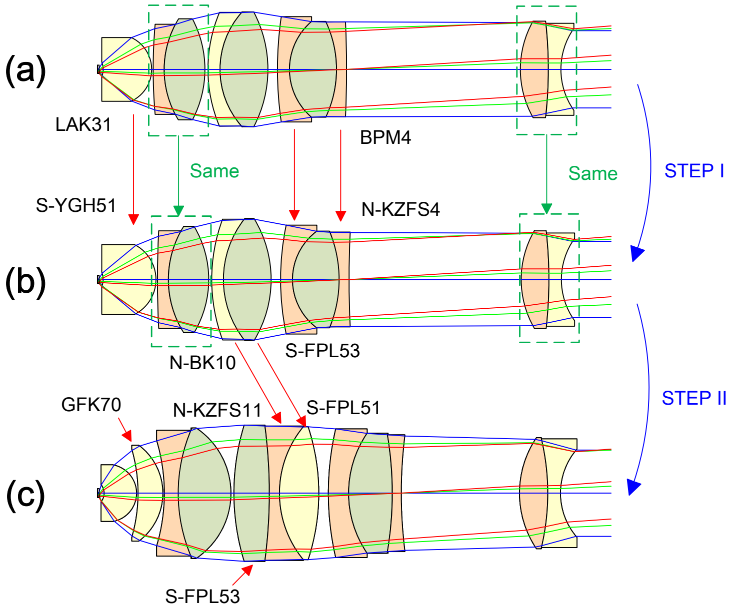

Figure 7.2.: Objective structures and material change during modification. (a) Initial 40×/0.85 objective with g-line to C-line correction. The surface curvatures are slightly adjusted to incorporate the extended spectrum. (b) Step I 40×/0.85 objective with i-line to t-line correction. (c) Step II 40×/0.95 objective with i-line to t-line correction.

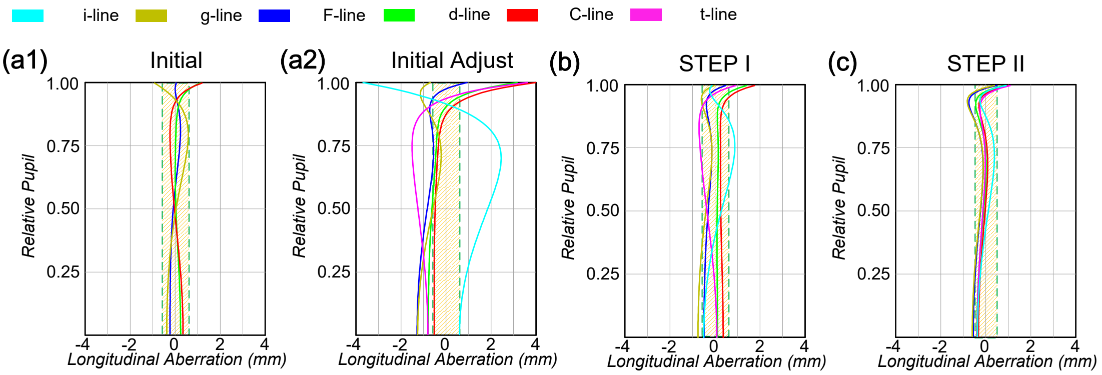

Figure 7.3.: Longitudinal aberration of the initial system and modified systems. The shaded region indicates the DoF of the d-line. (a1) Initial system with g-line to C-line apochromatic correction. (a2) Initial system with slightly adjusted surface curvatures. (b) Step I modified system with i-line to t-line apochromatic correction. (c) Step II modified system with i-line to t-line apochromatic correction and enlarged NA = 0.95.

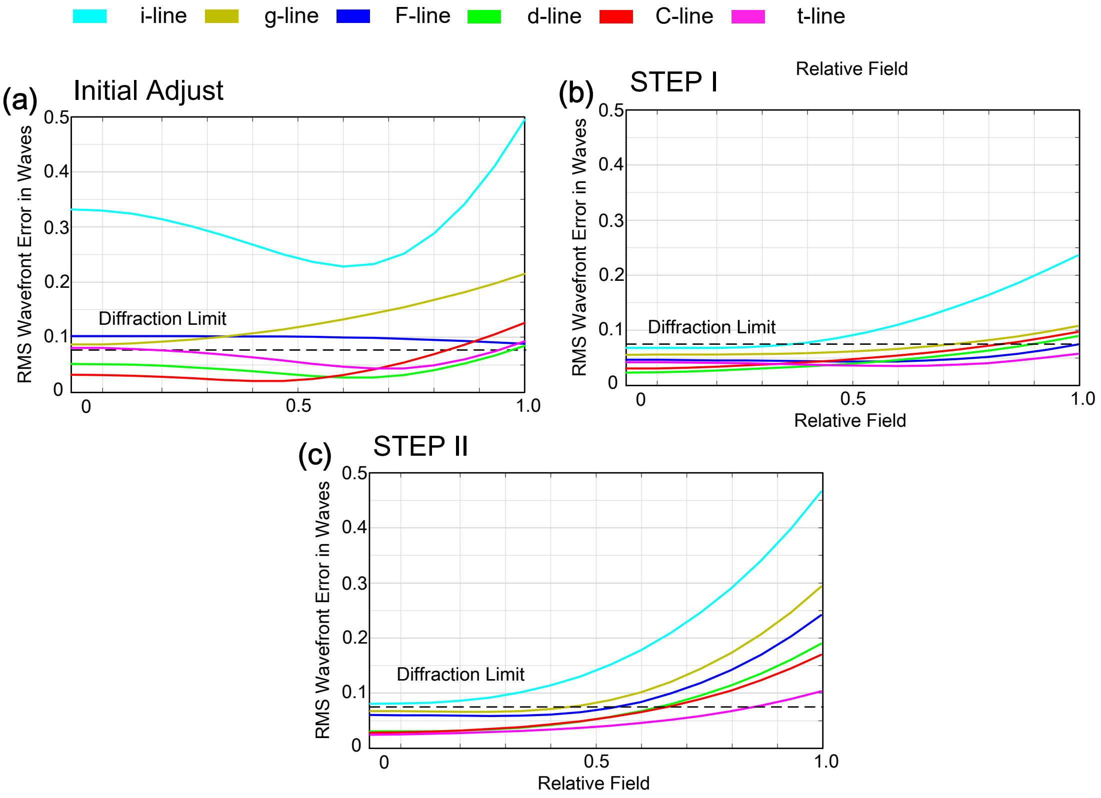

Figure 7.4.: RMS wavefront error of the initial system and modified systems. The dashed line shows the 0.0714 λ diffraction limit given by the Marechal criterion. (a) Initial system with slightly adjusted surface curvatures, corresponding to (a2) in Figure A7.4. (b) Step I modified system with i-line to t-line apochromatic correction. (c) Step II modified system with i-line to t-line apochromatic correction and enlarged NA = 0.95.

In the first step, to keep the “P(PN)0” type (d) optical power distribution, two lens modules are utilized locally in the front and middle group. To reduce the axial chromatic aberration, which results from the extended working spectrum, and to further restrain the spherical aberration, applying the front group lens module No. 6, the “Middle Glass” S-YGH51 ($n_d = 1.755,\ \nu_d = 52.32$) is used instead of the LAK31 ($n_d = 1.697,\ \nu_d = 56.42$) in the re-optimized front quasi-aplanatic meniscus lens owing to its higher refractive index and low dispersion. The material also has low autofluorescence, which is suitable for high-contrast fluorescence imaging. Furthermore, applying the middle group lens module No. 1 and No. 2, materials of the two negative components in the cemented triplet in the middle group are changed from BPM4 ($n_d = 1.613,\ \nu_d = 43.84,\ P_{ig} = 1.3229,\ P_{Ct} = 0.7875$) to N-KZFS4 ($n_d = 1.613,\ \nu_d = 44.49,\ P_{ig} = 1.3015,\ P_{Ct} = 0.7933$) to achieve better chromatic correction for the UV and IR range. The surface curvatures of the second cemented doublet and the triplet are re-optimized. Keeping identical first cemented doublet and rear lens as the initial system, axial chromatic aberration is apochromatic corrected from i-line to t-line, and the field performance is also corrected as diffraction-limited only except i-line.

In the second step, due to the enlarged NA, a single quasi-aplanatic lens is not sufficient to collect the high NA. Combining the lens module No. 3 and No. 6 of the front group, a GFK70 ($n_d = 1.569,\ \nu_d = 68.37$) aplanatic shell-lens is inserted behind the front lens. Furthermore, to smoothen the ray path and efficiently collect the high NA, adopting the lens module No. 5 of the middle group, the shape of the first cemented doublet is changed from bi-convex to meniscus. However, this feature slightly hampers the correction of spherochromatism and axial chromatic aberration. To correct the chromatic aberration and control the zonal error, the second cemented doublet is changed to a cemented triplet (middle group lens module No. 7), which is composed of weak apochromatic cementing on one side (S-FPL53+N-KZFS11) and strong Merte cementing (N-KZFS11+S-FPL51) on the other. Consequently, the axial chromatic aberration over the wide spectrum, spherical aberration including zonal error and the spherochromatism are well corrected for the high NA. However, since the rear group only consists of a single meniscus doublet, although the field curvature can be corrected, it is difficult to control the coma induced by the high NA, resulting in the tremendously increased wavefront error at the boundary field. To further improve the field performance, Gauss type or Petzval type rear groups should be utilized.

7.2 Synthesis of New Structures from Basic Lens Modules

In the second example, the basic lens modules are used to synthesize a Plan-apochromate 40×/1.20 SF20 oil-immersion objective with *class (c)* chromatic correction and *class 4* field correction. The systems should be corrected for infinite-conjugate with 200mm tube lens, and the parfocal length is fixed as 45mm. To gradually change the system structure for clear illustration, listed in Table 7.2, five intermediate steps are set. In the synthesis process, the pupil position is always fixed to realize telecentric object space. Both the spot-radius-based and wavefront-error-based merit functions are used during the synthesis process. Constraints of the element thickness and air spacing are given to assure manufacturability. Certain requirements of longitudinal aberration are also set in the merit function to realize improved zonal spherical aberration and spherochromatism correction. The system layouts of each step systems are demonstrated in Figure 7.5. Their corresponding longitudinal aberrations and RMS wavefront plots are given in Figure 7.6 and Figure 7.7, respectively.

Table 7.2.: System parameters of the 40×/1.20 SF20 oil-immersion objective with 5 intermediate steps.

Parameters	STEP I	STEP II	STEP III	STEP IV	STEP V	Final Goal
Magnification	10×	40×	40×	40×	40×	40×
NA	0.25	0.60	0.85	0.85	0.85	1.20 (Oil)
Spectral Range	F-C	F-C	F-C	g-C	g-C	g-C
Color Correction	Ach- *Class (a)*	Ach- *Class (a)*	Ach- *Class (a)*	Fluor- *Class (b)*	Apo- *Class (c)*	Apo- *Class (c)*
Field Correction	- *Class 1*	- *Class 1*	- *Class 1*	Plan- *Class 5*	Plan- *Class 5*	Plan- *Class 4*

Simple Petzval structure is calculated to realize the low NA Achromate step I system, which is shown in Figure 7.3(a). Simple crown glass K5 ($n_d = 1.522,\ \nu_d = 59.48$) and flint glass F2 ($n_d = 1.620,\ \nu_d = 36.37$) are utilized to form the two positive cemented doublets for axial chromatic correction. The aperture stop is placed at the back focal plane achieving the telecentric object space. The small NA, curved image and secondary spectrum are the most critical residual problems.

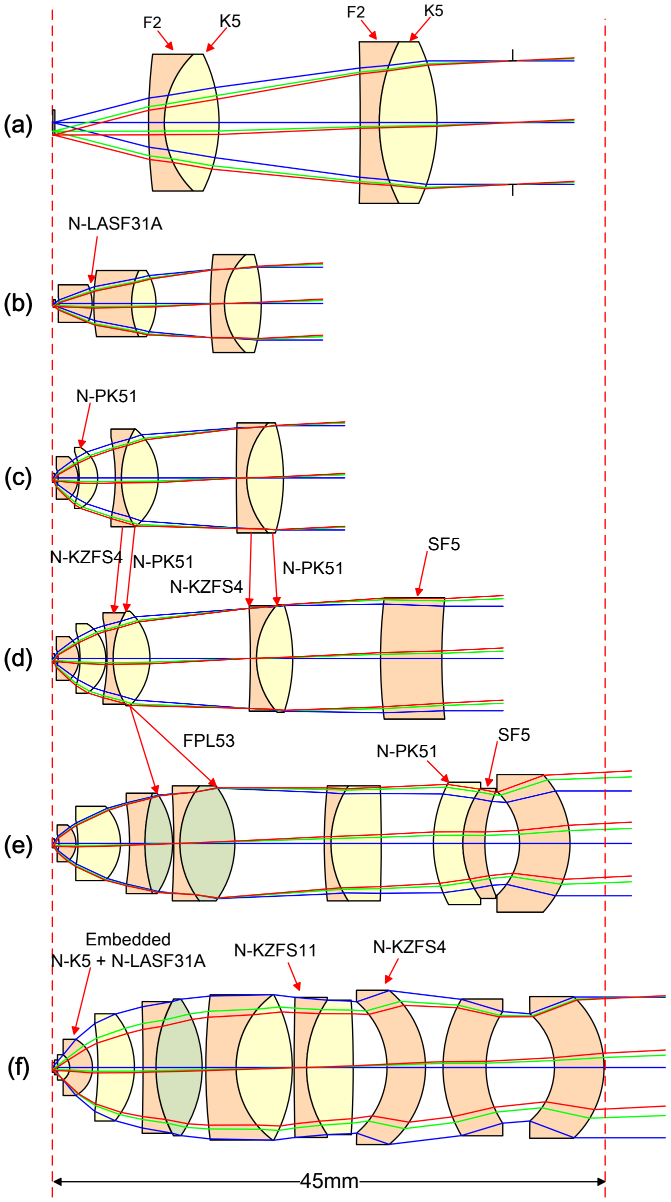

Figure 7.5.: Full process of the 40×/1.20 SF20 oil-immersion objective synthesis. (a) Step I 10×/0.25 Achromate objective. (b) Step II 40×/0.60 Achromate objective. (c) Step III 40×/0.85 Achromate objective. (d) Step IV 40×/0.85 Plan-fluorite objective. (e) Step V 40×/0.85 Plan-apochromate CORR objective. (f) Final design 40×/1.20 Plan-apochromate objective.

In the second step, the NA is first enlarged by applying front group lens module No.1, No.4 and No.5. An Amici lens with curved front surface is used as the front lens of the system in Figure 7.3(b), which is made of the Lanthanum dense flint N-LASF31A ($n_d = 1.833,\ \nu_d = 40.76$) glass with high refractive index and medium dispersion. Owing to its high index, the NA is effectively enlarged to 0.60 and the magnification is adapted to 40×. Taking advantage of lens module No.4, the field curvature of the step II system is not critical. But the residual secondary spectrum and lateral color significantly hamper the chromatic performance of the system.

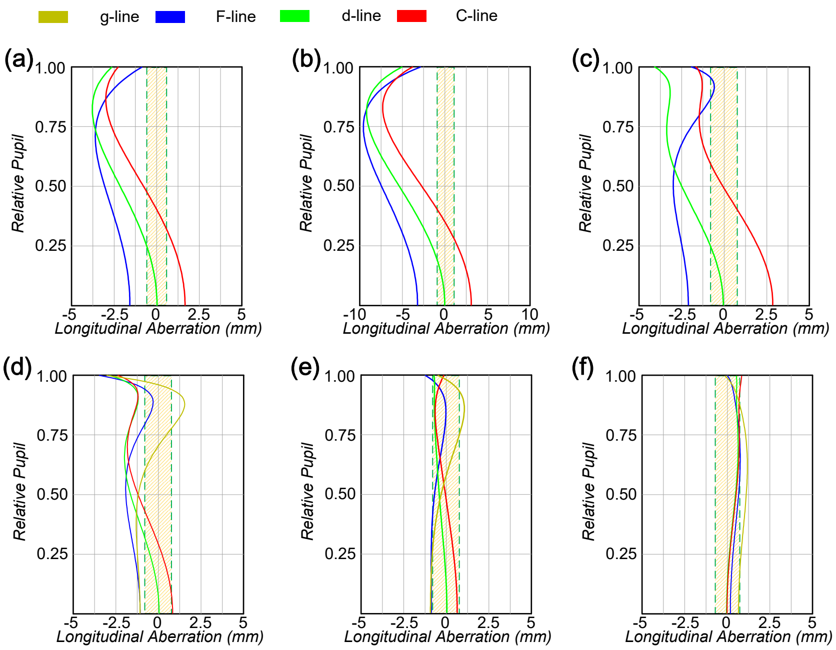

Figure 7.6.: Longitudinal aberration of the final design and synthesized intermediate systems. The shaded region indicates the DoF of the d-line. (a) Step I 10×/0.25 Achromate objective. (b) Step II 40×/0.60 Achromate objective. (c) Step III 40×/0.85 Achromate objective. (d) Step IV 40×/0.85 plan-fluorite objective. (e) Step V 40×/0.85 Plan-apochromate CORR objective. (f) Final design 40×/1.20 Plan-apochromate objective.

In the third step, the NA is further enlarged to 0.85. To control the induced chromatic aberration and restrain the spherical aberration, aplanatic shell lens made of N-PK51 ($n_d = 1.529,\ \nu_d = 76.98$) is inserted behind the front lens and the shape of the first cemented doublet is changed to meniscus, corresponding to the front group lens module No. 3, No. 6 and middle group lens module No. 5, respectively. Although the axial chromatic aberration is achromatic corrected for F-line to C-line, the residual spherical aberration is large. Furthermore, because of the high NA, the simple “two group” structure cannot control the coma and astigmatism. As a consequence, the full field performance is far away from being diffraction-limited.

Therefore, generating the “clear three group” structure is necessary to further improve the chromatic correction and field correction. To realize the medium magnification and high NA, the type (c) “P(PN)0” optical power distribution is selected. Corresponding to the rear group lens module No. 1 and No 6, a thick meniscus lens made of dense flint glass SF5 ($n_d = 1.673,\ \nu_d = 32.21$) is used as the rear group, which significantly compensates the field curvature and lateral color. Furthermore, to correct the high NA spherical aberration including zonal error and to control the secondary spectrum, the simple achromatic class pair K5+F2 is changed to Merte cementing with anomalous dispersive material N-KZFS4+N-PK51 (middle group lens module No.2 and No.3). Thereby, Fluorite level axial chromatic aberration correction is achieved, but the system suffers from large spherochromatism. The single rear lens cannot fully correct the residual coma, thus the performance of the boundary field is not diffraction-limited.

In the fifth step, the axial chromatic correction is further improved by inserting one more cemented doublet into the middle group and changing the N-PK51 glasses to more anomalous dispersive fluor crown FPL53 with strongly curved cementing surface (middle group lens module No.2). Furthermore, Gauss type rear group is utilized with its front part cemented by N-PK51 and SF5 (rear group lens module No.2 and No.7), which also significantly contributes to the correction of axial chromatic aberration and spherical aberration due to the large marginal ray height. Thereby, the apochromatic corrected axial chromatic aberration is achieved with well-corrected spherical aberration. The full field performance is nearly diffraction-limited.

To reach the final goal of an oil-immersion (type A oil) objective, regarding the front group lens module No.8, an embedded front lens with index-matched material should be used instead of the single quasi-aplanatic thick meniscus lens. Therefore, the N-K5 plano-convex small lens is embedded to the N-LASF31A meniscus lens. Furthermore, to control the higher-order spherical aberration for zonal error correction, glass pairs in the second and third cemented doublets in the middle group are changed to Merte cementing with N-PK51+N-KZFS11 (middle group lens module No.3). When it comes to the rear part, separated Petzval type rear group is used instead of the quasi-symmetric Gauss type (rear group lens module No. 3). The second and third lenses are still made of dense flint glass SF5 for lateral color correction. But the first meniscus lens selects anomalous dispersive material N-KZFS4 forms a reverse-bent structure, which can be used to adjust the higher-order spherical aberration and spherochromatism with its air lens effect. This rear group configuration is similar to the example demonstrated in Figure 6.14(a). As the result, the axial chromatic aberration from g-line to C-line is apochromatic corrected with well-controlled zonal error and spherochromatism. However, it is notable that due to the enlarged NA, it is increasingly difficult to correct the coma, therefore 20% vignetting is introduced to the field boundary to achieve the nearly diffraction-limited field correction.

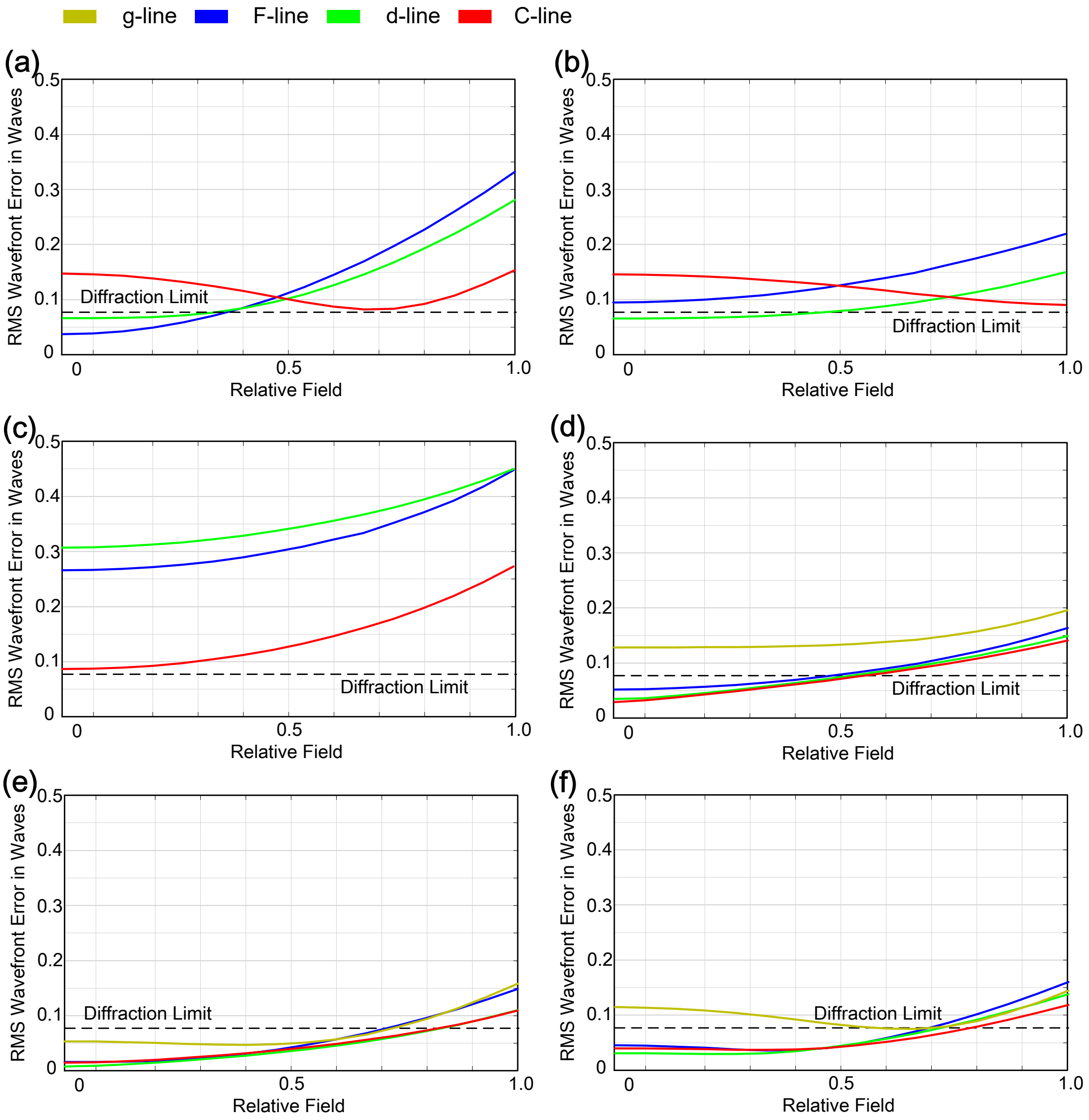

Figure 7.7.: RMS wavefront error of the final design and synthesized intermediate systems. The dashed line shows the 0.0714 λ diffraction limit given by the Marechal criterion. (a) Step I 10×/0.25 Achromate objective. (b) Step II 40×/0.60 Achromate objective. (c) Step III 40×/0.85 Achromate objective. (d) Step IV 40×/0.85 plan-fluorite objective. (e) Step V 40×/0.85 Plan-apochromate CORR objective. (f) Final design 40×/1.20 Plan-apochromate objective.

8. Conclusion

The main objective of this work was to achieve a new point of view of the microscope objective design, by which the structures of the systems can be decomposed to lens modules, and the objectives can be synthesized with systematic modular design approach.

To reach this aim, Chapter 4 first introduced the system database with 484 microscope objectives, which is built up with the patented data from 448 patents through the historical development. By systematically analyzing these systems, new classifications of the objectives are utilized for better understanding of the system complexity. Considering the system performance, instead of the traditional classification with three color correction classes and two field correction classes, there are seven color correction classes and seven field correction classes proposed. Furthermore, classifications based on six etendue zones and six working distance levels are brought up. Besides, the impacts of CORR function, parfocal length and tube lens arrangement on the system complexity are also discussed.

Utilizing these detailed classifications, the change of system structures and parameters for application and manufacturing addressing can be summarized. In Chapter 5, impacts of eight characteristic biomedical research applications and one semiconductor routine application are summarized. Impacts of four common manufacturing requests are also analyzed.

Subtracting off these hidden assumptions, the functionalities of system structures for aberration correction can be analyzed. In Chapter 6, the general aberration correction strategies, optical power distributions and material selection strategies for all the microscope objectives are discussed. Then focusing on the major Zone 1-4 objectives, which have 443 entries (91.5%) out of the database with 484 microscope objectives, lens modules are extracted and analyzed from each structural group, which is also a functional group for specific aberration restraint or correction. Ten modules for the front group, nine modules for the middle group and ten modules for the rear group are well sorted. Beside the behavior of aberration correction, some related application impacts and manufacturing and technology considerations are briefly discussed. Nine modules out of these 29 lens modules were well described in the literature. They are analyzed from the new point of view and compared with the new-found correction schemes.

Finally, utilizing these 29 lens modules as building blocks, as a reverse process, two examples are given in Chapter 7 with different considerations of system synthesis. First, as a typical system modification for new applications, the lens modules can be inserted locally to the available system by keeping the basic structure and optical power distribution for invariant manufacturing and technology considerations. Second, synthesizing the basic lens modules, it is feasible to generate arbitrary new structures for arbitrary applications. But this method entails a risk of over-engineering to the system design. In practical use, trade-off between the complexity and modularity might be made.

Thereby, the systematic analysis and design approach of the microscope objective is successfully achieved. But three aspects should be emphasized, which can be modified or extended in future. First, although the patents are good sources to acquire the manufacturing requests, most of the manufacturing and technology considerations are kept as secrets by the manufacturers. Furthermore, the production of the highly complicated microscope objectives also depends on the sophisticated mechanical design. To completely address the manufacturing requests, it is necessary to obtain more information from the industry. Second, this new point of view can be extended to other conventional optical systems, e.g., photographic objectives. To extend the etendue and create systems with medium NA and medium field size for future demands, both the building blocks from aperture-dominant systems and field-dominant systems should be systematically utilized. Third, it is promising to apply this modular design approach to the future AI-aided optical design. Turning the single unit from the surface property to the lens module property can reduce the complexity of the network. However, so far, the summarized lens modules are empirical models and the interfaces of the modules are not well defined. For pupil matching, the lens units should be re-scaled and re-optimized. Therefore, during the system synthesis, personal design experience is still used for more efficient optimization. To reach the final goal of automatic and systematic synthesis, analytical models must be built up.

Appendix I: Iterative Paraxial Raytracing

Compared with the conventional methods, marginal ray tracing using the new iterative approach is schematically illustrated in Figure A1.1. The RONA and RINA indicate the real object space and image space numerical apertures, respectively, whereas the PONA and PINA refer to the corresponding paraxial object space and image space numerical apertures. The h_R and h_P demonstrate the real marginal ray height and paraxial marginal ray height, respectively. The EnP and ExP represent the corresponding positions of the entrance pupil and the exit pupil. In addition, the blue sphere demonstrates the real pupil fulfilling the sine condition (or isoplanatism), whereas the red plane gives the pupil plane under paraxial approximation.

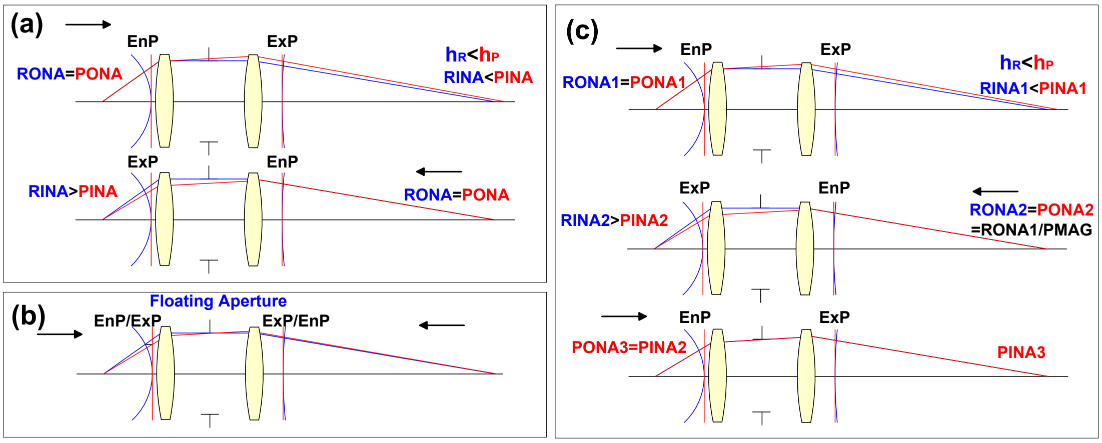

Figure A1.1.: Comparison of three raytracing methods. (a) Conventional raytracing method. The aperture is set by object space NA. (b) Conventional raytracing method. The aperture is defined by the floating aperture stop size. (c) The new iterative raytracing method with three iterations. The aperture is set by object space NA.

In Zemax/OpticStudio^{TM}, there are six aperture types defining the aperture size of the optical system. Given that the apertures of the microscope objectives are always specified by NA, it is intuitive to use the object space NA (ONA) to define the aperture for the conventional raytracing method (a). Under this circumstance, the software sets the real object NA (RONA) identical to the given value. Therefore, for the high NA systems, the paraxial angle can exceed the theoretical maximum value of 0.707. Consequently, the following paraxial ray heights might be far larger than the real ray heights, which is an unrealistic scenario. When the raytracing direction is reversed, the new RONA and PONA can be set with the low NA, which can be calculated as the objective specified NA divided by the paraxial magnification. The paraxial magnification is obtained from the paraxial chief ray tracing from the high NA side to the low NA side, which is reliable because of the small field size. As the deviations of the real and paraxial entrance pupils on the low NA space are very small, the resulting paraxial image space NA (PINA) on the high NA side represent the practical paraxial aperture, which is smaller than the real image space NA (RINA). Utilizing the conventional method (a), the real raytracing is quasi-consistent, whereas the paraxial raytracing is prone to large errors.

To keep the real raytracing and paraxial raytracing consistent for different raytracing directions, the conventional method (b) utilizes the type “Float by STOP size” to define the aperture size. When the “real ray aiming” is activated, the boundary of the aperture STOP, the spherical entrance pupil and the spherical exit pupil are conjugated with the real raytracing. Both the real and paraxial marginal ray tracing start from the aperture STOP, which locates in the middle of the systems. Therefore, the paraxial ray height h_P and real ray height h_R on the aperture STOP are identical. It is self-evident that the fulfillment of the “real ray aiming” and “paraxial ray aiming” cannot be achieved simultaneously. Hence, under this circumstance, the paraxial pupil edge cannot be accurately found. Although the resulting paraxial ray data are quasi-consistent for different raytracing directions, they might reach unrealistic values when the system has extremely high NA, e.g., NA>0.9.

In the new iterative approach (c), the first two steps of raytracing are identical to the conventional method (a), but after the PINA2 is achieved according to the raytracing from the low NA side to the high NA side, it is used as the ONA again to trace the paraxial ray back with the activation of the paraxial ray aiming. To further improve the accuracy of the paraxial NA, the obtained PINA3 can be used as the RONA4=PONA4 and then the raytracing is operated from the low NA side to the high NA side again for the next iteration. Typically, only with the demonstrated three steps, the accuracy of the paraxial data is sufficient to evaluate the aberrations.

Appendix II: Historical Review

A2.1 From Lister to Abbe

Figure A2.1 illustrates the early stage of the microscope objective evolution in the 19th century. Utilization of an aplanatic lens with achromatic correction, which was first introduced by Lister in 1830 with a pair of planoconvex cemented doublet, can be regarded as the start of modern microscope objective development. Petzval modified the design in 1843 by optimizing the planar surfaces to compensate spherical aberration, coma and astigmatism. Furthermore, because of the long separation of the two doublets, according to Petzval's law, the field curvature can also be controlled under low aperture and small field size. It is also notable that the aperture stop was sometimes placed at the rear focal plane of the objective, forming a telecentric object space. In fact, the modified Petzval type is nowadays well known as the Lister type two-group microscope objective.

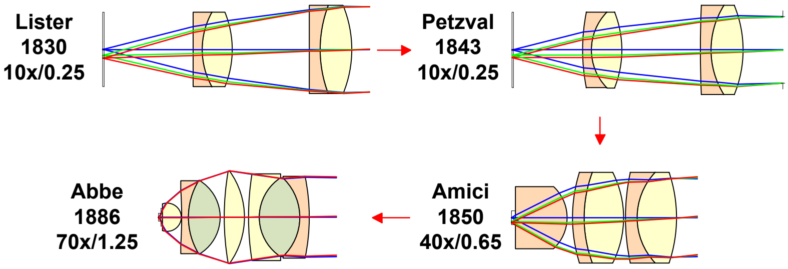

Figure A2.1.: Early stage of two-group microscope objective development in the 19th century.

However, these two simple two-group objective types can only correct small NA (~0.25). To afford the high NA, as the next evolutionary step, Amici introduced an aplanatic-vertex lens (Amici lens) as the front lens in 1850. According to the functionality of an aplanatic lens, the NA can be enlarged by a factor of approximately n^2 without introducing spherical aberration, where n is the refractive index of the lens material. Nevertheless, with the increasing NA, the field curvature of a large field becomes critical. To achieve a similar system throughput as Lister type, the field size of the Amici type objective must be reduced. Hence the Amici type can only be used for objectives with medium magnification and medium NA, e.g., 40×/0.65. By the end of the 19th century, the success of Carl Zeiss factory achieved lots of breakthroughs in creating new lens structures. Utilizing the Schott glasses and anomalous dispersive materials, Abbe invented the first Apochromate oil-immersion objective lens (70×/1.25). Until the inventions of Abbe, the fundamental forms of two-group microscope objectives were well developed without patenting and the design principles are very clear. Methods that use aplanatic surfaces to correct spherical aberration, flint and crown glasses (achromatic material selection) combination to compensate chromatic aberration, and anomalous dispersive material (apochromatic material selection) to correct secondary spectrum are well described in many literature.

A2.2 Lens Evolution until the First Peak Period

Development of two-group objectives continued in the first half of the 20th century. The conventional structures were patented by various companies during this period. There was a trend during this period to achieve larger field of view with extended working distance, excellent chromatic correction and field flatness. Thus, until the end of the first peak period of patenting, namely between 1965 and 1975, two major microscope objective types: the three-group objectives and the double-Gauss type objectives, were invented. The infinite-conjugate correction also became more popular. An overview of the lens evolution during this period is demonstrated in Figure A2.2.

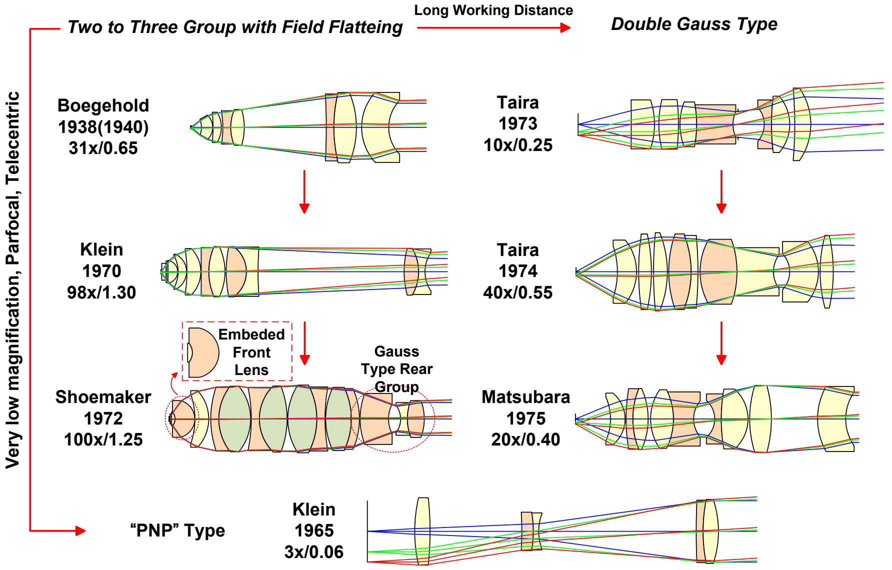

Figure A2.2.: Modern microscope objective development for field flattening and extended working distance. "PNP" type very low magnification telecentric parfocal objective was also invented during the first peak period.

In 1938, Boegehold first reported the well-known method for field curvature correction by using a thick meniscus lens in the rear group to compensate Petzval curvature [60]. After the World War II, two-group objectives were further modified with a complicated front group that corrects spherical aberration and axial chromatic aberration, and a remote rear group with a thick meniscus lens for field curvature and lateral color compensation, e.g., 98×/1.30 Klein 1970 [77]. The complicated front group can be divided into a high NA collecting front group, which typically consists of several aplanatic lenses, and an aberration correcting middle group, which typically comprises a set of cemented doublets or triplets. Development of these highly sophisticated objectives matured during the first peak period. As a milestone, Shoemaker patented the first “clear-three-group” Plan-apochromate oil-immersion objective in 1972 [78], which consists of an embedded front lens for NA enlargement and a quasi-symmetric Gauss type rear group for field correction. This system type became the basic structure of high NA immersion microscope objectives until now.

In the conventional high NA objectives, the use of the Amici lens results in a small working distance. To extend it to satisfy the demand from inverted microscope, lens modules from typical photographic objectives were adopted. Klein (4×/0.14) [77] and Taira (10×/0.25) [79] first utilized a modified double-Gauss structure to design a low magnification Plan-achromate microscope objective with a low NA. However, when the NA increases, the classical double-Gauss type cannot provide sufficient optical power with excellent aberration correction. Aplanatic-concentric lenses were inserted into the front group to enlarge the NA for long working distance without introducing spherical aberration, e.g., Taira 40×/0.55 [80]. Furthermore, to control the field curvature and coma, a thick meniscus lens was utilized as a rear group, which resembles the structure in “clear-three-group” systems, e.g., Matsubara 20×/0.40 [63].

Considering the very low magnification (1×~4×) objectives, to fulfill the requirements of telecentric objective space and parfocality, a special “Positive-Negative-Positive” (“PNP”) type was invented, which consists of a positive front group as the field lens, a negative middle group with cemented lenses and a positive rear group with cemented lenses and meniscus lenses [81]. Distributing the optical power into these three groups, the field curvature can be controlled and the telecentric object space can be achieved simultaneously. Nevertheless, since the distance between the lens front to the objective shoulder must be controlled within the parfocal length, it is increasingly difficult to design the systems with decreasing magnification. Therefore, there are very few objectives reaching 1× or lower magnifications.

A2.3 Advanced Lens Evolution after 1970s

Most of the basic structures of modern microscope objectives were invented before 1970. So far, the design principles for color correction, field flattening and working distance extension have been well discussed in literature and are well known to most optical designers. In the past 40 years, further developments were driven by the great variety of applications. However, the impact of these applications and manufacturing requests are not clear to most optical designers, and thus the new design principles are hidden under the shadow. The milestone steps of lens evolution are illustrated in Figure A2.3, where the objectives for biomedical research applications and semiconductor industry are utilized as the representative research application and routine application, respectively.

The first change was the creation of objectives with correction function (CORR). The CORR objectives appeared in the middle of 1970s, which were invented to adjust the tolerance of the cover glass (CG) thickness, which deviates from the standardized value, e.g., 0.17 mm [82]. Furthermore, microscope objectives developed for multi-immersion were first reported by Carl Zeiss in 1975 [83]. Around 1980, owing to the increasing demand to observer samples in cell culture dishes, inverted microscope became popular for biomedical applications. Consequently, the objectives should be designed for the dish thickness, e.g., 0.8-1.2 mm, and with long working distance [84]. Since the thickness of the dish was not standardized as the cover slip, it is necessary to design the objective with a wider range of CG adjustment.

In the 1980s, the application segmentation became clear: the research applications, especially for biomedical use, and the routine applications, especially for semiconductor inspection. Concerning the biomedical applications, fluorescence microscopy was the first game changer. Since UV light is widely used for excitation, the objective transmittance for the specific UV spectral lines (e.g., 340, 365 nm) should be improved for epifluorescence setup. Besides, to efficiently collect the weak fluorescence emitted from the specimen, the objective lens should be designed with a larger NA, which enhances the resolution simultaneously. From the beginning of 1980s, utilizing new types of glasses with better UV transmission, vendors patented microscope objectives specifically designed for fluorescence microscopy [85]. Through 1980s, invention of objectives with improved chromatic correction benefited from new glass types with anomalous dispersion. Various correction methods for CORR objectives were also developed, resulting in a set of highly sophisticated "clear-three-group" objectives.

In the 1990s, to fulfill the requirement from the widely used confocal setup, special design principles were exploited to create complicated rear groups, thus realizing nearly flattened field. For the confocal depth imaging, many water-immersion objectives were designed to replace the oil-immersion objectives to realize index matching for biological sample observation [86].

Coming into the 21st century, the biomedical research interest was changed from simple cell structure imaging to both observing the cell structures and the behavior of molecules, which should be observed with live cells. However, the live cell observation requires different environmental conditions from the conventional specimen observation, such as temperature and immersion medium. The multi-adjustment should be incorporated into the CORR objective design [71]. Another evolution was driven by the requests for high contrast imaging in fluorescence microscopy. To avoid the strong autofluorescence, glasses should be carefully selected, and system structure was also modified to reduce the stray light.

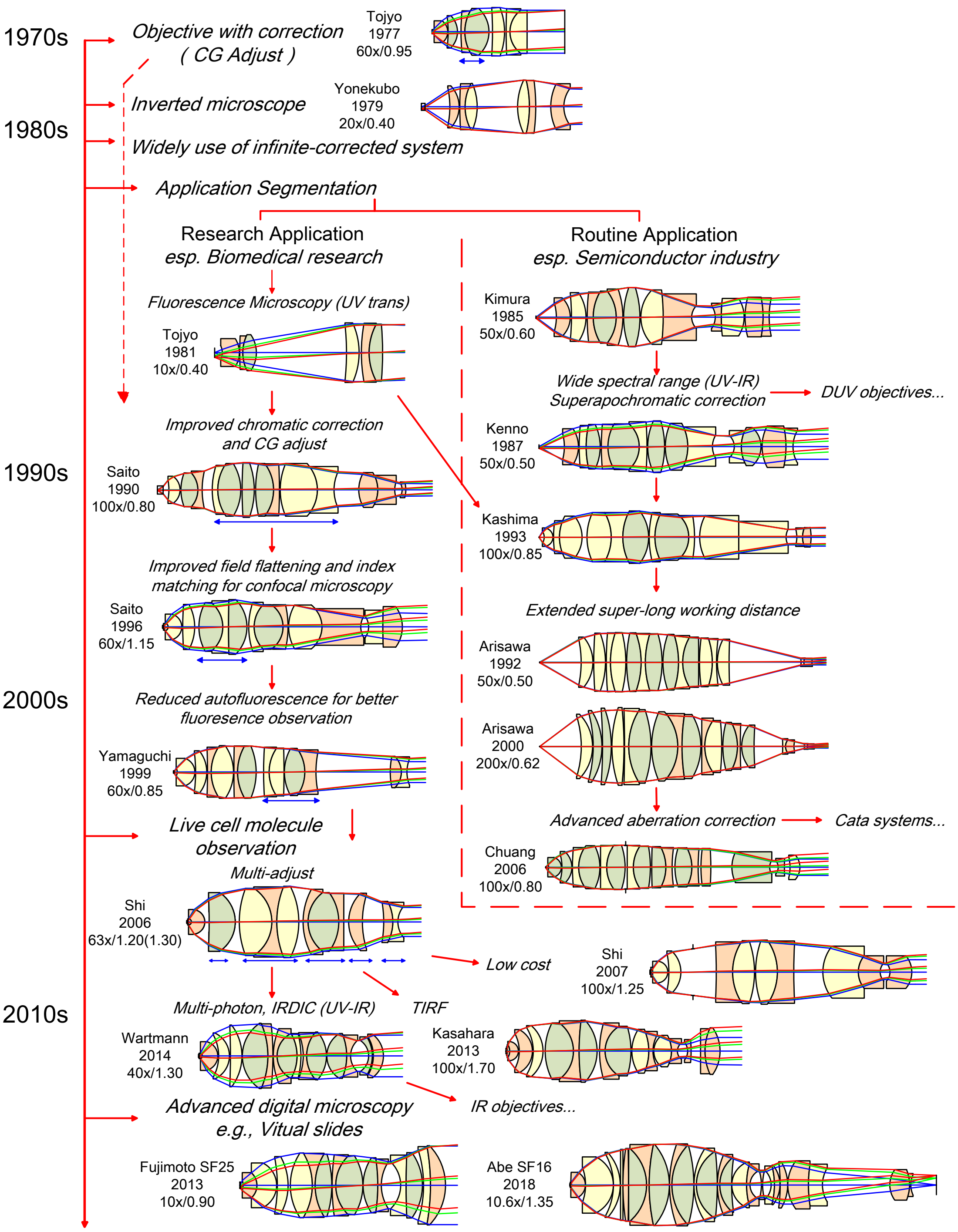

Figure A2.3.: Advanced modern microscope objective development corresponding to application segmentation. The blue arrows indicate the moving groups for CORR function.

When it comes to the semiconductor inspection objectives, after adopting the infinity optics in 1980s [87], the evolution mostly resulted from the extension of working spectrum. For one thing, because the YAG laser is used for laser processing during semiconductor device repairing, the microscope objective should be apochromatic corrected for the visible spectrum for observation, together with the specific wavelength of YAG laser and its harmonics for laser processing, which reaches IR at 1064nm and UV at 355nm [88]. In these objectives, the glass pairs should be carefully selected to realize the superapochromatic correction. For another, because the resolution is improved with decreasing wavelength, the same as lithographic projection systems, UV/DUV light sources were widely utilized for semiconductor inspection and operation. However, optical materials with excellent transmittance in DUV spectrum (wavelength below 280 nm) are limited. Hence the following two types of objectives were invented:

1. DUV objectives corrected for a very narrow bandwidth in DUV, e.g., 193, 248 nm, and a conjugated single visible or IR wavelength for autofocus. Since calcium fluoride and fused silica are the only two common materials that can be used for this wavelength, the system complexity significantly increases. They are excluded from further analysis and discussion.
2. UV-capable objectives achromatic corrected for visible spectrum and a conjugated UV wavelength. Due to the limit of material, the corrected UV wavelength is typically around i-line [89] and can reach 266 nm by using calcium fluoride and fused silica with certain sacrifice of visible correction [90].

The next evolution focused on further extension of the working distance. The conventional long working distance objectives can achieve maximum $\kappa \approx 2.0$. However, with increasing magnification, the effective focal length reduces, resulting in insufficient working distance for operation. Additional shell lenses and special power distribution were exploited to further enlarge the working distance. In the state-of-the-art 200× objective, the κ exceeds 13.0 [43]. After 2000, catadioptric layouts are used for semiconductor objectives to realize extreme aperture and field size. Furthermore, many designs focused on advanced field and chromatic correction, including the chromatic variation of coma, to generate uniform resolution over the full field [91]. Modern microscopy technologies, such as fluorescence microscopy and confocal microscopy, are also applied to semiconductor microscopy through its development from 1990s.

In the recent decade, the latest development of microscope objectives for biomedical use mostly focused on the application of advanced fluorescence microscopy. It is notable that many design principles utilized for semiconductor applications were also adopted. For instance, in multiphoton microscopy, IR light is used for excitation and the fluorescence is generated at UV and visible range. With epi-illumination setups, the microscope objective must be superapochromatic corrected from UV to IR [92], where the glass selection method is similar to what is used in the superapochromatic semiconductor objectives. The next trend of the advanced microscope objective design is to fulfill the requirements from the super-resolution methods. TIRF microscopy is particularly considered because of its requirement of system NA larger than 1.38. Utilizing special immersion oil, the state-of-the-art 100× objective lens can reach extreme NA of 1.70 [39]. Other objectives designed for popular localization microscopy methods were also proposed by the vendors. Moreover, based on the development of digital sensor, objective with high NA but low magnification is of interest to achieve high resolution with wide field, particularly for virtual slide microscopy. The objectives should be corrected for far larger etendue than the conventional systems (typically $G<0.9503$ mm^2). Their structures cannot be simply divided into three groups. Many of the utilized special structures significantly balance the higher-order aberrations but result in critical sensitivity. In recent years, new microscope objectives with highest etendue have been patented for virtual slide microscopy. The state-of-the-art system (Fujimoto 10×/0.90 SF25) achieves $G=3.976$ mm^2 [37]. Some other systems do not only realize high NA under low magnification, but also eliminate vignetting (Abe 10.6×/1.35 SF16) [93], which is similar to the advanced semiconductor objectives. However, consequently, the parfocal length and thread diameter cannot be controlled within the conventional value. It is notable that, despite these advanced features, in the recent decade, lots of simple microscope objectives have also been developed to ensure better system tolerance for low-cost mass production.

Appendix III: Overview of the Microscope Objective Database

An overview of the microscope objective database is given in Table A3.1, where the “Mag.” stands for the objective magnification and “F.N.” means the field number (intermediate image diameter SF). The conjugate types of the microscope objectives are given in “Conjugate”, where finite-conjugate systems are marked with “fin” and the tube lens focal lengths are given for the infinite-conjugate systems. The “Color”, “Field” and “W.D.” represent the color correction, field correction and working distance classes, respectively, which are defined in Chapter 4.2. All the systems are set with the raytracing direction from the high-NA object space to the low-NA image space to avoid the non-consistent setup in the image space, e.g., the conjugate type and tube lens arrangement.

When the systems are built up from the patents, if it is applied (for most of the cases), the longitudinal aberration curves are used as the criteria to evaluate the system performance. However, in some patents published before 2000, the claimed longitudinal aberration cannot be achieved by the patented structural data. Under this circumstance, the systems are reoptimized. To keep the intention of the patent, the structure of the system should be maintained, thus fixing the focal length, conjugate, pupil position and all the structural constraints according to the claims in the patents. Starting from the most sensitive group, the surface parameters and some air spacings are reoptimized without changing the materials. The merit function contains spot-based, wavefront-based and aberration-based operands. The final goal is to achieve the claimed longitudinal aberration and acceptable field performance. It is notable that, in many patents, the inventor only patented a lens structure without giving the imaging performance. Some of them can realize an imaging system, for which the original data is kept although the performance is poor. However, some of the patented data can not realize an imaging system. These systems must be reoptimized, but the criterion and merit functions are changed from case to case.

In most of the patents, only the refractive index and Abbe number are given to indicate the material type. However, some common index and Abbe number can be found in the catalogs of various material vendors. For basic achromatic correction *class (a)*, its impact on the system performance is slight. But when it comes to the extended spectrum correction, the material must be carefully fitted to realize the claimed longitudinal aberration. During the process of system construction, a table was summarized containing the preferred materials of each manufacturer. All the fitted glasses are checked again according to this table. In some patents from 1960s to 1990s, the patented index and Abbe number refer to abandoned materials. To solve this problem, I found some old glass catalogs containing dispersive data, e.g., Bausch & Lomb catalog. If the old material cannot be found, the glass should be directly modelled with its index, Abbe number and optimized partial dispersion data.

Table A3.1.: Overview of the 484 systems in the microscope objective database.

No.	Mag.	NA	F.N.	Conjugate	Inventor	Patent No.	Color	Field	W.D.
1	0.5	0.025	25	200mm	Ouchi	USP 6366398-1	(c)	(2)	(I)
2	1	0.025	30	200mm	Arisawa	JP H02-178608	(c)	(2)	(I)
3	1	0.03	22	100mm	Yamaguchi	JP 2007-011092	(c)	(2)	(I)
4	1	0.03	18	fin	Mori	USP 4027951-1	(a)	(2)	(I)
5	1	0.03	25	200mm	Yamaguchi	JP 2009-294518	(c)	(2)	(I)
6	1	0.05	25	200mm	Ouchi	USP 6366398-2	(c)	(2)	(I)
7	1.5	0.045	26.5	180mm	Suzuki	JP H07-306364	(c)	(2)	(I)
8	1.55	0.085	18	fin	Matsubara	JP S50-068538	(b)	(2)	(I)
9	1.8	0.05	30	fin	Taira	USP 3744881-1	(b)	(2)	(I)
10	2	0.055	30	200mm	Shinonaga	JP S62-062316	(c)	(2)	(I)
11	2	0.055	22	180mm	Kurata	JP H08-313814	(a)	(2)	(I)
12	2	0.08	18	fin	Mori	USP 4027951-2	(a)	(2)	(I)
13	2	0.1	25	200mm	Otaki	USP 6128128-1	(c)	(2)	(I)
14	2	0.1	25	200mm	Watanabe	USP 5774272	(c)	(2)	(I)
15	2	0.13	11	180mm	Hayashi	JP 2001-021812	(b)	(2)	(I)
16	2	0.15	22	180mm	Kawano	USP 6069734-1	(c)	(2)	(I)
17	2.5	0.07	26	180mm	Kimura	USP 4501474	(b)	(2)	(I)
18	2.5	0.07	24	182mm	Shoemaker	USP 3659925	(a)	(2)	(I)

No.	Mag.	NA	F.N.	Conjugate	Inventor	Patent No.	Color	Field	W.D.
19	2.5	0.075	18	fin	Ushida	USP 4592624-1	(a)	(2)	(I)
20	2.5	0.075	26.5	fin	Ushida	USP 4592624-2	(a)	(2)	(I)
21	3	0.06	24	200mm	Klein	USP 3176583	(a)	(2)	(I)
22	3	0.09	23	180mm	Suzuki	JP S64-015712	(a)	(2)	(III)
23	3.5	0.09	18	fin	Ziegler	USP 3262363	(a)	(2)	(I)
24	4	0.1	21	fin	Tojyo	USP 4101201	(a)	(2)	(I)
25	4	0.1	24	182mm	Shoemaker	USP 3975087	(a)	(2)	(I)
26	4	0.1	30	fin	Taira	USP 3647282	(a)	(2)	(I)
27	4	0.11	21	fin	Kawano	USP 5239413-1	(a)	(1)	(I)
28	4	0.13	30	fin	Tojyo	USP 4146304	(b)	(2)	(I)
29	4	0.13	30	fin	Tojyo	USP 4166674	(a)	(2)	(III)
30	4	0.13	18	200mm	Hayashi	USP 5532879	(a)	(2)	(I)
31	4	0.13	21	fin	Saito	USP 5216545-1	(a)	(2)	(I)
32	4	0.14	20	fin	Klein	USP 3537773-1	(a)	(1)	(III)
33	4	0.16	26.5	fin	Tojyo	USP 4227773	(a)	(2)	(III)
34	4	0.16	30	fin	Koizumi	JPB S49-020234	(c)	(2)	(I)
35	4	0.16	26.5	180mm	Sakakura	USP 7158310-1	(e)	(2)	(III)
36	4	0.16	30	fin	Koizumi	USP 3883231	(c)	(1)	(I)
37	4	0.2	28	fin	Nakamura	JP S61-275810-1	(c)	(2)	(III)
38	4	0.28	30	180mm	Furuya	USP 2017-0168281-1	(c)	(2)	(I)
39	4	0.35	22	180mm	Kawano	USP 6069734-2	(c)	(1)	(I)
40	5	0.1	18	fin	Ruben	USP 3115538	(c)	(2)	(I)
41	5	0.1	30	fin	Tojyo	JP S51-021837	(b)	(2)	(I)
42	5	0.13	24	200mm	Nakamura	JP H11-174338-1	(e)	(2)	(I)
43	5	0.13	25	200mm	Nakamura	JP H10-221597	(f)	(2)	(I)
44	5	0.14	30	200mm	Arisawa	JP H04-026813-1	(e)	(2)	(IV)
45	5	0.14	30	200mm	Shinonaga	JP S60-098417	(c)	(2)	(III)
46	5	0.7	16	180mm	Yokoi	JP H09-197283	(a)	(6)	(I)

No.	Mag.	NA	F.N.	Conjugate	Inventor	Patent No.	Color	Field	W.D.
47	6	0.2	12	fin	Klein	USP 3443862-1	(b)	(2)	(I)
48	5.88	0.36	26	164.5mm	Wartmann	USP 2015-248001-1	(d)	(1)	(I)
49	5.88	0.4	26	164.5mm	Wartmann	USP 2015-248001-2	(d)	(1)	(I)
50	7	0.25	18	fin	Bernhardt	USP 2822728	(a)	(2)	(I)
51	8	0.18	20	250mm	Klein	USP 3537773-2	(a)	(1)	(III)
52	10	0.2	25	200mm	Toshi	USP 9366850-1	(b)	(2)	(IV)
53	10	0.2	20	fin	Ruben	USP 3041934	(a)	(1)	(I)
54	10	0.21	24	200mm	Nakamura	JP H11-174338-2	(e)	(2)	(III)
55	10	0.25	22	200mm	Toshi	USP 8958154-1	(c)	(2)	(I)
56	10	0.25	21	fin	Kawano	USP 5239413-2	(a)	(1)	(I)
57	10	0.25	26.5	180mm	Konishi	USP 6034825-1	(a)	(2)	(I)
58	10	0.25	21	fin	Tojyo	USP 4150871	(a)	(2)	(III)
59	10	0.25	21	fin	Tojyo	USP 4283123	(a)	(2)	(III)
60	10	0.25	30	fin	Taira	USP 3744881-2	(b)	(2)	(III)
61	10	0.25	12	fin	Klein	USP 2713808-1	(a)	(2)	(I)
62	10	0.25	12	fin	Klein	USP 3443862-2	(c)	(2)	(I)
63	10	0.25	12	182mm	Muller	USP 3437398-1	(a)	(2)	(I)
64	10	0.25	16	fin	Petzval	-	(a)	(1)	(I)
65	10	0.25	18	fin	Hayamizu	JPB S39-027285	(a)	(1)	(I)
66	10	0.25	20	fin	Nagano	JP S57-062016	(b)	(2)	(I)
67	10	0.25	20	180mm	Shi	USP 7672057	(a)	(2)	(I)
68	10	0.25	20	225mm	Yamawaki	JP 2012-118340	(a)	(2)	(I)
69	10	0.25	21	fin	Tojyo	USP 4176912	(a)	(2)	(III)
70	10	0.25	22	200mm	Fukutake	USP 6128139	(a)	(2)	(I)
71	10	0.25	24	182mm	Shoemaker	USP 4054369	(a)	(1)	(I)
72	10	0.26	30	200mm	Arisawa	JP H04-026813-2	(e)	(2)	(IV)
73	10	0.28	30	200mm	Shinonaga	JP S60-070412-1	(c)	(2)	(IV)
74	10	0.3	26.5	fin	Nagaoka	USP 5729389-1	(b)	(2)	(I)

No.	Mag.	NA	F.N.	Conjugate	Inventor	Patent No.	Color	Field	W.D.
75	10	0.3	22	200mm	Ono	JP H11-352407-1	(f)	(2)	(I)
76	10	0.3	27	fin	Mizusawa	JP H07-261093	(a)	(2)	(III)
77	10	0.3	30	fin	Nagano	USP 4322136	(a)	(2)	(III)
78	10	0.3	18	180mm	Abe	USP 2018-0364466-1	(a)	(2)	(III)
79	10	0.3	20	182mm	Rybicki	USP 4326779	(b)	(2)	(I)
80	10	0.32	30	fin	Nakagawa	USP 3756698	(c)	(2)	(I)
81	10	0.33	18	180mm	Hatano	USP 6560032-1	(c)	(2)	(I)
82	10	0.37	25	164.5mm	Sprenger	DE 102012016973	(e)	(2)	(I)
83	10	0.4	18	fin	Ushida	USP 4403835-1	(a)	(2)	(I)
84	10	0.4	21	fin	Tojyo	USP 4279477	(b)	(1)	(I)
85	10	0.4	22	180mm	Kajitani	JP 2013-222078-1	(a)	(2)	(III)
86	10	0.4	26.5	180mm	Sakakura	USP 7158310-2	(e)	(2)	(I)
87	10	0.4	25	200mm	Morita	JP 2010-014856-2	(e)	(2)	(I)
88	10	0.4	25	200mm	Watanabe	JP 2010-224477-2	(e)	(2)	(I)
89	10	0.4	20	fin	Yamada	JP H08-082744	(c)	(2)	(I)
90	10	0.45	16	167.5mm	Kashima	USP 5191473	(a)	(2)	(I)
91	10	0.45	25	200mm	Otaki	USP 6128128-2	(c)	(2)	(I)
92	10	0.45	28	fin	Nakamura	JP S61-275810-2	(c)	(2)	(I)
93	10	0.5	22	200mm	Suenaga	USP 5920432-1	(c)	(4)	(I)
94	10	0.6	22	180mm	Abe	USP 2017-0261736	(a)	(7)	(VI)
95	10	0.6	22	180mm	Kajitani	JP 2012-173491	(a)	(6)	(I)
96	10	0.8	22	180mm	Yonetani	USP 7663807	(c)	(6)	(I)
97	10	0.9	25	180mm	Fujimoto	USP 8350904-1	(c)	(6)	(I)
98	10.6	0.9	15.9	fin	K. Abe	USP 9939622-1	(c)	(7)	(I)
99	10.6	1.35	15.9	fin	K. Abe	USP 9939622-2	(c)	(7)	(II)
100	11	1.17	5	fin	Blasenheim	USP 6510007	(c)	(3)	(II)
101	12	0.15	18	164.5mm	Bauersfeld	GB 306084	(a)	(2)	(IV)
102	13.5	0.35	10.8	fin	Maeda	USP 4002407	(b)	(1)	(I)

No.	Mag.	NA	F.N.	Conjugate	Inventor	Patent No.	Color	Field	W.D.
103	15	0.65	22.5	fin*	Miyashita	JP 2009-205063-1	(b)	(5)	(I)
104	16	0.65	18	200mm	Schulz	DE 102017108593	(a)	(4)	(I)
105	16	0.65	18	200mm	Schulz	DE 102017108595	(b)	(1)	(VI)
106	16	0.8	22	200mm	Watanabe	JP 2005-189732-1	(a)	(5)	(VI)
107	16	0.8	22	200mm	Watanabe	JP 2005-189732-2	(c)	(4)	(VI)
108	17	0.3	15	fin	Sonnefeld	USP 2050024-1	(a)	(2)	(I)
109	17	0.45	26.5	180mm	Yamawaki	JP 2007-328014-1	(b)	(2)	(I)
110	18	0.25	26.5	180mm	Hamamoto	JP 2008-102295	(b)	(2)	(IV)
111	18	0.35	22	180mm	Kajitani	JP 2013-222078-2	(a)	(2)	(III)
112	18	0.35	18	fin	Jakubal	DE 1272579	(a)	(2)	(I)
113	20	0.25	22	200mm	Ono	JP H11-352407-2	(f)	(2)	(IV)
114	20	0.3	25	200mm	Toshi	USP 9366850-2	(b)	(2)	(IV)
115	20	0.35	25	200mm	Toshi	JP 2010-066445-1	(c)	(2)	(IV)
116	20	0.35	20	fin	Murayama	USP 5757552-1	(a)	(2)	(IV)
117	20	0.35	24	200mm	Nakamura	JP H11-174338-3	(e)	(2)	(IV)
118	20	0.35	26.5	180mm	Kusaka	JP H09-265044	(c)	(2)	(IV)
119	20	0.4	21	fin	Kawano	USP 5239413-3	(a)	(1)	(I)
120	20	0.4	25	200mm	Yoshida	USP 7848027-1	(c)	(2)	(IV)
121	20	0.4	17	180mm	Takahashi	JP 2007-206404	(f)	(2)	(IV)
122	20	0.4	18	200mm	Amamiya	JP H06-250090-1	(a)	(2)	(IV)
123	20	0.4	20	fin	Mori	JPB S47-037455	(a)	(1)	(IV)
124	20	0.4	21	fin	Suenaga	JP S64-063915	(b)	(2)	(IV)
125	20	0.4	21	fin	Yamagishi	USP 4563060	(a)	(2)	(III)
126	20	0.4	21	fin	Yonekubo	USP 4174151	(a)	(2)	(I)
127	20	0.4	21	180mm	Togino	USP 4521083	(a)	(2)	(III)
128	20	0.4	30	200mm	Arisawa	JP H05-196873-1	(e)	(2)	(IV)
129	20	0.4	31	fin	Matsubara	USP 3925910-1	(a)	(2)	(III)
130	20	0.4	31	fin	Matsubara	USP 3925910-2	(a)	(2)	(III)

No.	Mag.	NA	F.N.	Conjugate	Inventor	Patent No.	Color	Field	W.D.
131	20	0.4	20	fin	Kobaya	USP 3540798	(a)	(2)	(I)
132	20	0.4	20	fin	Matsuki	USP 3514185	(a)	(2)	(I)
133	20	0.4	20	fin	Suzuki	USP 4989957-1	(a)	(2)	(III)
134	20	0.4	20	200mm	Takahashi	JPB S38-026630	(a)	(2)	(I)
135	20	0.4	21	fin	Kurihara	USP 4624535	(a)	(2)	(I)
136	20	0.4	21	180mm	Uetake	JPB S43-015237	(b)	(2)	(I)
137	20	0.4	22	200mm	Fukutake	USP 5889618	(a)	(2)	(I)
138	20	0.4	25	200mm	Ryzhikov	USP 5808807	(a)	(2)	(I)
139	20	0.4	29	200mm	Tojyo	USP 4232941	(c)	(2)	(I)
140	20	0.4	30	164.5mm	Knorr	DE 973566	(a)	(1)	(I)
141	20	0.44	16	fin	Unknown	~ USP 4403835	(a)	(1)	(I)
142	20	0.45	22	200mm	Ito	JP H10-142509	(a)	(2)	(IV)
143	20	0.45	22	200mm	Suenaga	USP 5940220-1	(b)	(2)	(IV)
144	20	0.45	25	200mm	Kudo	JP 2000-035542	(a)	(2)	(I)
145	20	0.45	30	200mm	Shinonaga	JP S60-070412-2	(c)	(2)	(IV)
146	20	0.45	18	180mm	Abe	USP 2018-0364466-2	(d)	(2)	(IV)
147	20	0.46	25	200mm	Yoshida	USP 9030750-1	(c)	(2)	(I)
148	20	0.46	21	fin	Saito	USP 5216545-2	(a)	(2)	(I)
149	20	0.46	30	fin	Itaya	USP 4212515	(a)	(2)	(I)
150	20	0.49	26.5	fin	Nagaoka	USP 5729389-2	(a)	(1)	(I)
151	20	0.5	26.5	180mm	Konishi	USP 6034825-2	(a)	(4)	(I)
152	20	0.5	24	200mm	Nakagawa	JP 2010-134405-1	(f)	(3)	(IV)
153	20	0.5	12	182mm	Muller	USP 3355234	(a)	(1)	(I)
154	20	0.5	20	fin	Tomimatsu	USP 6219189-1	(b)	(1)	(I)
155	20	0.5	22	200mm	Mizusawa	JP H09-197285	(a)	(5)	(I)
156	20	0.5	24	182mm	Shoemaker	USP 3552830	(a)	(5)	(I)
157	20	0.5	25	200mm	Mizusawa	USP 5798870	(b)	(5)	(I)
158	20	0.6	12	182mm	Muller	USP 3437398-2	(c)	(4)	(I)

No.	Mag.	NA	F.N.	Conjugate	Inventor	Patent No.	Color	Field	W.D.
159	20	0.6	25	164.5mm	Shi	DE 10317746	(c)	(4)	(I)
160	20	0.65	21	fin	Tojyo	USP 4280757	(b)	(3)	(I)
161	20	0.65	22	200mm	Miyashita	USP 7245425	(c)	(4)	(I)
162	20	0.68	22	180mm	Fujita	USP 8705178	(b)	(4)	(I)
163	20	0.7	22	200mm	Matsumoto	USP 9869879	(c)	(4)	(I)
164	20	0.75	27	fin*	Miyashita	JP 2009-205063-2	(b)	(5)	(I)
165	20	0.75	22	200mm	Toshi	USP 8958154-2	(c)	(4)	(I)
166	20	0.75	13	fin	Yamada	JP H08-082746	(c)	(5)	(I)
167	20	0.75	22	200mm	Suenaga	USP 5920432-2	(b)	(4)	(I)
168	20	0.75	22	200mm	Yamahiro	JP 2003-098438	(c)	(5)	(I)
169	20	0.75	25	200mm	Ito	USP 5729391	(c)	(4)	(I)
170	20	0.75	28	fin	Nakamura	JP S61-275811	(c)	(5)	(I)
171	20	0.75	18	fin	Suenaga	JP H08-082745	(c)	(5)	(I)
172	20	0.75	25	200mm	Ito	JP H11-249024	(c)	(4)	(I)
173	20	0.8	22	180mm	Kasahara	USP 6501603-1	(c)	(4)	(I)
174	20	0.8	22	180mm	Konishi	USP 5739957-1	(b)	(4)	(I)
175	20	0.8	25	164.5mm	Wartmann	DE 2017218169-1	(c)	(1)	(I)
176	20	0.8	26.5	180mm	Hasegawa	JP H08-136816	(d)	(4)	(I)
177	20	0.8	26.5	180mm	Suzuki	JP H05-119264	(c)	(4)	(I)
178	20	0.85	25	164.5mm	Wartmann	DE 2017218169-2	(d)	(1)	(I)
179	20	0.9	18	164.5mm	Nobis	USP 9696536	(d)	(4)	(I)
180	20	0.9	30	180mm	Fujimoto	USP 7982961	(c)	(6)	(I)
181	20	0.94	22	180mm	Kasahara	USP 6501603-2	(c)	(4)	(VI)
182	20	0.95	25	180mm	Fujimoto	USP 8350904-2	(c)	(6)	(I)
183	20	0.95	30	180mm	Abe	USP 9746658-1	(c)	(7)	(I)
184	20	0.95	22	200mm	Watanabe	JP 2007-133071-1	(c)	(4)	(II)
185	20	0.95	22	200mm	Watanabe	JP 2007-133071-2	(c)	(4)	(II)
186	20	1	20	164.5mm	Wartmann	USP 7382542-1	(d)	(6)	(VI)

No.	Mag.	NA	F.N.	Conjugate	Inventor	Patent No.	Color	Field	W.D.
187	20	1	23	164.5mm	Matthae	USP 8988780	(c)	(6)	(VI)
188	20	1	22	200mm	Yoshida	JP 2011-075982-1	(d)	(6)	(II)
189	20	1	23	164.5mm	Wartmann	DE 102011109783	(g)	(6)	(II)
190	20	1.45	30	180mm	Abe	USP 9746658-2	(c)	(7)	(II)
191	24	0.25	12	fin	Luneburg	USP 2538841	(a)	(1)	(I)
192	25	0.4	30	fin	Maeda	USP 3989317	(a)	(1)	(I)
193	25	0.5	12	fin	Klein	USP 2713808-2	(a)	(5)	(I)
194	25	0.5	14	fin	Klein	USP 3592530	(a)	(3)	(I)
195	25	0.6	10	107mm	Tanaka	USP 5555133	(c)	(3)	(I)
196	25	0.8	18	164.5mm	Shi	USP 7782539	(c)	(4)	(II)
197	25	1.05	18	180mm	Saito	USP 7869132	(e)	(4)	(II)
198	25	1.1	25	200mm	Yamaguchi	JP 2015-135440-1	(e)	(4)	(II)
199	25	1.1	22	200mm	Yoshida	JP 2011-075982-2	(d)	(4)	(II)
200	30	0.55	20	fin	Tomimatsu	USP 6219189-2	(b)	(4)	(I)
201	30	0.65	18	fin	Ruben	USP 3174396	(a)	(3)	(I)
202	30	0.65	18	fin	Ziegler	USP 3272072	(a)	(1)	(I)
203	30	1.1	22	180mm	Kasahara	USP 8358469-1	(c)	(4)	(II)
204	31	0.65	9	164.5mm	Boegehold	USP 2206155	(a)	(3)	(I)
205	39	0.65	18	fin	Bertele	DE 1164700	(a)	(5)	(I)
206	40	0.42	26.5	180mm	Konuma	JP H09-090230	(c)	(4)	(IV)
207	40	0.5	18	fin	Yamada	JP S60-063513	(b)	(4)	(IV)
208	40	0.5	20	fin	Murayama	USP 5757552-2	(a)	(5)	(IV)
209	40	0.5	21	fin	Yamagishi	USP 4591243	(a)	(4)	(IV)
210	40	0.55	18	fin	Yamada	JP S60-260016	(b)	(4)	(IV)
211	40	0.55	24	182mm	Sussmann	USP 4231637-1	(a)	(3)	(III)
212	40	0.55	30	fin	Taira	USP 3806231	(a)	(4)	(III)
213	40	0.55	18	fin	Ushida	USP 4403835-2	(a)	(3)	(I)
214	40	0.55	20	fin	Suzuki	USP 4989957-2	(a)	(5)	(III)

No.	Mag.	NA	F.N.	Conjugate	Inventor	Patent No.	Color	Field	W.D.
215	40	0.55	26.5	180mm	Fujimoto	JP 2002-202457-1	(b)	(4)	(I)
216	40	0.6	18	200mm	Mizusawa	JP H10-221609	(a)	(4)	(IV)
217	40	0.6	22	200mm	Suenaga	USP 5940220-2	(b)	(4)	(IV)
218	40	0.6	22	180mm	Yamawaki	JP 2005-352021	(c)	(4)	(IV)
219	40	0.6	25	fin	Esswein	USP 4953962-1	(a)	(4)	(IV)
220	40	0.6	26.5	180mm	Hayashi	JP 2003-161887	(c)	(4)	(IV)
221	40	0.65	21	fin	Kawano	USP 5239413-4	(a)	(1)	(I)
222	40	0.55	13.5	182mm	Sussmann	USP 4231637-2	(a)	(5)	(III)
223	40	0.65	12	fin	Klein	USP 2713808-3	(a)	(3)	(I)
224	40	0.65	18	fin	Uetake	USP 3623792-1	(a)	(1)	(I)
225	40	0.65	18	fin	Uetake	USP 3623792-2	(a)	(1)	(I)
226	40	0.65	20	fin	Ruben	USP 3102158	(a)	(4)	(I)
227	40	0.65	20	180mm	Kajitani	USP 6441966-1	(b)	(3)	(I)
228	40	0.65	20	200mm	Sharma	USP 6914728	(b)	(4)	(I)
229	40	0.65	21	fin	Nakahashi	USP 4279476	(a)	(1)	(I)
230	40	0.65	21	fin	Tojyo	USP 3893752	(a)	(1)	(I)
231	40	0.65	21	fin	Saito	USP 5216545-3	(a)	(1)	(I)
232	40	0.65	25	164.5mm	Esswein	USP 4362365	(a)	(1)	(I)
233	40	0.65	30	fin	Goto	USP 3879111	(a)	(4)	(I)
234	40	0.66	12	fin	Sussman	USP 4418988	(a)	(1)	(I)
235	40	0.66	24	182mm	Shoemaker	USP 3552831	(a)	(3)	(I)
236	40	0.66	24	182mm	Shoemaker	USP 3902791	(a)	(4)	(I)
237	40	0.66	25	182mm	Shoemaker	USP 3868175	(a)	(3)	(I)
238	40	0.7	26.5	fin	Nagaoka	USP 5729389-3	(a)	(1)	(I)
239	40	0.7	30	fin	Tojyo	USP 4208099	(a)	(5)	(I)
240	40	0.7	30	fin	Uetake	USP 4184747	(a)	(5)	(I)
241	40	0.75	18	200mm	Coussot	USP 4084885-1	(a)	(5)	(I)
242	40	0.75	18	fin	Klein	DE 1186234	(a)	(4)	(I)

No.	Mag.	NA	F.N.	Conjugate	Inventor	Patent No.	Color	Field	W.D.
243	40	0.75	22	180mm	Kajitani	JP 2013-222078-3	(a)	(4)	(I)
244	40	0.75	25	200mm	Misawa	USP 5699196	(b)	(4)	(I)
245	40	0.78	22	180mm	Akahane	USP 2017-0184830	(b)	(5)	(I)
246	40	0.8	20	182mm	Rybicki	USP 4379623	(b)	(4)	(I)
247	40	0.8	25	180mm	Abe	JP H08-292374-1	(c)	(4)	(VI)
248	40	0.85	26.5	180mm	Saito	USP 5444573	(c)	(4)	(I)
249	40	0.85	26.5	180mm	Sakakura	JP 2006-133248	(e)	(4)	(I)
250	40	0.85	30	fin	Uetake	USP 3572902	(c)	(3)	(I)
251	40	0.9	22	200mm	Suenaga	USP 5920432-3	(c)	(4)	(I)
252	40	0.9	26.5	180mm	Sakakura	USP 7158310-3	(e)	(4)	(I)
253	40	0.93	26.5	180mm	Suzuki	USP 5270860	(c)	(4)	(I)
254	40	0.95	18	fin	Yamada	JP S61-275812-1	(c)	(4)	(I)
255	40	0.95	18	200mm	Mizusawa	US H1763	(c)	(4)	(I)
256	40	0.95	25	200mm	Yamaguchi	JP 2010-134218	(e)	(4)	(I)
257	40	0.95	30	fin	Taira	JP S51-135545	(c)	(3)	(I)
258	40	1	18	fin	Tomimatsu	USP 5805346-1	(a)	(5)	(II)
259	40	1	20	180mm	Suzuki	USP 5502596	(c)	(4)	(II)
260	40	1	25	200mm	Watanabe	USP 5798869	(c)	(4)	(II)
261	40	1	26.5	180mm	Adachi	JP H08-292373-1	(c)	(4)	(II)
262	40	1	25	164.5mm	Sprenger	DE 102008020345	(e)	(4)	(VI)
263	40	1.1	22	200mm	Watanabe	USP 7889432	(e)	(4)	(VI)
264	40	1.15	20	164.5mm	Shi	USP 9488817-1	(c)	(4)	(II)
265	40	1.15	22	200mm	Suenaga	JP H10-333044	(c)	(4)	(II)
266	40	1.2	22	180mm	Kasahara	USP 8358469-2	(c)	(4)	(II)
267	40	1.2	22	200mm	Hiraga	JP 2004-029067	(c)	(4)	(II)
268	40	1.2	23	200mm	Okuyama	USP 2003-0043473	(c)	(4)	(II)
269	40	1.2	25	164.5mm	Matthae	USP 7268953	(f)	(4)	(II)
270	40	1.25	22	180mm	Fujimoto	JP 2014-048342	(c)	(4)	(II)

No.	Mag.	NA	F.N.	Conjugate	Inventor	Patent No.	Color	Field	W.D.
271	40	1.25	22	200mm	Yamaguchi	USP 8199408	(d)	(4)	(II)
272	40	1.3	20	164.5mm	Wartmann	USP 7382542-2	(d)	(4)	(II)
273	40	1.3	22	200mm	Yamahiro	JP H11-174339-1	(b)	(4)	(II)
274	40	1.3	25	164.5mm	Brehm	DE 102008006826	(d)	(4)	(II)
275	40	1.3	25	200mm	Furutake	USP 5982559	(b)	(4)	(II)
276	40	1.3	25	164.5mm	Wartmann	USP 9645380-1	(g)	(4)	(II)
277	40	1.3	30	180mm	Abe	USP 9746658-3	(c)	(7)	(II)
278	40	1.38	26.5	180mm	Abe	USP 2018-0113293-1	(c)	(4)	(II)
279	40	1.4	25	164.5mm	Wartmann	DE 102009037743	(d)	(4)	(II)
280	40	1.4	30	180mm	Abe	USP 9746658-3	(c)	(7)	(II)
281	42	0.66	18	182mm	Muller	USP 3132200	(a)	(1)	(I)
282	43	0.24	22	180mm	Y. Suzuki	USP 8928987	(c)	(2)	(I)
283	45	0.8	12	182mm	Muller	USP 3437398-3	(c)	(5)	(II)
284	50	0.4	25	200mm	Toshi	USP 9366850-3	(b)	(2)	(IV)
285	50	0.4	20	200mm	Nakajima	JP H11-167067	(f)	(2)	(IV)
286	50	0.42	30	200mm	Arisawa	JP H05-196873-2	(e)	(2)	(IV)
287	50	0.42	30	200mm	Arisawa	JP H07-020385-1	(f)	(2)	(IV)
288	50	0.42	30	200mm	Shinonaga	JP S63-023119	(c)	(2)	(IV)
289	50	0.45	25	200mm	Toshi	JP 2010-066445-2	(c)	(2)	(IV)
290	50	0.45	22	180mm	Abe	JP H06-175034	(e)	(2)	(IV)
291	50	0.45	24	200mm	Nakamura	JP H11-174338-4	(e)	(2)	(IV)
292	50	0.5	22	200mm	Ito	USP 6181480	(f)	(4)	(IV)
293	50	0.5	26.5	180mm	Kenno	JP S62-049313-1	(f)	(4)	(III)
294	50	0.5	30	200mm	Arisawa	JP H04-220615	(c)	(5)	(IV)
295	50	0.52	24	200mm	Nakagawa	JP 2010-134405-2	(f)	(5)	(IV)
296	50	0.55	22	180mm	Yokoi	JP H08-297247-2	(a)	(5)	(IV)
297	50	0.55	25	200mm	Yoshida	USP 7848027-2	(c)	(5)	(IV)
298	50	0.55	18	200mm	Amamiya	JP H06-250090-2	(a)	(4)	(IV)

No.	Mag.	NA	F.N.	Conjugate	Inventor	Patent No.	Color	Field	W.D.
299	50	0.55	22	200mm	Watanabe	JP H11-223774	(d)	(4)	(IV)
300	50	0.55	25	200mm	Hiraga	USP 6560033	(b)	(4)	(IV)
301	50	0.55	27	180mm	Togino	USP 4540248	(b)	(4)	(IV)
302	50	0.55	30	200mm	Shinonaga	JP S60-070412-3	(c)	(5)	(IV)
303	50	0.6	18	180mm	Abe	USP 2018-0364466-3	(d)	(4)	(IV)
304	50	0.6	22	180mm	Kimura	JP S60-063512	(a)	(5)	(III)
305	50	0.65	25	200mm	Watanabe	JP 2008-122592	(a)	(5)	(III)
306	50	0.65	25	fin	Esswein	USP 4953962-3	(a)	(3)	(I)
307	50	0.7	18	fin	Mori	JP S60-205521	(a)	(3)	(V)
308	50	0.7	26.5	180mm	Yamawaki	JP 2007-328014-2	(b)	(4)	(V)
309	50	0.8	22	200mm	Toshi	USP 8958154-3	(c)	(4)	(V)
310	50	0.8	25	200mm	Yoshida	USP 9341832-1	(c)	(5)	(V)
311	50	0.8	25	200mm	Hiraga	JP 2000-002838	(c)	(4)	(I)
312	50	0.8	26.5	180mm	Yamawaki	JP 2003-075724-1	(c)	(4)	(I)
313	50	0.85	18	fin	Ruben	USP 3138651	(a)	(3)	(I)
314	50	0.85	20	182mm	Danner	USP 4417787	(a)	(3)	(I)
315	50	0.9	22	180mm	Kitagawa	USP 5748372	(a)	(4)	(V)
316	50	0.9	16	fin	~Boegehold	~USP 1578259	(c)	(1)	(I)
317	50	0.95	20	180mm	Smirnov	USP 9285687	(d)	(5)	(I)
318	50	0.95	25	164.5mm	Matthae	DE 10318264	(c)	(4)	(I)
319	50	0.95	26.5	180mm	Saito	JP H07-287169	(c)	(4)	(I)
320	55.9	1.4	25	200mm	K. Suzuki	JP 2003-015046-1	(d)	(4)	(II)
321	59.6	1.4	25	200mm	K. Suzuki	JP 2003-015046-2	(d)	(4)	(II)
322	60	0.6	26.5	180mm	Kenno	JP S62-049313-2	(e)	(4)	(IV)
323	60	0.7	18	fin	Shimizu	USP 4666256	(a)	(5)	(V)
324	60	0.7	22	180mm	Abe	USP 5739958	(b)	(4)	(V)
325	60	0.7	22	200mm	Suenaga	USP 5940220-3	(a)	(5)	(V)
326	60	0.7	22	200mm	Watanabe	JP H10-133118	(a)	(5)	(V)

No.	Mag.	NA	F.N.	Conjugate	Inventor	Patent No.	Color	Field	W.D.
327	60	0.7	26.5	180mm	Shimizu	USP 4588264-1	(a)	(4)	(V)
328	60	0.8	20	180mm	Kajitani	USP 6441966-2	(c)	(4)	(I)
329	60	0.85	25	200mm	Yamaguchi	USP 5861996	(a)	(4)	(I)
330	60	0.95	18	fin	Yamada	JP S61-275812-2	(c)	(4)	(I)
331	60	0.95	21	fin	Matsubara	USP 4037934	(b)	(3)	(I)
332	60	0.95	21	180mm	Tojyo	USP 4059342	(a)	(4)	(I)
333	60	0.95	25	180mm	Abe	JP H08-292374-2	(c)	(4)	(VI)
334	60	1	22	200mm	Watanabe	JP 2006-341170	(b)	(5)	(VI)
335	60	1.1	26.5	180mm	Kasahara	JP 2003-172879	(c)	(4)	(VI)
336	60	1.1	18	fin	Suenaga	JP H11-023976	(b)	(4)	(II)
337	60	1.15	21	fin	Saito	USP 5530590	(c)	(4)	(II)
338	60	1.15	26.5	180mm	Yamamoto	JP 2009-037060	(c)	(4)	(VI)
339	60	1.2	26.5	180mm	Adachi	JP H08-292373-2	(b)	(4)	(II)
340	60	1.2	18	200mm	Mizusawa	JP H09-258107	(b)	(4)	(II)
341	60	1.2	20	fin	Suenaga	USP 5532878	(b)	(4)	(II)
342	60	1.2	25	200mm	Hiraga	JP 2004-184826	(c)	(4)	(II)
343	60	1.2	25	200mm	Yamaguchi	USP 2005-0207021	(d)	(4)	(II)
344	60	1.25	22	200mm	Yoshida	USP 7889433	(e)	(4)	(II)
345	60	1.4	25	200mm	Yamaguchi	JP 2015-135440-2	(d)	(4)	(II)
346	60	1.4	25	200mm	Yoshida	USP 9030750-2	(c)	(4)	(II)
347	60	1.4	18	fin	Shimizu	JP S61-240218	(c)	(4)	(II)
348	60	1.4	18	fin	Hatano	USP 6560032-2	(c)	(4)	(II)
349	60	1.4	18	180mm	Suzuki	USP 5517360	(c)	(4)	(II)
350	60	1.4	22	180mm	Konishi	USP 7486445	(d)	(4)	(II)
351	60	1.4	22	200mm	Mandai	JP 2003-337285	(c)	(4)	(II)
352	60	1.4	22	200mm	Watanabe	JP 2002-341249	(c)	(4)	(II)
353	60	1.4	25	200mm	Yamaguchi	JP 2000-035541	(c)	(4)	(II)
354	60	1.4	25	200mm	Yamaguchi	USP 6519092-1	(c)	(4)	(II)

No.	Mag.	NA	F.N.	Conjugate	Inventor	Patent No.	Color	Field	W.D.
355	60	1.4	26.5	180mm	Fujimoto	JP 2006-113287	(c)	(4)	(II)
356	60	1.4	26.5	180mm	Fujimoto	USP 6747804-1	(c)	(4)	(II)
357	60	1.4	26.5	180mm	Kasahara	USP 6501603-3	(c)	(4)	(II)
358	60	1.4	29	fin	Asoma	USP 4537472	(c)	(4)	(II)
359	60	1.45	22	200mm	Mandai	USP 7046451-1	(c)	(4)	(II)
360	60	1.45	26.5	180mm	Fujimoto	JP 2002-350734-1	(c)	(4)	(II)
361	60	1.48	22	180mm	Fujimoto	USP 7199938-1	(c)	(4)	(II)
362	60	1.5	22	180mm	Abe	USP 2018-0113293-2	(c)	(4)	(II)
363	63	0.8	18	200mm	Coussot	USP 4084885-2	(a)	(4)	(I)
364	63	0.8	21	fin	Tojyo	USP 4251131	(a)	(1)	(I)
365	63	1	20	164.5mm	Wartmann	USP 2006-0018030	(e)	(5)	(VI)
366	63	1.2	20	164.5mm	Shi	USP 9488817-2	(c)	(4)	(II)
367	63	1.2	20	164.5mm	Shi	USP 7349162	(c)	(4)	(II)
368	63	1.4	25	164.5mm	Wartmann	USP 9645380-2	(g)	(4)	(II)
369	65	0.8	18	fin	Kupka	DE 1272578	(a)	(4)	(I)
370	80	0.95	18	250mm	Klein	USP 3380793	(a)	(4)	(I)
371	90	1.3	18	fin	Ziegler	USP 3297393-1	(a)	(1)	(II)
372	95	1.25	18	fin	Hayamizu	JPB S38-024630	(b)	(4)	(II)
373	97	1.2	18	fin	Sharma	AO 24 P2577	(a)	(1)	(II)
374	98	1.3	16	fin	Ziegler	USP 3297393-2	(a)	(1)	(II)
375	98	1.3	25	fin	Klein	USP 3524694	(a)	(4)	(VI)
376	100	0.5	24	200mm	Nakamura	JP H11-174338-5	(e)	(5)	(IV)
377	100	0.5	30	200mm	Arisawa	JP H04-026813-5	(e)	(5)	(IV)
378	100	0.5	30	200mm	Arisawa	JP H07-020385-2	(f)	(5)	(IV)
379	100	0.5	26.5	180mm	Kusaka	USP 6069744-1	(c)	(5)	(IV)
380	100	0.6	25	200mm	Toshi	USP 9366850-4	(b)	(5)	(IV)
381	100	0.6	26.5	180mm	Yamamoto	JP 2008-145787	(b)	(4)	(IV)
382	100	0.67	30	200mm	Arisawa	JP 2005-258148	(f)	(4)	(IV)

No.	Mag.	NA	F.N.	Conjugate	Inventor	Patent No.	Color	Field	W.D.
383	100	0.7	25	200mm	Toshi	JP 2010-066445-3	(c)	(5)	(V)
384	100	0.7	30	200mm	Arisawa	JP 2003-167199	(e)	(5)	(V)
385	100	0.7	30	200mm	Shinonaga	JP S62-062317	(c)	(5)	(V)
386	100	0.8	25	200mm	Yoshida	USP 7848027-3	(c)	(5)	(V)
387	100	0.8	18	180mm	Abe	USP 2018-0364466-3	(d)	(4)	(V)
388	100	0.8	18	fin	Yamada	JP S60-247613	(c)	(4)	(V)
389	100	0.8	21	fin	Saito	USP 5076676	(c)	(4)	(V)
390	100	0.8	25	200mm	Yamaguchi	JP 2000-206414	(c)	(5)	(V)
391	100	0.8	26.5	fin	Suzuki	JP H04-040409	(b)	(5)	(V)
392	100	0.8	26.5	180mm	Fujimoto	JP 2002-202457-2	(c)	(4)	(V)
393	100	0.8	20	180mm	Chuang	USP 7245438	(c)	(5)	(I)
394	100	0.8	20	164.5mm	Ulrich	USP 5103341	(b)	(4)	(I)
395	100	0.85	18	fin	Yamada	JP S60-241009	(c)	(4)	(V)
396	100	0.85	26.5	180mm	Yamawaki	JP 2007-328014-3	(b)	(5)	(V)
397	100	0.85	16	360mm	Kashima	JP H05-196874	(f)	(4)	(I)
398	100	0.9	25	200mm	Yoshida	USP 9341832-2	(c)	(5)	(V)
399	100	0.9	18	180mm	Shimizu	USP 4588264-2	(b)	(4)	(V)
400	100	0.9	25	200mm	Hiraga	JP 2000-241710	(b)	(4)	(V)
401	100	0.9	25	250mm	Riesenberg	DD 288244	(c)	(4)	(V)
402	100	0.9	25	200mm	Watanabe	JP 2009-192988	(c)	(4)	(V)
403	100	0.9	30	200mm	Arisawa	JP H04-220616	(c)	(4)	(V)
404	100	0.9	10	fin	Mori	USP 3661446	(a)	(4)	(I)
405	100	0.9	18	fin	Matsubara	USP 3822931	(a)	(4)	(I)
406	100	0.9	18	182mm	Rybicky	USP 4261654	(b)	(4)	(I)
407	100	0.9	21	fin	Saito	USP 5216545-4	(a)	(4)	(I)
408	100	0.9	26.5	180mm	Yamawaki	JP 2003-075724-2	(c)	(4)	(I)
409	100	0.95	16	fin	Asoma	USP 4505553	(c)	(4)	(I)
410	100	0.95	20	160mm	Ravizza	USP 2644362	(a)	(3)	(I)

No.	Mag.	NA	F.N.	Conjugate	Inventor	Patent No.	Color	Field	W.D.
411	100	0.95	20	180mm	Saito	USP 6188514	(c)	(4)	(I)
412	100	0.95	25	182mm	Danner	USP 4384765	(a)	(4)	(I)
413	100	0.95	25	164.5mm	Matthae	DE 10316415	(d)	(5)	(I)
414	100	0.95	26.5	180mm	Suzuki	JP H09-101462	(c)	(4)	(I)
415	100	1.1	10	180mm	Kashima	USP 5631779	(c)	(5)	(II)
416	100	1.1	10	180mm	Kashima	USP 5406421	(f)	(5)	(II)
417	100	1.1	18	200mm	Watanabe	USP 6700710	(b)	(4)	(VI)
418	100	1.13	16	180mm	Klein	USP 2644943-1	(a)	(4)	(II)
419	100	1.15	18	fin	Tomimatsu	USP 6219189-3	(b)	(4)	(II)
420	100	1.2	15	250mm	Sonnefeld	USP 2050024-2	(a)	(3)	-
421	100	1.23	21	fin	Saito	USP 5216545-5	(a)	(1)	(II)
422	100	1.25	22	200mm	Toshi	USP 8958154-4	(c)	(4)	(II)
423	100	1.25	12	182mm	Shoemaker	USP 3659924	(a)	(5)	(II)
424	100	1.25	12	182mm	Sussman	USP 4376570	(a)	(3)	(II)
425	100	1.25	18	200mm	Tomimatsu	USP 5805346-2	(a)	(4)	(II)
426	100	1.25	18	fin	Yonekubo	JP S54-079053	(b)	(4)	(II)
427	100	1.25	20	200mm	Sharma	USP 6882481	(b)	(4)	(II)
428	100	1.25	20	180mm	Shi	USP 7907348	(a)	(5)	(II)
429	100	1.25	23	200mm	Ryzhikov	USP 5898524	(a)	(5)	(II)
430	100	1.25	23.5	180mm	Hiyakumura	JP S58-192013	(b)	(4)	(II)
431	100	1.25	24	182mm	Shoemaker	USP 3659923	(a)	(4)	(II)
432	100	1.25	24	182mm	Shoemaker	USP 3902793	(a)	(4)	(II)
433	100	1.25	25	200mm	Fukumoto	JP 2010-008527	(a)	(4)	(II)
434	100	1.25	25	200mm	Ryzhikov	USP 5886827	(a)	(4)	(II)
435	100	1.3	25	200mm	Yoshida	USP 9030750-3	(c)	(5)	(II)
436	100	1.3	10	fin	Bertele	USP 3530436	(a)	(3)	(II)
437	100	1.3	12	182mm	Shoemaker	USP 3700311	(c)	(4)	(II)
438	100	1.3	12	182mm	Shoemaker	USP 3746428	(c)	(4)	(II)

No.	Mag.	NA	F.N.	Conjugate	Inventor	Patent No.	Color	Field	W.D.
439	100	1.3	18	180mm	Hatano	USP 6560032-3	(c)	(4)	(II)
440	100	1.3	20	182mm	Shoemaker	USP 4373785	(a)	(4)	(II)
441	100	1.3	22	200mm	Yamahiro	JP H11-174339-2	(b)	(4)	(II)
442	100	1.3	25	fin	Connor	USP 3711186	(c)	(4)	(II)
443	100	1.3	25	200mm	Kudo	USP 5978147	(b)	(4)	(II)
444	100	1.3	30	fin	Goto	JP S51-072343	(c)	(4)	(II)
445	100	1.33	22	180mm	Fujimoto	JP 2007-034020	(c)	(4)	(II)
446	100	1.35	20	fin	Goto	USP 3912378	(c)	(1)	(II)
447	100	1.35	26.5	180mm	Saito	JP H05-142477	(c)	(4)	(II)
448	100	1.35	22	180mm	Yamawaki	USP 2015-0146304	(c)	(4)	(II)
449	100	1.37	30	fin	Nakagawa	USP 4232940	(c)	(4)	(II)
450	100	1.4	18	fin	Yamada	JP S61-275813	(c)	(4)	(II)
451	100	1.4	22	180mm	Konishi	USP 5739957-2	(c)	(4)	(II)
452	100	1.4	22	200mm	Watanabe	JP 2004-061589	(c)	(4)	(II)
453	100	1.4	26.5	180mm	Saito	JP H06-160721	(c)	(4)	(II)
454	100	1.41	22	180mm	Kasahara	JP 2006-195125-1	(c)	(4)	(II)
455	100	1.44	22	180mm	Fujimoto	JP 2006-259548	(c)	(4)	(II)
456	100	1.45	20	164.5mm	Matthae	USP 6504653	(b)	(5)	(II)
457	100	1.45	22	200mm	Mandai	USP 7046451-2	(c)	(4)	(II)
458	100	1.45	26.5	180mm	Fujimoto	USP 6747804-2	(c)	(4)	(II)
459	100	1.46	26.5	180mm	Fujimoto	JP 2002-350734-2	(c)	(4)	(II)
460	100	1.49	25	164.5mm	Wartmann	USP 8724227	(b)	(4)	(II)
461	100	1.65	6.6	180mm	Suzuki	USP 5659425	(c)	(3)	(II)
462	100	1.65	25	200mm	Yamaguchi	USP 6519092-2	(c)	(4)	(II)
463	100	1.67	18	200mm	Watanabe	JP 2002-098903	(c)	(4)	(II)
464	100	1.7	22	180mm	Kasahara	USP 9323036	(c)	(4)	(II)
465	102	1.4	16	fin	Klein	USP 2644943-2	(a)	(4)	(II)
466	105	1.7	4	164.5mm	Knorr	DE 970649	(a)	(1)	-

No.	Mag.	NA	F.N.	Conjugate	Inventor	Patent No.	Color	Field	W.D.
467	140	0.4	20	fin	Kurita	USP 4521086	(a)	(2)	(III)
468	150	0.7	26.5	180mm	Kusaka	USP 6069744-2	(c)	(5)	(V)
469	150	0.9	25	200mm	Yoshida	USP 9341832-3	(c)	(5)	(V)
470	150	0.9	26.5	180mm	Fujimoto	JP 2002-202457-3	(c)	(5)	(V)
471	150	0.9	26.5	180mm	Fujimoto	JP H08-286112	(c)	(4)	(V)
472	150	0.93	26	250mm	Shimada	JP H11-160624-1	(a)	(5)	(I)
473	150	0.95	18	200mm	Amamiya	USP 5636058	(c)	(4)	(I)
474	150	0.95	18	fin	Yamada	JP S60-209715-1	(c)	(5)	(I)
475	150	1.2	25	200mm	Ono	JP H11-218687	(c)	(4)	(II)
476	150	1.45	22	180mm	Kasahara	JP 2006-195125-2	(c)	(4)	(II)
477	160	0.8	23	250mm	Klein	USP 4009945	(b)	(5)	(I)
478	160	0.95	18	fin	Yamada	JP S60-209715-2	(c)	(5)	(I)
479	160	1.43	18	200mm	Bauer	USP 9488818	(c)	(4)	(II)
480	200	0.62	30	200mm	Arisawa	USP 6016226	(c)	(5)	(IV)
481	200	0.95	18	fin	Yamada	JP S60-209715-3	(c)	(5)	(I)
482	250	0.8	26.5	180mm	Kusaka	USP 6069744-3	(c)	(5)	(V)
483	250	0.9	26.5	180mm	Suzuki	USP 5132845	(c)	(5)	(V)
484	250	0.93	26	250mm	Shimada	JP H11-160624-2	(a)	(5)	(I)

Combining the seven color correction levels and seven field correction levels, the number of systems that belong to the 49 new microscope objective types are listed in Table A3.2.

Table A3.2.: Number of systems belonging to the 49 color and field correction classes.

Number of Systems		**Color Correction Classes**							**Sum**
		(a)	**(b)**	**(c)**	**(d)**	**(e)**	**(f)**	**(g)**	
Field Correction Classes	**(1)**	33	4	5	3	0	0	0	45
	(2)	55	19	32	1	14	6	0	127
	(3)	16	3	5	0	0	1	0	25
	(4)	32	35	103	15	9	5	2	201
	(5)	23	10	27	2	4	3	0	69
	(6)	2	0	5	2	0	0	1	10
	(7)	1	0	6	0	0	0	0	7
Sum		162	71	183	23	27	15	3	**484**

Appendix IV: Color Correction Classes

Conventionally, only the axial chromatic aberration correction was considered to evaluate the chromatic correction of the microscope objective. However, when the performance of the modern systems is carefully compared, the difference between each color correction class is not only indicated by the axial chromatic aberration correction, but it can also be seen from the spherochromatism correction. Moreover, due to the strategy of color correction, the chromatic focal shift curves have various shapes. The detailed differences can be distinguished by the plots of longitudinal aberration and chromatic focal shift shown in Table A4.1. The numerical apertures of all the selected systems are narrowed down to 0.8 and the longitudinal aberration is calculated in the object space. Thereby, identical depth of focus (DoF) could be used as a reference for comparison. For instance, at the central wavelength d-line, it is DoF = 0.918 µm for dry objectives and DoF = 1.392 µm for oil-immersion objectives.

Table A4.1.: Representative objectives from seven chromatic correction classes with their chromatic focal shift and longitudinal aberration plots. In the chromatic focal shift plot, the red dashed lines give the corrected spectrum while the green lines indicate the depth of focus (DoF).

Objective system	**Chromatic focal shift**	**Longitudinal aberration**
(a) Achromate 60×/0.85 Yamaguchi USP 5861996 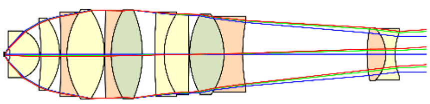 **Cemented doublet with two different crown glasses*	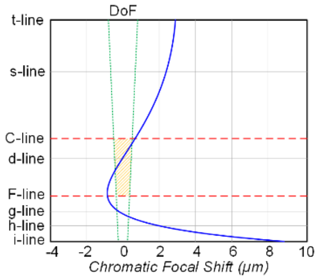	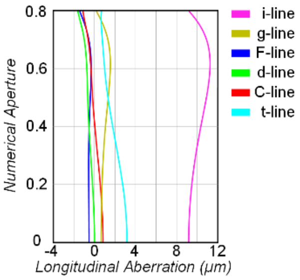
(b) Fluorite 160×/0.95 Klein USP 4009945 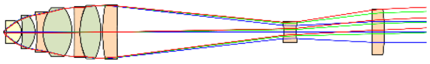	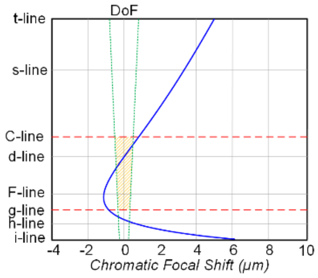	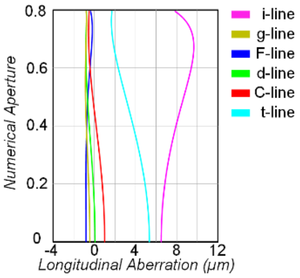

Objective system	**Chromatic focal shift**	**Longitudinal aberration**
(c) Apochromate 20×/0.95 Fujimoto USP 8350904 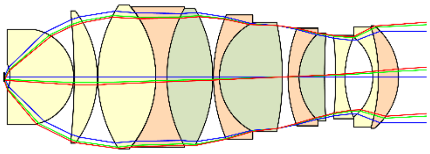	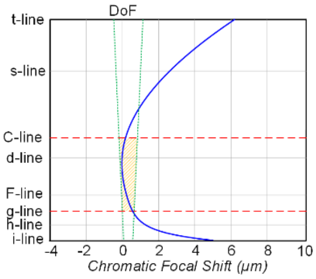	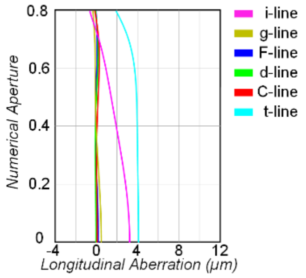
(d) Improved VIS Apochromate (g-s) 55.9×/1.40 O Suzuki JP 2003-015046 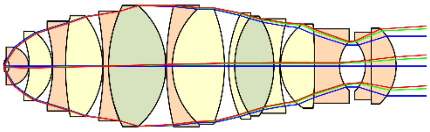 **Rear cemented doublet with two different flint glasses*	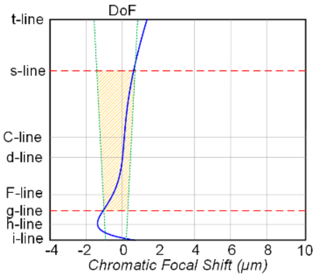	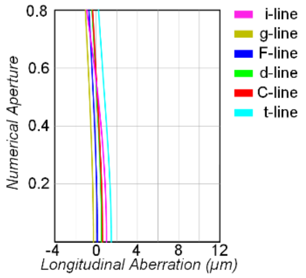
(e) UV Superapochromate (351nm-C) 100×/0.85 Kashima JP H05-196874 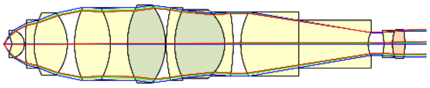 **Cemented doublet with two different crown glasses*	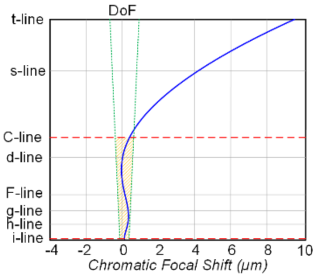	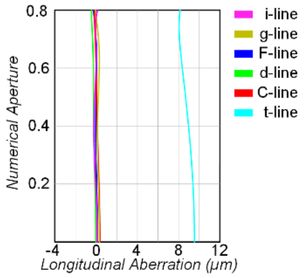
(f) IR Superapochromate (h-t) 40×/0.95 Yamaguchi JP 2010-134218 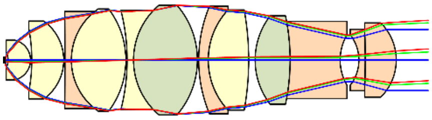 **Rear cemented doublet with two different flint glasses*	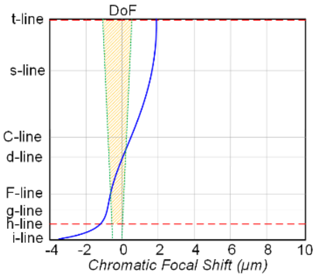	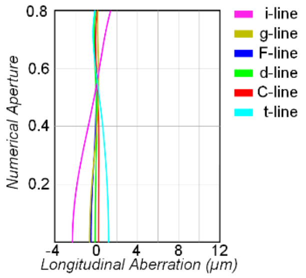
(g) UV-IR Superapochromate (i-t) 40×/1.30 O Wartmann USP 9645380 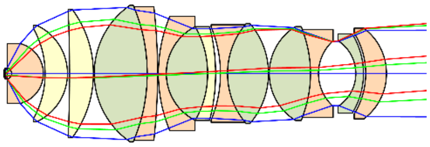	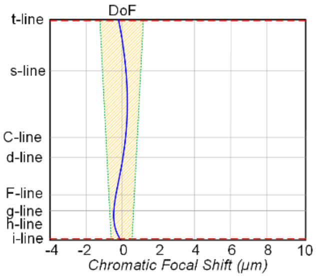	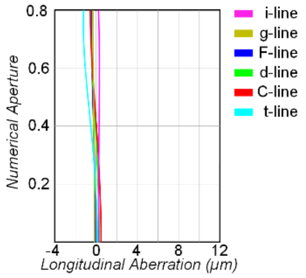

Concerning the conventional Achromate, Fluorite and Apochromate from *class (a)* to *class (c)*, based on the basic achromatism principle, typically the chromatic focal shift curve only has one inflection point within the corrected spectrum. The slope around the inflection point, as well as saddle point, is relatively small. Thus, the chromatic focal shift from g-line to C-line or F-line to C-line can be controlled within 1×~2.5×DoF. In some advanced Apochromate objectives, such as the example *class (c)* system, utilizing special glass combinations, the area around the saddle point could be corrected rather flat. Consequently, the maximum chromatic focal shift is only half of the DoF. By comparing the longitudinal aberration curves, typically there is a large residual spherochromatism in the *class (a)/(b)* objectives. But when it comes to the *class (c)*, both the paraxial chromatic error (longitudinal chromatic aberration) and the chromatic aberration at the full aperture are well corrected, which means that the spherochromatism is removed.

When the corrected spectrum is extended to the UV and/or IR range, the longitudinal aberration should be corrected with at least two inflection points on the chromatic focal shift curve. The *class (d)* improved VIS Apochromate 55.9×/1.40 objective has three inflection points. The chromatic focal shift is therefore very flat and controlled within the DoF through the full spectrum. The *class (e)* UV superapochromate only considers the short wavelength side. Three saddle points can be found from i-line to C-line, which utilizes glasses with specific blue side partial dispersion. However, because the red side is not controlled, the focus of the wavelength above C-line system, only the chromatic focal shift in the visible range is shifted significantly. When it comes to the *class (f)* system, only the chromatic focal shift in the visible range is apochromatic corrected within the DoF. The correction of C-line to t-line, although takes the advantage of DoF enlargement of long wavelength, only realizes Fluorite level correction. As the state-of-the-art, the class (g) system selects glasses with rather equivalent partial dispersion in blue side and red side. Hence, the two saddle points are found in NIR and NUV, and the general curve is flat. Consequently, the chromatic focal shift from i-line to t-line is controlled within the DoF. Comparing the examples from *class (d)* to *class (g)*, they can be always classified as Apochromate according to conventional definition. However, their exact correction of the boundary wavelength might be distinctive. The difference mostly results from glass selection.

The high-performance objectives above the Apochromate *class (c)* mostly correct spherochromatism at the full aperture. Some extreme cases even correct the spherochromatism for all the aperture zones, such as the system (d). This advanced feature is useful in the objective with iris and the application utilizing laser with apodization. Under these circumstances, although the effective NA is smaller than the designed value, nearly identical longitudinal correction can be maintained.

Appendix V: Field Correction Classes

The representative systems of these seven classes and their field performance are shown in Table A5.1. All the systems are *class (c)* apochromatic corrected from g-line to C-line. All the transverse aberrations are calculated for the whole system, which is a combination of the objective and its tube lens.

Table A5.1.: Representative objectives from each field correction class with their field curvature and transverse aberration fan plots. Field curvature is plotted for central wavelength d-line. In the plot, the S stands for sagittal focal shift and the T represents the tangential focal shift. According to different definition, the best image shell could be found between the sagittal shell and tangential shell. Except *class 2*, where the DoF is very large under low NA, 2.5×DoF is shown as the reference to evaluate the level of field curvature correction.

Objective system	**Field curvature**	**Transverse aberration**
(a) *Class 1* 100×/1.35 O SF20 Goto USP 3912378 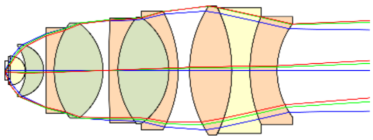	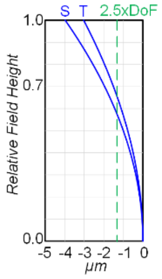	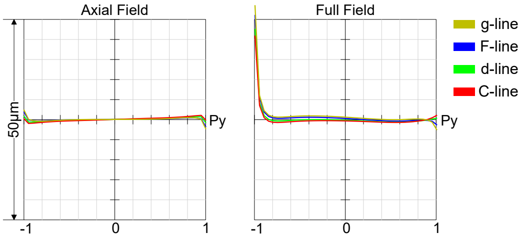
(b) *Class 2* 20×/0.40 SF29 Tojyo USP 4232941 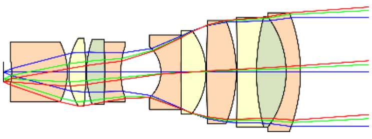	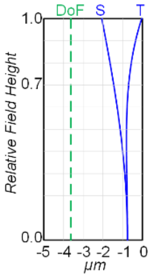	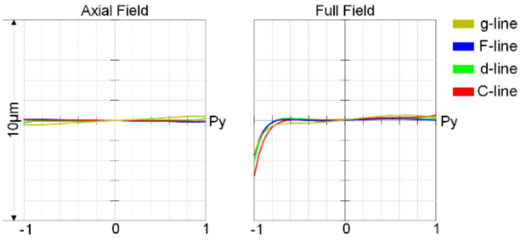
(c) *Class 3* 100×/1.65 O SF6.6 Suzuki USP 5659425 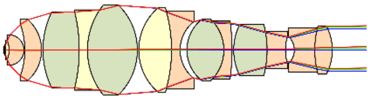 **Rear cemented doublet with two different flint glasses*	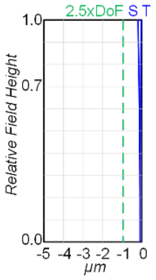	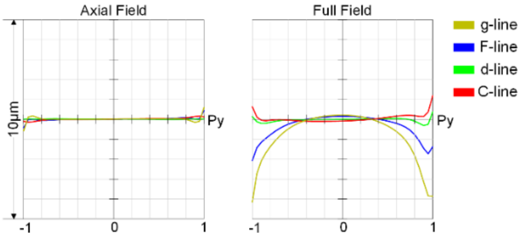

Objective system	Field curvature	Transverse aberration
(d) *Class 4* 100×/0.95 SF20 Saito USP 6188514 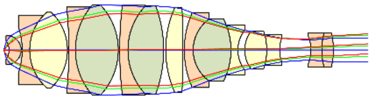 **Rear cemented doublet with two different flint glasses*	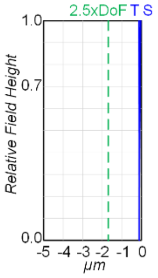	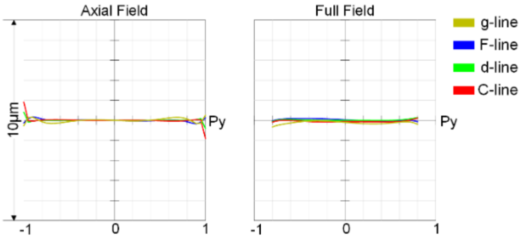
(e) *Class 5* 100×/0.95 SF25 Matthae DE 10316415 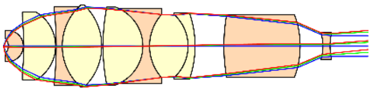 **Cemented quartet with two different crown glasses cemented together*	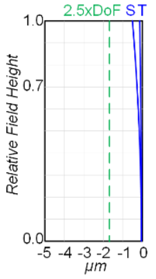	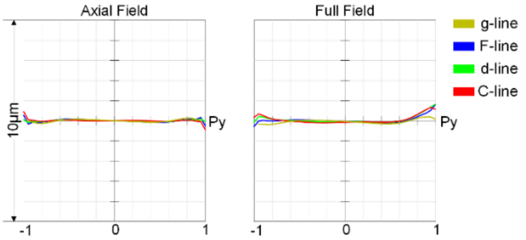
(f) *Class 6* 10×/0.90 SF25 Fujimoto USP 8350904 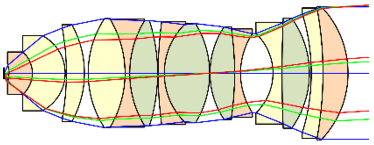	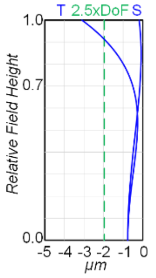	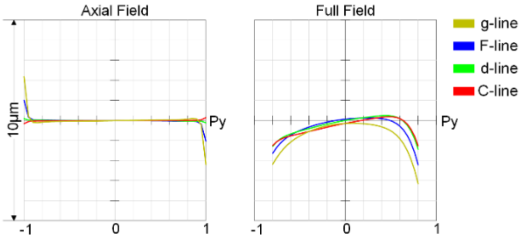
(g) *Class 7* 20×/1.45 SF30 Abe USP 9746658 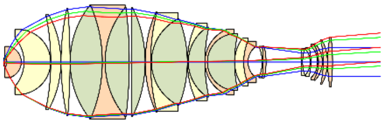	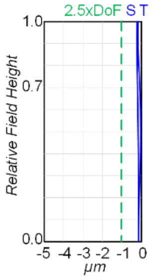	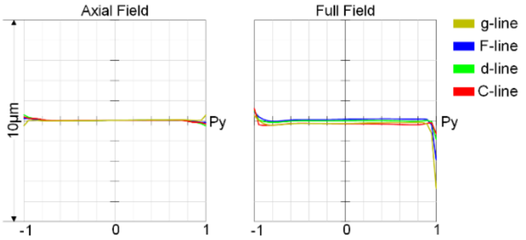

According to the transverse aberration fans of the axial field, all the systems are nearly perfectly corrected for spherical aberration and axial chromatic aberration. In the *class 1* system (a), only the rear cemented meniscus triplet compensates the field curvature. The positive power is still too strong, thus generating a negative Petzval curvature. As a result, the focal shift of the edge field is approximately 5×DoF, two times larger than the Plan limit. The system also suffers from large amount of astigmatism. However, because the cemented meniscus triplet contributes a lot to coma compensation, with a little vignetting, although the field curvature is large, the resolution of the off-axial field is acceptable. The *class 2* system (b) utilizes the double-Gauss structure. The field curvature can be compensated by the meniscus lenses, and coma is also well controlled by the quasi-symmetric layout. Adopted from photographic objective design, the double-Gauss type is useful in working distance extension and field correction, but it only works for the low NA applications. The field curvature of *class 3* system (c) is perfectly corrected for very a small object diameter of 0.066 mm. Coma of F-line and d-line are also controlled well for this small field. However, the objective suffers from chromatic variation of coma, resulting in the tremendous coma of g-line and C-line. The *class 4* system (d) is a typical high magnification high NA objective, with low etendue $G = 0.044$ mm^2. The field curvature is corrected perfectly, but 20% vignetting was introduced to cut off the exploding coma at the edge field. On the contrary, the *class 5* system (e) is designed for identical magnification and NA as (d) but with larger field. Comparing the rear part of these two systems, the system (e) did not use the popular Gauss type rear group. The thick positive lens forms a special air lens together with the following strong negative lens, which compensates field curvature and corrects coma simultaneously. System (f) and system (g) were invented for virtual slides application, with extremely high etendue $G_f = 3.976$ mm^2 and $G_g = 3.715$ mm^2, respectively. The *class 6* system (f) is designed for standardized infinity optics and with parfocal length of 90 mm. The chief ray height at the rear group is large, which induced coma, and the vignetting of the off-axial fields is introduced by both the first and last cemented meniscus doublet as field diaphragms. However, according to the transverse aberration plot, even if 20% vignetting is utilized, coma rises dramatically at the boundary aperture. Field curvature correction is also hampered. Although the best image shell still lies within 2.5×DoF, because of the large astigmatism, the tangential shift exceeds the limit. In the state-of-the-art system (g), all the field aberrations are well controlled. Nevertheless, the parfocal length is sacrificed. The distance from the object to the objective shoulder is approximately 300 mm, far larger than the standardized parfocal length from 45 to 105 mm. Furthermore, the diameter of the objective exceeds 100 mm, which is also five times larger than the typical diameter of NA = 1.45 objectives.

Appendix VI: Impact of Applications

Table A6.1.: Impact of applications on the systems parameters of microscope objectives.

Applications		Etendue		Spectral range		Field correction	Working distance	CORR function	Others
		NA	Magnification	Transmittance	Color correction				
Conventional objective		-	-	VIS	Basic Ach-/Fluor-/Apo- *Class (a)-(c)*	Only field curvature *Class 1-3*	-	CG	-
Conventional IM		↓	-	VIS	Basic Ach-/Fluor-/Apo- *Class (a)-(c)*	Only field curvature *Class 1-3*	LD↑	Large range CG	-
Confocal setup		↑	↓	VIS	Apo- *Class (c)-(d)*	Petzval + Field aberration *Class 4-7*	-	Immersion/Depth	-
Fluorescence Microscopy	General	↑	↓	UV-VIS	Apo-/UV-VIS (i-C) Superapo- *Class (c)-(g)*	Petzval + Field aberration *Class 4-7*	-	CG/Immersion	Autofluorescence↓
	General live cell	↑	↓	UV-IR	VIS-IR (g-t) Superapo- *Class (d)/(f)/(g)*	Petzval + Field aberration *Class 4-7*	LD	Temperature	Possible CG/Immersion/Temperature CORR
	Multiphoton	↑	↓	UV-IR	UV-IR (i-t) Superapo- *Class (f)/(g)*	Petzval + Field aberration *Class 4-7*	LD	Depth	-
	TIRF	↑↑↑	↑	UV-VIS	Apo- *Class (c)-(d)*	Only field curvature *Class 3-4*	Fixed	CG/Temperature	-
Virtual slide microscopy		↑↑	↓↓↓	UV-VIS	Apo- *Class (c)-(d)*	Petzval + Field aberration↑↑ *Class 6-7*	-	Depth	-
Semiconductor inspection		↑	↑	VIS+UV/IR	Basic Ach-/Fluor-/Apo- UV Superapo-/IR Superapo- *Class (a)-(f)*	Petzval + Field aberration↑↑↑ *Class 5*	LD↑↑↑	(Large range CG)	-

Abbreviations

↑:	Enlarged/Improved	↑↑:	Significantly enlarged/Improved	↑↑↑:	Greatly enlarged/Improved	↓:	Reduced	↓↓↓:	Greatly reduced
IM:	Inverted microscope	TIRF:	Total internal reflection fluorescence microscopy			CORR:	Environmental correction	CG:	Cover glass thickness
VIS:	Visible spectrum	UV:	Ultraviolet	IR:	Infrared radiation	Ach-:	Achromate	Fluor-	Fluorite
Apo-:	Apochromate	Superapo-:	Superapochromate	LD:	Long working distance				

Appendix VII: Front Group Materials and Layouts

If the front lenses are made of optical material with higher refractive index (n_d>1.90), the front group can collect larger NA with the same bending, which can relax the middle group design and avoid hyper-hemisphere. Only a limited number of dense flint or Lanthanum dense flint glasses (LASF) can reach this high refractive index. According to Section 6.3, SF dense flint glasses are not preferred in the modern high- performance microscope objective, due to the limited transmittance and capability of chromatic correction. Furthermore, these glasses typically have poor stability and manufacturability. Consequently, the LASF glasses with excellent stability and superb transparency in blue are commonly selected for the front aplanatic lens. The most popular candidates are LASF35 ($n_d = 2.022,\ \nu_d = 29.06$) from Schott and S-LAH79 ($n_d = 2.003,\ \nu_d = 28.27$) from Ohara. However, due to the large dispersion, the aplanatic lens made of these LASF glasses would introduce tremendous chromatic aberration. To reduce this effect, first, as introduced in Section 6.3, the materials with medium refractive index ($n_d = 1.60 \sim 1.90$) and medium dispersion ($\nu_d = 40 \sim 60$) are preferred. Second, based on the front group structure consisting of a vertex-aplanatic lens and shell-lenses, it is possible to design the shell-lenses with materials with low refractive index and low dispersion. Typically, these two methods can also be used together.

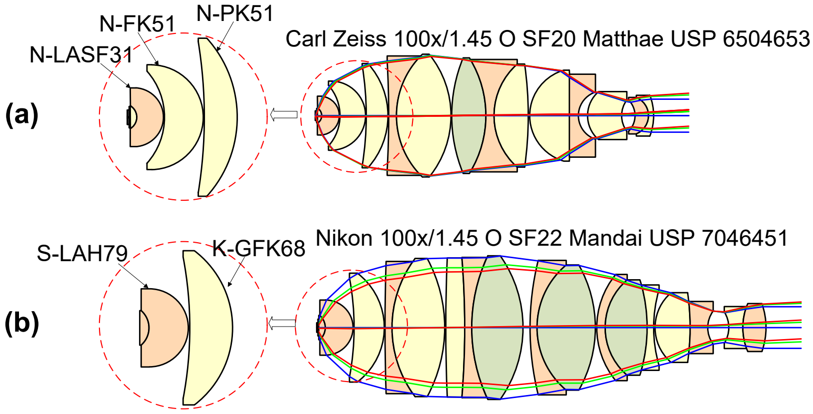

Figure A7.1.: 100×/1.45 oil-immersion objectives with different material selection in the front group. (a) N-LASF31 is utilized with the embedded front lens made of N-BK7, which refractive index is nearly matched to the immersion oil. (b) S-LAH79 is utilized with the embedded front lens made of another flint glass KF6, whose refractive index is nearly matched to the immersion oil.

Figure A7.1 demonstrates a comparison of two 100×/1.45 oil-immersion objectives with nearly equivalent performance. The front lenses are designed to be quasi-vertex-aplanatic with an embedded structure. However, concerning the material selection, the system (a) from Carl Zeiss utilized both two methods, selecting medium-index, medium dispersive glass N-LASF31 ($n_d = 1.881$, $\nu_d = 41.01$) in the front aplanatic embedded lens, followed by two shell-lenses made of low-index, low dispersive glass N-FK51 ($n_d = 1.487$, $\nu_d = 84.47$) and N-PK51 ($n_d = 1.529$, $\nu_d = 76.98$), while the system (b) from Nikon only used the second method, selecting S-LAH79 for the front lens and producing the shell lens with medium index, low dispersive material K-GFK68 ($n_d = 1.592$, $\nu_d = 68.37$). Consequently, the system (b) requires more elements in the middle group to correct the larger residual chromatic aberration.

If the high-index LASF glass in system (b) is changed to N-LASF31A or S-LAH59 instead of S-LAH79, the resulting front group structure is the most popular solution for high NA objective design. Taking advantage of the relatively high refractive index and relatively low dispersion of these medium-index LASF and the following GFK70 ($n_d = 1.569$, $\nu_d = 68.37$) or GFK68 from Sumita, the high NA could be efficiently collected without introducing tremendous chromatic aberration.

When it comes to the high-contrast fluorescence microscopy, under the common epi-fluorescence setup, the excitation light enters the objective from the rear part and reaches the highest intensity at the front group, where it is easy to generate autofluorescence [94]. Therefore, the materials used in the front group should be carefully selected with low fluorescence efficiency. Marked as the forbidden zone in Figure 2.4, the high dispersive glasses with Abbe number ν_d lower than 35 and Abbe number ν_d lower than 50 together with d-line refractive index lower than 1.62 typically have large autofluorescence efficiency. However, the materials fulfilling the conditions of $25 \leq \nu_d \leq 41$ and $1.65 \leq n_d \leq 1.80$ have low autofluorescence and can be used for the high-contrast fluorescence imaging. To match the requirement of low fluorescence, the high-index LASF glasses cannot be used, whereas the medium-index LASF glasses, such as N-LASF31A, are favorable. However, for some systems with high NA and high etendue, it is necessary to use the high-index material to relax the complexity of the middle group. Therefore, special crystals with extremely high refractive index and low autofluorescence have been developed, e.g., LiTaO3 ($n_d = 2.187,\ \nu_d = 23.9$). But they are only used in a limited number of special products [95].

Table A7.1.: Comparison of the front lenses in practical microscope objectives.

System Layout and Front Group	Spherical Aberration	Field Curvature (FC) and Axial Chromatic Aberration (ACA, F-C)
(a) High NA dry objective 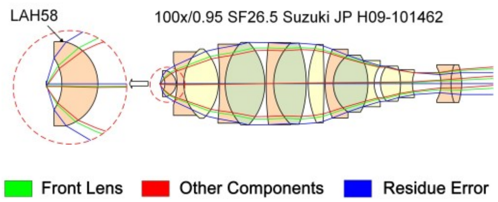 	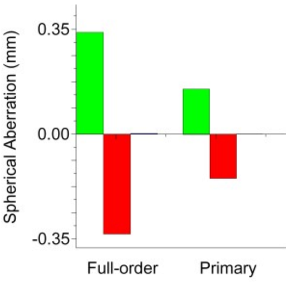 	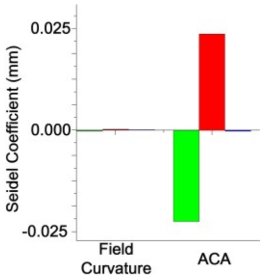
(b) Embedded front lens for immersion objective 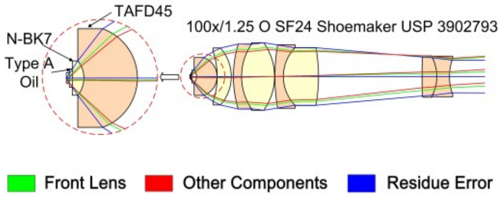 	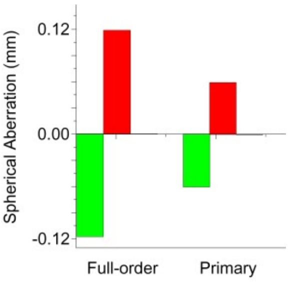 	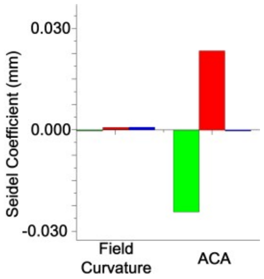
(c) Monolithic front lens for immersion objective 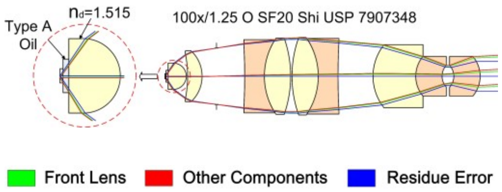 	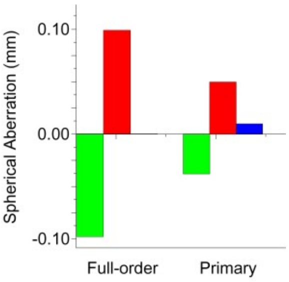 	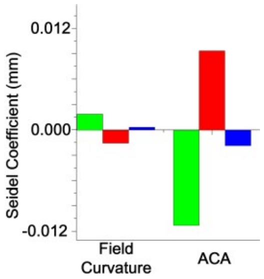
(d) Optical contact bonding front lens 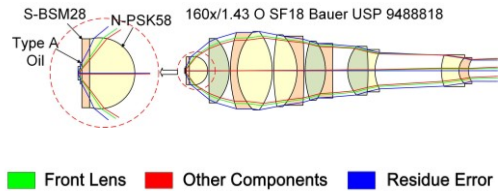 	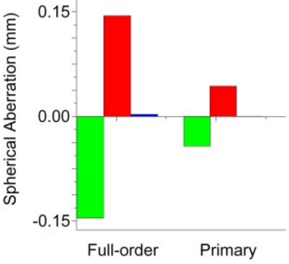 	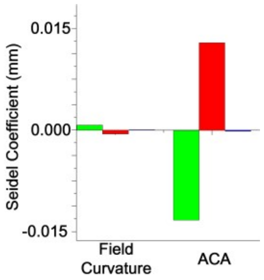

The functionalities of the aberration correction, the front lens of a high NA dry objective, the typical embedded front lens for the immersion objective, the monolithic front lens for immersion objective and the novel front lens utilizing optical contact bonding technology are compared in Table A7.1 with practical examples.

The system (a) utilized a thick meniscus front lens made of LAH58 ($n_d = 1.883,\ \nu_d = 40.78$). Owing to its relatively high index and relatively low dispersion, the high NA = 0.95 is effectively obtained without tremendous axial chromatic aberration. The material also has relatively low autofluorescence efficiency to improve the contrast of fluorescence image. In order to realize the acceptable free working distance of 0.38 mm, the designed concave front surface cannot fulfill the aplanatic condition. Therefore, it generates a large positive spherical aberration with tremendous higher-order contribution, which is different from the slight negative spherical aberration generated by the other systems. However, because of the thick meniscus shape, the element is nearly free of the Petzval curvature. Consequently, the middle group of system (a) becomes very complicated as it compensates the spherical aberration, while the rear group becomes relatively simple due to the relaxation of the field curvature correction.

The systems (b)-(d) are immersion objectives with Type A oil as immersion liquid. The conventional embedded lens used in system (b) selected N-BK7 as the index-matched material and the high index TAFD45 ($n_d = 1.954,\ \nu_d = 32.32$) glass for the rear meniscus part. The front lens is quasi-aplanatic, introducing slight spherical aberration. The field curvature is also restrained by generating a slight positive Petzval curvature according to Equation (6.5). However, due to the large dispersion of TAFD45, the introduced axial chromatic aberration is greater.

The system (c) used a monolithic v-a lens made of a glass with a d-line index of 1.515 and Abbe number about 61, which is matched to the immersion liquid. Taking advantage of the low dispersion, the introduced axial chromatic aberration only has half of the value of the system (b) under identical NA. However, due to its low index, compared with system (b), the rear curvature has a greater bent, reaching the limit of hemisphere. Furthermore, the monolithic front lens generates tremendous negative Petzval curvature, which is then compensated by the “Gauss type” rear group.

Appendix VIII: Rear Groups for Lateral Color Correction

Utilizing three basic structures demonstrated in Section 6.4.3, historically, the distance between the middle group and rear group was enlarged to control the lateral color. The longer separation exploits the first term of Equation (6.6). The light propagates along the long air distance and creates a larger separation of chief ray away from the optical axis. Thus, the rear group significantly contributes to lateral color correction. As illustrated in Figure A8.1, there is a 25.52 mm long separation between the middle group and rear group of the 40×/0.65 objective [96]. Moving the rear group towards the middle group by 6 mm and reoptimizing the rear group to realize the same resolution, the lateral color from the tube lens, front and middle group nearly remain the same, but the contribution from the rear group significantly drops, resulting in the under corrected lateral chromatic aberration.

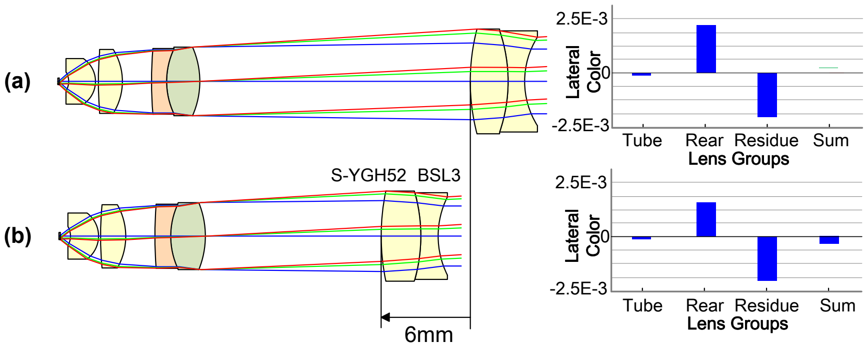

Figure A8.1.: Lateral color correction with long separation of middle and rear group of a 40×/0.65 objective. The cemented single meniscus rear group consists of two crown glasses as S-YGH52 and BSL3. (a) Original design with excellent compensated lateral color. (b) Reoptimized system with reduced separation and hampered lateral color correction.

However, in the highly sophisticated objectives with extended etendue, more components are used in the middle group, which requires large axial space. To match the standardized parfocal length, the air spacing between the middle and rear group is limited. Therefore, thick lenses made of high index materials are often used to achieve large ray bundle separation with reduced distance. In the example 63×/1.00 water dipping objective with Gauss type rear group [92] as shown in Figure A8.2, the thick S-LAH59 ($n_d = 1.816$, $\nu_d = 46.62$) meniscus lens effectively separates the off-axial ray bundles and the last S-NBH51 ($n_d = 1.750,\ \nu_d = 35.30$) meniscus lens contributes significantly to the lateral color control. Notably, according to Kingslake and Johnson [97] it is possible to thicken a lens element by providing a large amount of under-corrected spherical aberration within the glass, which can be used to reduce zonal error. Thus, when the marginal ray height in the rear group is high, the thick lens could also effectively contribute to zonal error correction and even achromatization [13].

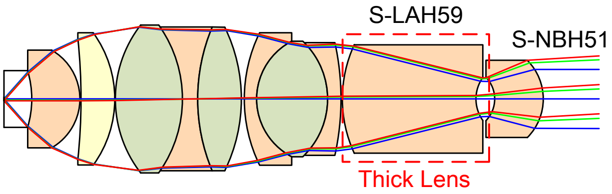

Figure A8.2.: Ray bundle separation with thick lens with high refractive index in 63×/1.00 water dipping objective.

According to Equation (6.6), controlling the lateral color is also associated with the axial chromatic aberration of the rear group. In the conventional Zone 1 and Zone 2 systems, due to the small NA and field size, the residual lateral color from the front group and middle group is not critical. Therefore, achromatic glasses are usually selected. In the example system in Figure A6.1, the rear doublet is cemented by a Middle Glass S-YGH52 ($n_d = 1.787$, $\nu_d = 50.00$) with flint behavior and a typical crown glass BSL3 ($n_d = 1.498$, $\nu_d = 65.03$). To realize the achromatism of the negative doublet, the positive element is made of flint S-YGH52, while the negative component is designed with low dispersive crown BSL3.

When it comes to the system suffering from large residual lateral color, to further increase the contribution of rear group, it is necessary to enlarge the second term of Equation (6.6) as axial color contribution. Therefore, the dense flint glasses with high index and large dispersion are widely used, which is the so-called dense flint principle. According to Section 6.3, due to the consideration of general color correction and autofluorescence suppression, the medium dispersive SF glasses are most favorable, e.g., the S-LAH59 and S-NBH51 used in the Figure A6.2 example system. The dense flint lenses also generate residual axial chromatic, which should be compensated by the middle group. It is notable that the dense flint glasses usually have relatively low transmittance in UV range. Therefore, when they are used in the objectives for UV applications, such as UV fluorescence excitation, the lens thickness should be reduced.

To finely adjust the chromatic aberration, as a special approach, the cemented doublets used in the rear group can be designed with buried surface. The buried surface is formed by two cemented elements with nearly identical refractive indexes but distinctive dispersions. By simply controlling the curvature of the cementing surface, the chromatic aberration is adjusted without disturbing monochromatic aberrations. Therefore, cementing two dense flint glasses is an efficient technology to control lateral color. An example 60×/1.40 oil-immersion objective [42] is shown in Figure A8.3. Based on the quasi-symmetric structure with strongly curved surfaces, the coma, astigmatism and Petzval curvature of the rear group are well balanced. However, because of the distinctive glass selection, the chromatic aberration does not show symmetric behaviors over the six surfaces. The first cemented meniscus doublet selects typical achromatic material GFK70 ($n_d = 1.569,\ \nu_d = 71.32$) and S-LAH63 ($n_d = 1.804,\ \nu_d = 39.59$), while the second meniscus doublet is comprised of S-LAH63 and FD60 ($n_d = 1.805,\ \nu_d = 25.46$), thus forming a buried surface. Consequently, the second cementing surface only contributes to chromatic correction. This cemented lens takes advantage of both the dense flint principle and buried surface.

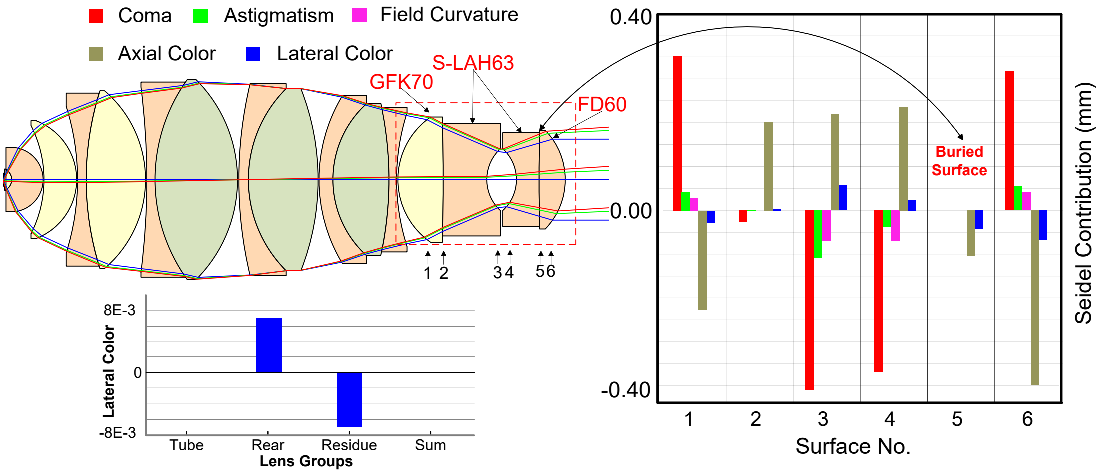

Figure A8.3.: 60×/1.40 oil-immersion objective with buried surface cementing in the rear group.

Appendix IX: CORR Solutions

Utilizing the three solutions listed in Section 6.5, the CORR function is realized in the modern microscope objectives. From the earliest solution with a removable element to the latest solution utilizing air lens effect, better correction performance is achieved, and it is feasible to implement multi-adjustment for environmental parameters including cover glass (CG) thickness, immersion liquid, temperature and imaging depth. But as a byproduct, the mechanical structure becomes tremendously complicated. In this appendix, the CG correction is used as the example to generally demonstrate the three solutions.

The CORR objectives were originally developed for the inverted microscope. Since the thickness and material of the glass vessel, e.g., cell culture dish, are not standardized, a wide range CG correction is required. Utilizing a removable/replaceable element at the front part of the objective, the change of CG can be compensated without changing the other parts of the system. Figure A9.1 shows a Plan-fluorite 25×/0.60 long W.D. objective [98] designed for observation through a cell culture dish with an inverted microscope or liquid crystal display substrate for industrial inspection. Both the dish and the substrate have the shape of a plane plate, which can be considered a cover glass.

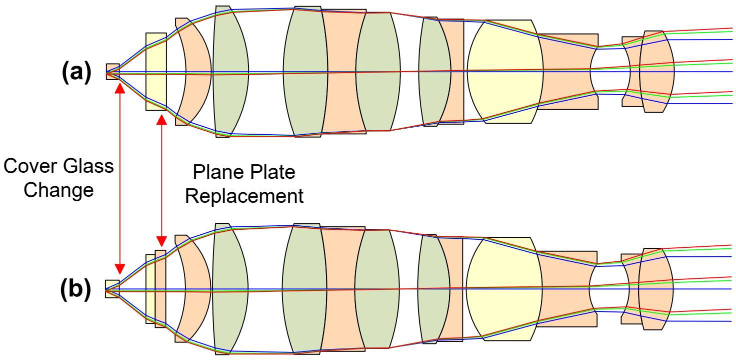

Figure A9.1.: The 25×/0.6 SF10 long W.D. objective (a) used with 1.1 mm plastic plane plate. (a) used with 1.2 mm glass plane plate.

Under case (a), a plastic ($n_d = 1.591,\ \nu_d = 31.00$) plane plate with 1.1 mm thickness is used. The corresponding replaceable element is made of low-dispersive and low-cost NSL5 glass ($n_d = 1.523,\ \nu_d = 59.89$) with thickness of 1.76 mm. When another 1.2 mm NSL5 plane plate is used instead of the plastic one under case (b), to compensate the induced spherical aberration and chromatic focal shift resulting from the distinctive dispersion, a 0.7 mm plane plate made of PBM28 glass ($n_d = 1.689,\ \nu_d = 31.08$), which has similar dispersion as the plastic material, is attached to a 0.8 mm NSL5 plane plate as a new replaceable element. Only by changing the replaceable element, the corrected configuration maintains identical axial chromatic correction and slightly changed spherical aberration without focal shift, which can be seen from Figure A9.2. Although the solution with removable/replaceable element can achieve nearly consistent corrected performance, it cannot realize continuous CG adjustment. Each replaceable element is produced for a specific CG thickness and material, which is not comfortable for practical applications with arbitrary CG thickness within its fabrication tolerance. Furthermore, for high NAs (>0.7), the design of this replaceable compensating component is nearly impossible, due to the tremendous higher-order spherical aberration induced at the plane plate.

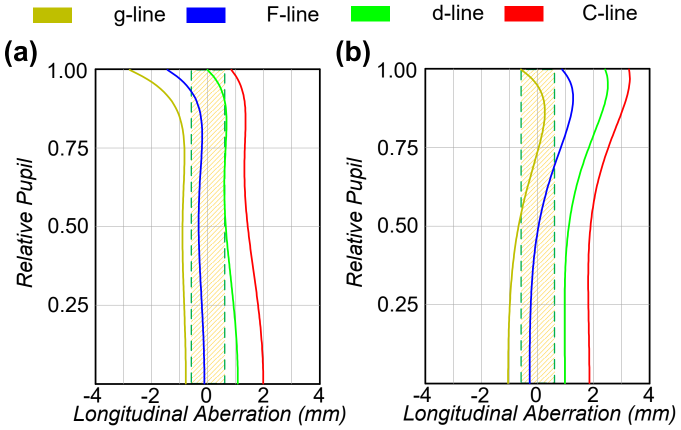

Figure A9.2.: Longitudinal aberration of the 25×/0.6 objective shown in Figure A9.1. The shaded region indicates the DoF of the d-line. (a) Used with 1.1 mm plastic plane plate. (b) Used with 1.2 mm glass plane plate.

From the 1980s, adopting the idea from zooming photographic objectives, a setup with moving components in the middle group becomes the most popular solution. In the early patents in the 1980s and 1990s, to achieve a wide range of CG correction with short track of movement, a positive component with strong optical power was utilized. Figure A9.3 demonstrates three CG configurations of a Plan-achromate 40×/0.55 objective [99], which can correct 0-2 mm CG thickness. Apart from the slight adjustment of the W.D., 1 mm CG thickness change can be compensated by about 1 mm movement of the second cemented doublet. However, because of the great optical power (f = 26.97 mm) of the moving component and the lack of the compensation group, the focus is significantly shifted. According to the longitudinal aberration of the three configurations shown in Figure A9.4, from case (a) to case (c), the focal shift of the d-line is about three times the depth of focus (DoF = 10 mm), which is not negligible. Because of the strong power of the moving component, from case (a) to case (c), the working object NA is changed from 0.54 to 0.52, while the magnification is changed from 41× to 38×. These disadvantageous features change the resolution of the objective and hamper the calibration of the instrument. Furthermore, since the moving component is not free of axial chromatic aberration, its movement also hampers the chromatic correction of the objective lens. Although generally achromatic performance is maintained during the CG change, the exact axial chromatic aberration correction is significantly changed. In case (a), the chromatic focal shift of the F-line and the d-line are well corrected, but it changes to the correction of the d-line and the C-line in case (c). It is also notable that when the ray height increases, the strong positive lens may also introduce a large amount of higher-order spherical aberration. Therefore, this solution is also not applicable to high NA objectives.

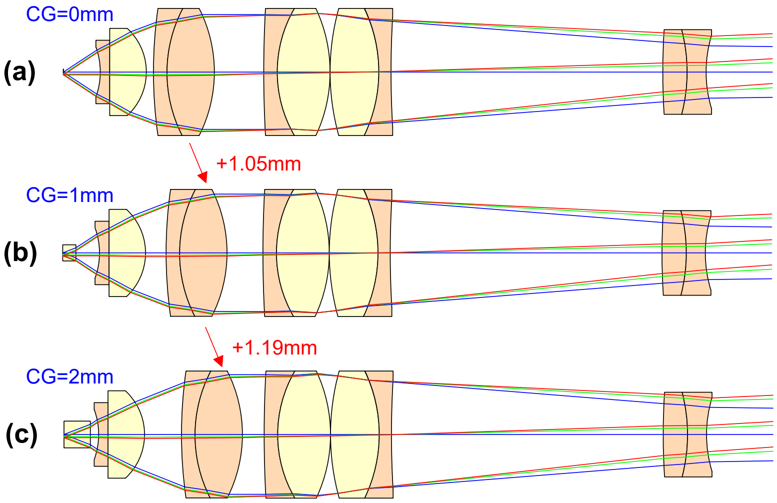

Figure A9.3.: The 40×/0.55 SF18 0–2 mm CG CORR objective using a moving component with strong optical power in the middle group. Although all the components in the moving doublet and the rear doublet are colored with light orange, they are made of different types of flint glasses. (a) Without CG. (b) CG with 1 mm thickness. (c) CG with 2 mm thickness.

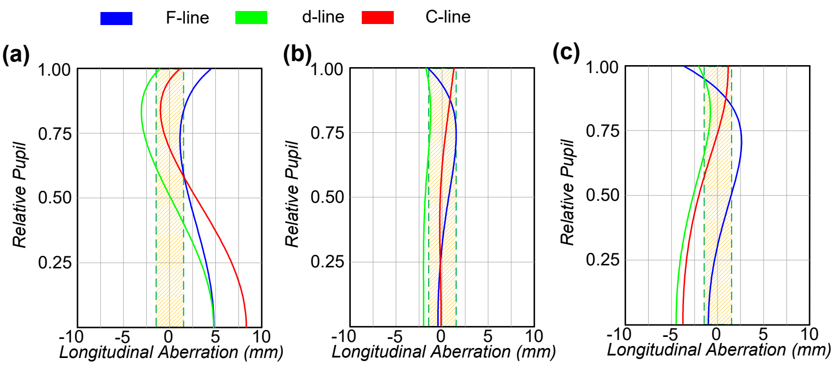

Figure A9.4.: Longitudinal aberration of the 40×/0.55 objective shown in Figure A9.3. The shaded region indicates the DoF of the d-line. (a) Without CG. (b) CG with 1 mm thickness. (C) CG with 2 mm thickness.

To reduce the focal shift and control the chromatic change, a weak power moving component corrected for axial chromatic aberration is used in most of the modern CORR objectives. Depending on the moving track length, they can be further classified into two types. First, it is beneficial to realize a wide-range CG correction by using a long track movement. However, because of the limit of parfocal length, it is impossible to incorporate this feature to the objective with high NA, e.g., NA > 0.9 dry objectives and immersion systems, where the lens tube is usually filled with glasses. Therefore, the CORR objectives with NA > 0.9 for inverted microscopes have not been found. Second, the short track movement can realize small CG thickness deviation within the fabrication tolerance for high NA dry objectives, water-immersion objectives and oil-immersion TIRF objectives. Figure A9.5 shows a Plan-achromate 60×/0.70 objective lens [100] having 0.7-1.7 mm CG CORR function, which was designed for an inverted microscope with long moving track. The movable cemented triplet has very weak optical power ($f = -534.31$ mm) and utilizes achromatic glass pair with anomalous dispersive material FPL53 ($n_d = 1.439$, $\nu_d = 94.96$) and “Middle Glasses” LAL14 ($n_d = 1.697$, $\nu_d = 55.53$) and SK16 ($n_d = 1.620$, $\nu_d = 60.29$) to correct axial chromatic aberration. Because of the weak power, compared with the 40×/0.55 objective shown in Figure A9.3, for the large-range CG correction, the moving track should be extended. However, according to Figure A9.6, both the chromatic performance and focal position are better maintained.

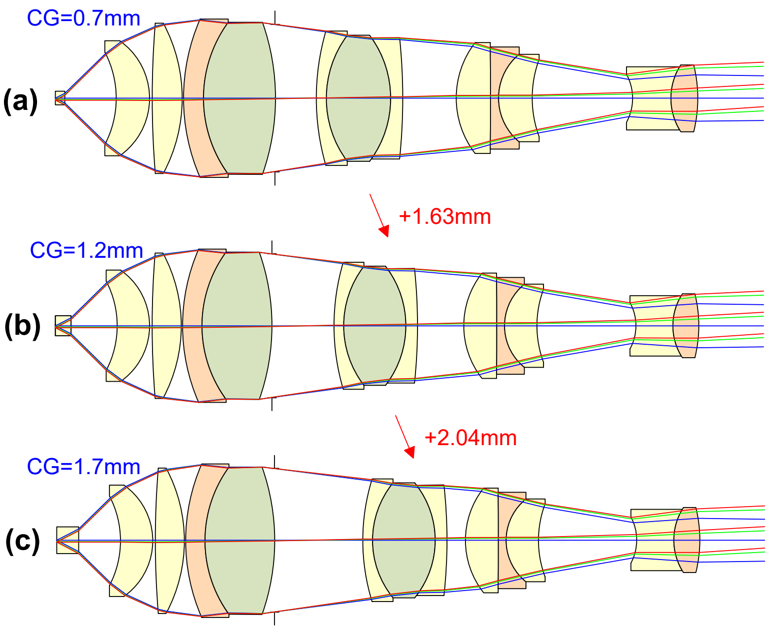

Figure A9.5.: The 60×/0.70 SF18 0.7-1.7 mm CG CORR objective using weak power moving component in the middle group with long moving track. (a) CG with 0.7 mm thickness. (b) CG with 1.2 mm thickness. (c) CG with 1.7 mm thickness.

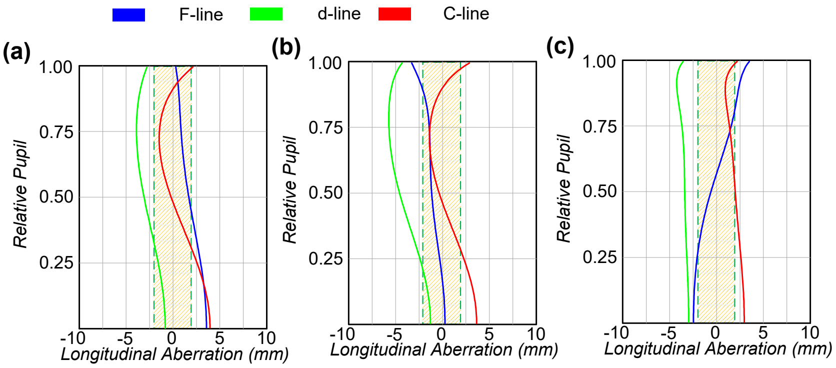

Figure A9.6.: Longitudinal aberration of the 60×/0.70 objective shown in Figure A9.5. The shaded region indicates the DoF of the d-line. (a) CG with 0.7 mm thickness. (b) CG with 1.2 mm thickness. (c) CG with 1.7 mm thickness.

An example of the short track movement is given in Figure A9.7 with a Plan-apochromate 40×/1.20 water immersion objective with 0.11-0.18 mm CG CORR function [101]. The correction function can be understood as the movement of the weak power cemented triplet ($f=-88.50$ mm), it can also be understood as the adjustment of the air lens thickness between the triplet and the Gauss type rear group. Although the optical track length of the objective is changed during the correction, the mechanical design for the moving component can be simplified. According to Figure A9.8, both the chromatic performance and focal position are maintained.

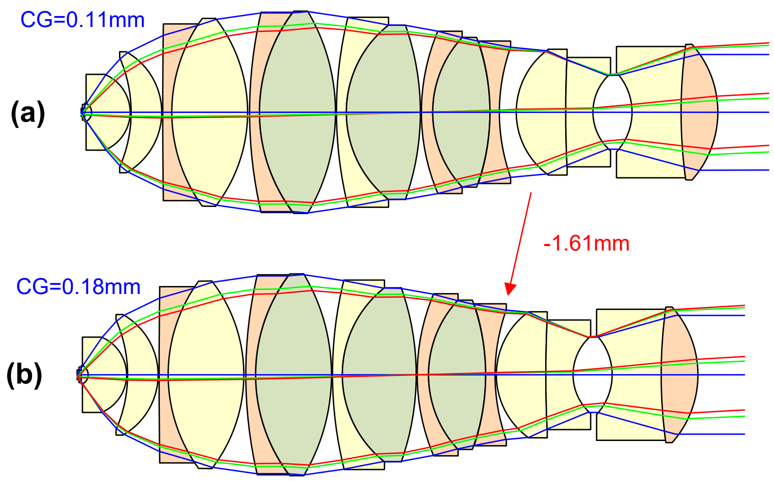

Figure A9.7.: The 40×/1.20 SF23 0.11–0.18 mm CG CORR water-immersion objective using weak power moving component in the middle group with short moving track. (a) CG with 0.11 mm thickness. (b) CG with 0.18 mm thickness.

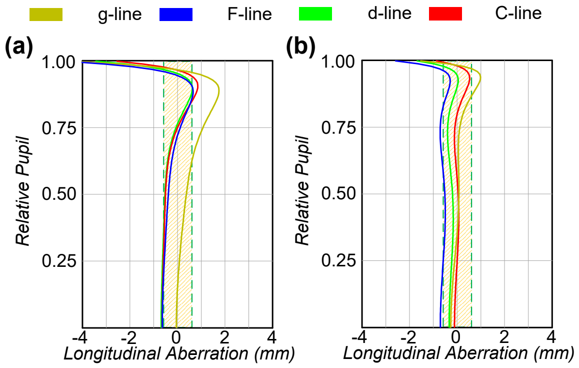

Figure A9.8.: Longitudinal aberration of the 40×/1.20 objective shown in Figure A9.7. The shaded region indicates the DoF of the d-line. (a) CG with 0.11 mm thickness. (b) CG with 0.18 mm thickness.

To further maintain the system performance during the correction and to adjust other environmental conditions, utilization of the air lens effect is the optimal solution. In state-of-the-art systems, e.g., the 63×/1.20(1.30) multi-immersion objective [71] in Figure A9.9, five air lenses are adjusted to correct the CG thickness from 0.15 to 0.19 mm, the temperature from 23°C to 37°C and the immersion liquid as water and glycerin. The objective used five air lens thicknesses, where the spherical aberration is the most sensitive. During the CG correction from 0.15 to 0.19 mm, the component pair E2 and E4 should be moved toward opposite directions, as well as the component pair E5 and E6. In fact, the CORR function realized by multiple air lenses can also be understood as a zooming system with mechanical compensation, while the previously discussed CORR objectives with a single moving component correspond to the zooming systems with optical compensation.

According to Figure A9.10, owing to the mechanical compensation, the focal position is nearly fixed, while the axial chromatic aberration and spherochromatism are also kept constant during the correction. However, the mechanical design for the moving components becomes tremendously complicated.

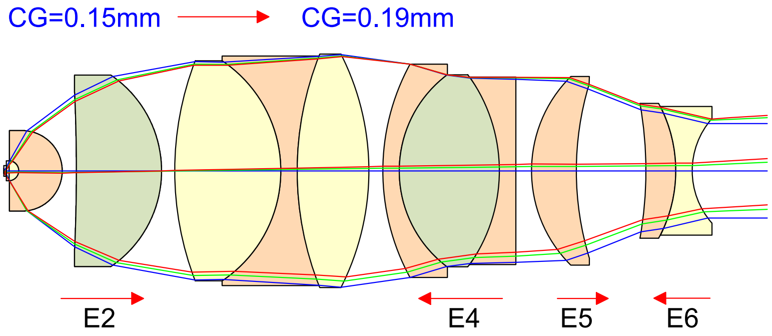

Figure A9.9.: The 63×/1.20 SF20 0.15-0.19 mm CG CORR water-immersion objective using five air lenses.

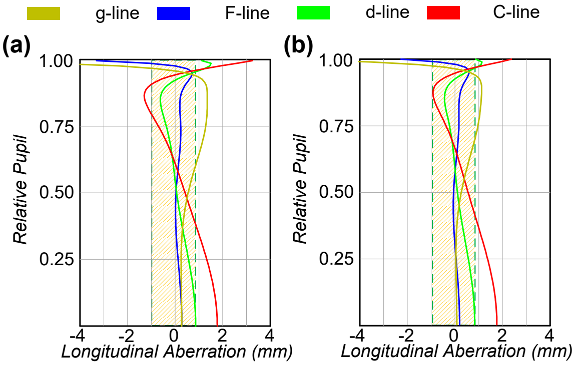

Figure A9.10.: Longitudinal aberration of the 63×/1.20 objective shown in Figure A9.9. The shaded region indicates the DoF of the d-line. (a) CG with 0.15 mm thickness. (b) CG with 0.19 mm thickness.

References

1. A. H. Bennett, *The Development of the Microscope Objective.* Journal of the Optical Society of America, 1943. **33**(3): p. 123-128.
2. H. Beyer, *Historischer Rückblick*, in *Handbuch der Mikroskopie*. 1988, Verlag Technik. p. 13-23.
3. H. Gross, F. Blechinger, and B. Achtner, *Handbook of Optical Systems, Survey of Optical Instruments*. 2008: Wiley.
4. H. Boegehold, *Das optische System des Mikroskops*. . Vol. 1. 1958, Berlin: VEB Verlag Technik.
5. W. Klein, *'Aufbau und Korrektion der Mikroskopobjektive.* Jahrbuch für Optik und Feinmechanik, 1976: p. 47-86.
6. H. Riesenberg, *Optisches System des Mikroskops*, in *Handbuch der Mikroskopie*. 1988, Verlag Technik. p. 24-107.
7. B. G. Broome. *Microscope objectives and their evolution to optical disk objectives*. in *Lens Design*. 1992. SPIE.
8. W. J. Smith, *Modern lens design*. Vol. 2. 2005: McGraw-Hill New York.
9. M. J. Kidger, *Intermediate optical design*. 2004: SPIE Bellingham, WA.
10. M. Laikin, *Lens Design*. 2006, Boca Raton: CRC Press.
11. H. C. Claussen, *Microscope Objectives with Plano-Correction.* Applied Optics, 1964. **3**(9): p. 993-1003.
12. C. G. Wynne, *Flat-field microscope objective.* Journal of Scientific Instruments, 1961. **38**(3): p. 92.
13. H. Takenaka. *Recent Trends in the Design of Microscope Objectives*. in *1985 International Lens Design Conference*. 1986. International Society for Optics and Photonics.
14. A. Miks and J. Novak, *Analysis and synthesis of planachromats.* Applied Optics, 2010. **49**(17): p. 3403-3410.
15. N. Liu, Y. Zhang, and F. Fang. *A novel method of lens initial structure selection: study on structures-aperture relationship of finite image distance achromatic spherical microscope objective with larger numerical aperture*. 2007.
16. D. N. Frolov, *Synthesis of the optical systems of lens objectives for microscopes.* Journal of Optical Technology, 2002. **69**(9): p. 614.
17. D. N. Frolov, R. M. Raguzin, and V. A. Zverev, *Optical system of a modern microscope.* Journal of Optical Technology, 2002. **69**: p. 610.
18. D. N. Frolov, O. A. Vinogradova, A. D. Frolov, and A. G. Tabachkov. *The construction of frontal components of objectives for microscope: optical design*. in *Optical Design and Testing VIII*. 2018. International Society for Optics and Photonics.
19. D. N. Frolov, O. A. Vinogradova, V. N. Frolov, and P. S. Vakulov. *Optical design and unification of objectives: CCF PlanApo for 28 mm observation in the microscope*. in *Optics, Photonics, and Digital Technologies for Imaging Applications V*. 2018.
20. E. Husserl, *The Paris Lectures*. 1964: Springer Netherlands.
21. D. Shafer, *My 50 Years of Optical Design Using Husserl's Phenomenology*. 2016.
22. Y. Zhang and H. Gross, *Systematic design of microscope objective Part I: system review and analysis.* Advanced Optical Technologies, 2019. **8**(4): p. 1-35.
23. H. Piller, *Microscope Photometry*. 1977, Heidelberg: Springer-Verlag Berlin.
24. H. Gross, *Handbook of Optical Systems, Fundamentals of Technical Optics*. 2005: Wiley.

25. W. T. Welford, *Aberrations of Optical Systems*. 1986: Taylor & Francis.
26. H. Gross, *Higher Order Spherical Aberration Revisited*, in *EOSAM 2018*. 2018: Delft.
27. Y. Zhang and H. Gross, *Systematic design of microscope objectives Part II: lens modules and design principles.* Advanced Optical Technologies, 2019. **8**(4).
28. J. Sasián, *Introduction to Aberrations in Optical Imaging Systems*. 2012: Cambridge University Press.
29. H. Gross, H. Zügge, M. Peschka, and F. Blechinger, *Handbook of Optical Systems, Aberration Theory and Correction of Optical Systems*. 2007: Wiley.
30. A. Berner, E. Kasperkiewicz, Y. Zhang, and H. Gross, *3rd-order spherochromatism surface contribution and its intrinsic and induced aberration parts.* J. Opt. Soc. Am. A, 2018. **35**(8): p. 1368-1378.
31. Zemax LLC, *ZEMAX User's Manual*. 2015.
32. H. H. Hopkins, *Canonical and real-space coordinates used in the theory of image formation*, in *Applied Optics and Optical Engineering*. 1983, Academic Press: New York. p. 307-369.
33. Lambda Research Corporation, *OSLO User's Manual*. 2018.
34. Synopsys®, *CODE V Setup and Operation Reference Manual*. 2018.
35. H. Boegehold, *Group of lenses.* US 1578259, 1926, Carl Zeiss SMT GmbH
36. C. Schulz and C. Schumann, *Immersionsobjektiv für ein Mikroskop.* DE102017108595, 2018, Leica Microsystems CMS GmbH
37. Y. Fujimoto and Y. Kawano, *Microscope for Virtual-Slide Creating System.* US 8350904, 2013, Olympus Optical Co.
38. R. Shi, *Microscope Objective.* US 7672057, 2010, Carl Zeiss Jena GmbH
39. T. Kasahara, *Immersion microscope objective and microscope using the same.* US 9323036, 2013, Olympus Optical Co.
40. T. Suzuki, *Immersion Microscope Objective.* US 5659425, 1997, Olympus Optical Co.
41. K. Watanabe, *Immersion microscope objective lens (in Japanese).* JP 2002-098903, 2002, Nikon Corporation
42. K. Yamaguchi, *Immersion Microscope Objective Lens.* US 6519092, 2003, Nikon Corporation
43. K. Arisawa, *Objective lens for a microscope.* US 6016226, 2000, Mitutoyo Corporation
44. K. H. Schade, P. Euteneuer, and A. Müller-Rentz, *HCS – ein Optiksystem mit Zukunft.* MITTEILUNGEN FÜR WISSENSCHAFT UND TECHNIK, 1998.
45. Y. Ouchi, *Observation Apparratus.* US 6366398, 1996, Nikon Corporation
46. R. Wartmann, *Hochaperturiges Immersionsobjektiv.* DE 102009037743, 2009, Carl Zeiss Microscopy GmbH
47. K. Abe, *Objective for microscope.* US 9746658, 2017, Olympus Optical Co.
48. K. Carlsson, et al., *Three-dimensional microscopy using a confocal laser scanning microscope.* Optics Letters, 1985. **10**(2): p. 53-55.
49. J. B. Pawley, *Handbook of biological confocal microscopy*. 2006: Springer.
50. T. Wilson, *Confocal Microscopy*. 1990: Academic Press.
51. M. Matthae and G. Herbst, *Planapochromatically-corrected microscope objective.* US 20130100537, 2013, Carl Zeiss Microscopy GmbH
52. S. Kashima, *Objective lens.* US 7042648, 2003, Olympus Optical Co.
53. T. Suzuki, *High magnification objective lens system.* US 5132845, 1990, Olympus Optical Co.
54. R. Shi, *Microscope objective.* US 7907348, 2007, Carl Zeiss MicroImaging GmbH

55. A. H. Shoemaker, *Five member oil immersion microscope objective.* US 3902793, 1975, American Optical Corporation
56. T. Bauer and C. Schulz, *Immersion objective for microscopes and use thereof.* US 20140247502A1, 2016, Leica Microsystems CMS GmbH
57. Y. Fujimoto and T. Kasahara, *Immersion objective lens system for microscope.* US 7199938, 2007, Olympus Optical Co.
58. M. Mandai and K. Yamaguchi, *Immersion MIcroscope Objective Lens.* US 7046451, 2006, Nikon Coporation
59. C. Metz, *Neue Okulare zur Ebnung der Gesichtsfelder der Apochromate.* Zeitschr. für wiss. Mikroskopie, 1920. **37**: p. 49-52.
60. H. Boegehold, *Microscope Objective.* US 2206155, 1940, Carl Zeiss SMT GmbH
61. T. Toshi and M. Akiko, *Microscope objective lens.* US 8958154, 2008, Nikon Corporation
62. K. Suzuki, *Immersion microscope objective lens (in Japanese).* JP 2003-015046, 2003, Nikon Corporation
63. M. Matsubara, *Objective lens systems for use in microscopes.* US 3925910, 1975, Olympus Optical Co.
64. H. Konishi, *Objective lens system for fluorescence microscopes.* US 5739957, 1998, Olympus Optical Co.
65. Y. Fujimoto and D. Nishiwaki, *Objective lens system for microscope.* US 6747804, 2001, Olympus Optical Co.
66. H. Konishi, Y. Fujimoto, K. Kusaka, and T. Kasahara, *Immersion type microscope objective.* US 7486445, 2008, Olympus Optical Co.
67. Y. Saito, *High magnification microscope objective lens (in Japanese).* JP H05-142477, 1993, Olympus Optical Co.
68. M. Yamahiro, *Immersion microscope objective lens (in Japanese).* JP H11-174339, 1999, Nikon Corporation
69. W. Merte, H. Richter, and M. von Rohr, *Das photographische Objektiv*. Handbuch der wissenschaftlichen und angewandten Photographie. 1932, Wien: Springer.
70. Y. Zhang and H. Gross. *Systematic design of microscopic lenses*. Proc. SPIE 10590, *International Optical Design Conference 2017*, 10590-0G
71. R. Shi, *Immersion microscope objective.* US 7349162, 2008, Carl Zeiss Jena GmbH
72. D. Shafer, *Optical Design And The Relaxation Response*, in *Recent Trends In Optical Systems Design; Computer Lens Design Workshop*. 1987. p. 2-9.
73. M. Matthae, W. Kleinschmidt, and G. Herbst, *Apochromatically Corrected Microscope Objective.* US 7268953, 2007, Carl Zeiss Microimaging GmbH
74. W. Klein, *Microscope objective.* US 4009945, 1967, Ernst Leitz GmbH
75. R. Shi, W. Kleinschmidt, G. Herbst, H. Richter, and C. Hoyer, *Immersion Objective and Light Microscope.* US 9488817, 2013, Carl Zeiss Microscopy GmbH
76. Y. Saito, *Microscope objective.* US 5444573, 1995, Olympus Optical Co.
77. W. Klein, *Microscope plano objective.* US 3537773, 1970, Ernst Leitz GmbH
78. A. H. Shoemaker, *Eight component 100x microscope ojbective.* US 3700311, 1972, American Optical Corp.
79. A. Taira, *Microscopic Objective.* US 3744881, 1973, Olympus Optical Co.
80. A. Taira, *Objective lens systems having a large working distance and adapted for use in microscopes.*

US 3806231, 1974, Olympus Optical Co.

81. W. Klein, *Wide field microscope objective.* US 3176583, 1965, Ernst-Leitz GmbH
82. T. Tojyo, *Microscope objective with correction means.* US 4059342, 1977, Olympus Optical Co.
83. Carl Zeiss Microscopy GmbH, *Objectives from Carl Zeiss Exceeding Your Expectations*. 2007.
84. K. Yonekubo, *Microscope objective lens system.* US 4174151, 1977, Olympus Optical Co.
85. T. Tojyo, *Objective lens system for microscopes.* US 4279477, 1981, Olympus Optical Co.
86. Y. Saito, *Liquid-immersion type objective lens system for microscopes.* US 5530590, 1996, Olympus Optical Co.
87. T. Kimura, *Microscope objective lens (in Japanese).* JP S60-63512, 1985, Olympus Optical Co.
88. T. Togino, *Microscope objective lens (in Japanese).* JP S62-49313, 1987, Olympus Optical Co.
89. S. Kashima, *NUV objective lens (in Japanese).* JP H05-196875, 1993, Olympus Optical Co.
90. I. Ito, *Microscope objective.* US 6181480, 2001, Nikon Corporation
91. Y.-H. Chuang, D. Shafer, and J. J. Armstrong, *Broad band objective having improved lateral color performance.* US 7245438, 2007, KLA-Tencor Technologies Co.
92. R. Wartmann and J. Sprenger, *Liquid Immersion Microscope Objective.* US 20060018030, 2006, Carl Zeiss Microscopy GmbH
93. K. Abe, *Microscope optical system.* US 9939622, 2018, Olympus Optical Co.
94. X. Lu, O. Rodenko, Y. Zhang, and H. Gross, *Efficient simulation of autofluorescence effects in microscope lenses.* Applied Optics, 2019. **58**(13): p. 3589-3596.
95. Y. Fujimoto, *Microscope objective lens (in Japanese).* JP 2006-113287, 2006, Olympus Optical Co.
96. K. Kajitani, *Microscope Objective Lens and Microscope Using the Same.* US 6441966, 2002, Olympus Optical Co.
97. R. Kingslake and R. B. Johnson, *Lens design fundamentals*. 2009: academic press.
98. T. Tanaka, *Objective lens for microscope.* US 5555133, 1996, Olympus Optical Co.
99. K. Ushida, *Objective lens for microscope.* US 4403835, 1983, Nikon Corporation
100. Y. Shimizu, *Microscope objective lens.* US 4666256, 1987, Nikon Corporation
101. Y. Okuyama, *Liquid immersion type microscope objective lens.* US 20030043473, 2003, Nikon Corporation

List of Figures

List of Tables

List of Abbreviations

NA	Numerical Aperture
SF	Field number (Intermediate image diameter)
RMS	Royal Microscopical Society
UIS	Universal Infinity System
CFI	Chrome-Free Infinity-corrected system
ICS	Infinity Color Corrected System
HCS	Harmonic Component/Compound System
DoF	Depth of Focus
OSC	Offence against Sine Condition
TIRF(M)	Total Internal Reflection Fluorescent (Microscopy)
AO	American Optical corporation
VIS	Visible spectrum
UV	Ultraviolet spectrum
IR	Infrared spectrum
NUV	Near-ultraviolet spectrum
NIR	Near-infrared spectrum
DUV	Deep-ultraviolet spectrum
SWIR	Short-wave-infrared spectrum
W.D.	Working Distance
CORR	Correction function/collar
CG	Cover Glass
IM	Inverted Microscope
CLSM	Confocal Laser-Scanning Microscope
TIR	Total Internal Reflection
ACA	Axial Chromatic Aberration
LCA	Lateral Chromatic Aberration (Lateral color)
SA	Spherical Aberration

FC	Field Curvature
ZSA	Zonal Spherical Aberration (Zonal error)
SPHCRM	Spherochromatism
AST	Astigmatism
ONA	Object space Numerical Aperture
RONA	Real Object space Numerical Aperture
PONA	Paraxial Object space Numerical Aperture
RINA	Real Image space Numerical Aperture
PINA	Paraxial Image space Numerical Aperture

List of Symbols

ν_d	d-line Abbe number
D_{img}	Intermediate image diameter (SF)
m_{obj}	Objective lens magnification
y_{obj}	Object height
f_{tube}	Tube lens focal length
f_{obj}	Objective lens focal length
G	2D etendue
D_{ExP}	Exit pupil diameter
u	Paraxial marginal ray angle
U	Real marginal ray angle (image space primed)
n	Object space refractive index (image space primed)
i	Angle of incidence of paraxial marginal ray (image space primed)
I	Angle of incidence of real marginal ray (image space primed)
A	Refraction invariant of paraxial marginal ray
$\bar{i}$	Angle of incidence of paraxial chief ray (image space primed)
$\bar{A}$	Refraction invariant of paraxial chief ray
Ω	Lagrange invariant
c	Curvature of the refractive surface
h	Paraxial marginal ray height at the surface
H	Chord length between the real marginal ray incidence point and surface vertex
$S_I \sim S_V$	Seidel coefficients
$\Delta s'_{\text{SPH}}$	Full-order spherical aberration
$S_{\text{FSPH}j}$	Full-order spherical aberration contribution coefficient of the surface No. j
$S_{\text{HSPH}j}$	Higher-order spherical aberration contribution coefficient of the surface No. j
$C_I \sim C_{II}$	Chromatic Seidel coefficients

D_{Airy}	Diameter of the Airy disk
R_E	Rayleigh length
Φ	Optical power
P	Partial dispersion
κ	Relative working distance factor
r	Retrofocus factor
h_{exit}	Marginal ray height of the exit ray bundle
h_{max}	Maximum marginal ray height in the middle part of the objective
t	Telephoto ratio
L	Overall length of the objective lens
D_{Thread}	Thread diameter
D	Diameter of exit marginal ray bundle
s	Symmetry factor
R_{Ptz}	Radius of the Petzval shell
ω_j	Relative marginal ray height
$\overline{\omega}_j$	Relative chief ray height

Acknowledgement

I would like to express my deepest gratitude to my supervisor Prof. Herbert Gross. I still remember our first meeting on 01.11.2013 about Delano diagram, at which time he was the reason that I decided to come to Jena. After these six years, I am completely convinced that I made a good decision and what I learnt is far beyond my expectation. Through my study in the past six years, his guidance, immense knowledge and constant encouragement profoundly influenced and inspired me. With his generous patience, I can gradually grow up and broaden my view in the field of optical design.

Many thanks also go to my colleagues in the Optical System Design group for their kindness and constant emotional support. The great working environment established the crucial basis of all the research works. I am honored to appear in every group photo and share the nice moment with them. Although our “container” has disappeared, the nice memories would always last and continue in the IAP building. I greatly appreciate the colleagues who offered the guidance and support over the years.

Last but not the least, I would like to thank my parents for giving birth to me and supporting me spiritually throughout my life. No matter struggling in the Western Europe or east Asia, no matter wandering in the desert or on the sea, on my way to chase my dream, they are always the strongest backing of mine.

Ehrenwörtliche Erklärung

Ich erkläre hiermit ehrenwörtlich, dass ich die vorliegende Arbeit selbständig, ohne unzulässige Hilfe Dritter und ohne Benutzung anderer als der angegebenen Hilfsmittel und Literatur angefertigt habe. Die aus anderen Quellen direkt oder indirekt übernommenen Daten und Konzepte sind unter Angabe der Quelle gekennzeichnet.

Bei der Auswahl und Auswertung folgenden Materials haben mir die nachstehend aufgeführten Personen in der jeweils beschriebenen Weise entgeltlich/unentgeltlich geholfen:

- Herbert Gross, Betreuer.

Weitere Personen waren an der inhaltlich-materiellen Erstellung der vorliegenden Arbeit nicht beteiligt. Insbesondere habe ich hierfür nicht die entgeltliche Hilfe von Vermittlungs- bzw. Beratungsdiensten (Promotionsberater oder andere Perso-nen) in Anspruch genommen. Niemand hat von mir unmittelbar oder mittelbar geldwerte Leistungen für Arbeiten erhalten, die im Zusammenhang mit dem Inhalt der vorgelegten Dissertation stehen.

Die Arbeit wurde bisher weder im In- noch im Ausland in gleicher oder ähnlicher Form einer anderen Prüfungsbehörde vorgelegt.

Die geltende Promotionsordnung der Physikalisch-Astronomischen Fakultät ist mir bekannt.

Ich versichere ehrenwörtlich, dass ich nach bestem Wissen die reine Wahrheit gesagt und nichts verschwiegen habe.

Jena, 25.07.2019

Ort, Datum Unterschrift d. Verfassers

Curriculum Vitae

Name:	Zhang, Yueqian
Date of birth:	15.08.1991 in Tianjin, P. R. China

Education:

09/1998 – 06/2003	Primary School
	Tianjin Hedong First Central Primary School (Tianjin, China)
09/2003 – 06/2004	Primary School
	Tianjin Experimental Primary School (Tianjin, China)
09/2004 – 06/2009	Middle & High School (Graduation exam)
	Tianjin Yaohua High School (Tianjin, China)
09/2009 – 06/2013	Bachelor of Engineering in Optical Engineering
	Zhejiang University (Hangzhou, China)
10/2013 – 10/2015	Master of Photonics
	Friedrich-Schiller-Universiät, Jena

Working experience:

11/2015 – 06/2016	Research assistant
	Fraunhofer-Institut für Angewandte Optik und Feinmechanik
07/2016 – 01/2020	Research assistant and doctoral candidate
	Group: Optical System Design (Prof. Dr. Herbert Gross)
	Institute of Applied Physics
	Friedrich-Schiller-Universiät, Jena

Publications

Journal Articles

1. Y. Zhang and H. Gross, *Systematic design of microscope objective Part I: system review and analysis.* Advanced Optical Technologies, 2019. **8**(5): p. 313-347.
2. Y. Zhang and H. Gross, *Systematic design of microscope objectives Part II: lens modules and design principles.* Advanced Optical Technologies, 2019. **8**(5): p. 349-384.
3. Y. Zhang and H. Gross, *Systematic design of microscope objectives Part III: lens modules and design principles.* Advanced Optical Technologies, 2019. **8**(5): p. 385-402.
4. A. Broemel, C. Liu, Y. Zhong, Y. Zhang, H. Gross, *Freeform surface descriptions. Part II: Application benchmark.* Advanced Optical Technologies, 2017. **6**(5): p. 337-347.
5. A. Berner, E. Kasperkiewicz, Y. Zhang, H. Gross, *3rd-order spherochromatism surface contribution and its intrinsic and induced aberration parts.* J. Opt. Soc. Am. A, 2018. **35**(8): p. 1368-1378.
6. X. Lu, O. Rodenko, Y. Zhang, H. Gross, *Efficient simulation of autofluorescence effects in microscope lenses.* Appl. Opt., 2019. **58**(13): p. 3589-3596.
7. X. Lu, Y. Zhang, H. Gross, *General analysis and optimization strategy to suppress autofluorescence in microscope lenses.* Appl. Opt., 2019. **58**(27): p. 7404-7415.

Conference Proceedings

1. Y. Zhang and H. Gross. *Systematic design of microscopic lenses*. Proc. SPIE 10590, *International Optical Design Conference 2017*, 2017, 10590-0G.
2. Y. Zhang, Y. Chen, H. Gross, P. Hartmann, and S. Reichel. *Investigation of striae tolerance in optical system*. Proc. SPIE 10690, Optical Design and Engineering VII, 2018, 10690-0M.
3. A. Berner, Y. Zhang, and H. Gross. *Induced* 3^{rd} *order spherochromatism*. Proc. SPIE 10690, Optical Design and Engineering VII, 2018, 10690-0J.
4. S. Heist, M. Landmann, M. Steglich, Y. Zhang, P. Kühmstedt, and G. Notni. *Pattern projection in the short-wave infrared (SWIR): accurate, eye-safe 3D shape measurement*.

Proc. SPIE 10991, Dimensional Optical Metrology and Inspection for Practical Applications VIII, 2019, 10991-0J.

5. Z. Hou, Y. Zhang, and F. Bociort. *Design Using Saddle Point Construction in Complex Lens Systems*. Proc. EOSAM, 2018

Talks (only own)

1. Y. Zhang and H. Gross. *Systematic design of microscopic lenses*. in: *International Optical Design Conference 2017*, Denver (2017).
2. Y. Zhang, Y. Chen, H. Gross, P. Hartmann, and S. Reichel. *Investigation of striae tolerance in optical system*. In: *SPIE Optical Systems Design 2018*, Frankfurt am Main (2018).